Igor Penido de Mello

Graduated in

Chemical Engineering

Method development for assessment of membrane characteristics in Membrane Bioreactor (MBR)

Dissertation for obtaining the master's degree in Membrane Engineering

Erasmus Mundus Master in Membrane Engineering

Advisor: Andreas Fischer, Project Manager R&D, Microdyn-Nadir GmbH*
Co-Advisor: Dominik Schreier, Manager Engineering Europe, Microdyn-Nadir GmbH*
*Today: MANN+HUMMEL Water & Fluids Solutions GmbH

Jury:

Chair: Isabel Coelhoso, Associate Professor, Universidade Nova de Lisboa
Members: André Ayral, Professor, Université de Montpellier
João Crespo, Professor, Universidade Nova de Lisboa
Vlastmil Fíla, Associate Professor, UCT Prague

FACULDADE DE CIÊNCIAS E TECNOLOGIA
UNIVERSIDADE NOVA DE LISBOA

July 2021

Igor Penido de Mello

Graduated in

Chemical Engineering

METHOD DEVELOPMENT FOR ASSESSMENT OF MEMBRANE CHARACTERISTICS IN A MEMBRANE BIOREACTOR (MBR)

Dissertation presented to Faculdade de Ciências e Tecnologia, Universidade Nova de Lisboa for obtaining the master's degree in Membrane Engineering

July 2021

ERASMUS MUNDUS MASTER IN MEMBRANE ENGINEERING FOR A SUSTAINABLE WORLD EM3E-4SW

With the support of the Erasmus+ Programme of the European Union

Method development for assessment of membrane characteristics in Membrane Bioreactor (MBR)

The Erasmus Mundus Master in Membrane Engineering for a Sustainable Word (EM3E-4SW) is an education program financed by the European Commission - Education, Audiovisual and Culture Executive Agency (EACEA), under Project Number-574441-EPP-1-2016-1-FR-EPPKA1-JMD-MOB. It is also supported by the European Membrane Society (EMS), the European Membrane House (EMH) and a large international network of industrial companies, research centers and universities.

www.em3e-4sw.eu
em3e-4sw-project@umontpellier.fr

Confidentiality note

This master's thesis is a truncated version of the original dissertation. The original work is protected from being revealed to the public by a non-disclosure agreement, as it is the result of a Research and Development project of an organization external to the EM3E-4SW master's program. Only this version, approved by the author and MANN+HUMMEL Water & Fluid Solutions GmbH, may be published, distributed or made available to third parties after respecting the three (3) years period after the thesis defense, held on July 23, 2021. Therefore, before July 23, 2024, no version of this work shall be published, distributed or made available to third parties.

“I began to realize how important it was to be an enthusiast in life. If you are interested in something, no matter what it is, go at it full speed. Embrace it with both arms, hug it, love it and above all become passionate about it. Lukewarm is no good.”

Roald Dahl

Acknowledgments

I would like to express my immense gratitude to

My family – Rosamélia, Marcelo, Alex and Marina – for the unconditional love and support during the whole course of the master's program;

My friends: those in Brazil, those I had the chance to make during these amazing two years of study and those that I luckily found in Wiesbaden and made me feel so welcome;

My professors – in Montpellier, Toulouse, Prague and Lisbon – for putting together this rich multidisciplinary educational program and for inspiring us students to achieve our dreams;

My advisor, Andreas Fischer, for the insightful guidance, admirable dedication, generous feedback and personal deference;

My co-advisor, Dominik Schreier, for the openness and trust;

Prof. Claudia Galinha, for the valuable advising;

MICRODYN NADIR – now MANN+HUUMEL – and all colleagues that I met there and helped me throughout this project.

Abbreviations

BOD	Biological oxygen demand
CAPEX	Capital costs
CAS	Conventional activated sludge
COD	Chemical oxygen demand
CST	Capillary suction time
DO	Dissolved oxygen
DOTM	Direct observation through the membrane
EPS	Extracellular polymeric substances
F/M	Food to microorganism ratio
HRT	Hydraulic retention time
Jc	Critical flux
$Jsus$	Sustainable flux
L_p	Permeability
LMH	Liters per hour per square meter (L h^{-1} m^{-2})
MBR	Membrane bioreactor
MF	Microfiltration
MLD	Megaliters per day
MLSS	Mixed liquor suspended solids
MWCO	Molecular weight cut-off
NF	Nanofiltration
OPEX	Operational costs
PES	Polyethersulfone
PVC	Polyvinyl chloride
PVDF	Polyvinylidene fluoride
RO	Reverse osmosis
R&D	Research and development
SD	Standard deviation
SIMC	Simplified internal mode control
SMP	Soluble microbial products
SRT	Solid retention time
TMP	Transmembrane pressure
UF	Ultrafiltration
USD	US-Dollars
ZN	Ziegler-Nichols

Abstract

Membrane bioreactors treat wastewater and produce effluent with quality above traditional methods. Their cost, however, remains higher than competing processes. The occurrence of membrane fouling contributes to these costs insofar as it increases the need for membrane area and air scouring. Manufacturers thus require environments comparable to real plant conditions in order to test products that overcome these drawbacks. This work aimed, in this context, to develop a filtration method that could be used to investigate the characteristics and resistance to fouling of different membranes. The project involved the identification of causes for the difficulties observed in previous attempts, the pursue of solutions, their integration in the system and finally the execution of several filtration trials. Diverse filtration protocols explored the behaviors of polyethersulfone laminated flat membrane sheets through permeation in different media: water, bentonite suspension and activated sludge. These protocols, based on flux-step methods, determined the rate of transmembrane pressure rise, which characterizes fouling, to then assess parameters such as the critical and sustainable fluxes. The method validated the different behaviors of two membrane materials, namely polyethersulfone and polyvinylidene fluoride, which had very different permeabilities, similar values for the critical flux but distinct sustainable fluxes. The higher sustainable flux of the polyvinylidene fluoride membranes was due to lower residual fouling rates, reflecting the higher resistance of this material to irreversible sorption of macromolecules and colloids. The setup built may be improved to allow the simultaneous testing of two membrane sheets. Yet, the method constructed can possibly be applied to differentiate membranes of varied materials, evaluate the effect of aeration intensity or asses sludge filterability.

Keywords: Submerged membrane bioreactor, wastewater, fouling, critical flux, sustainable flux

Table of contents

Figures

Tables

1. Introduction

The increasing size and number of membrane bioreactors (MBRs) for wastewater treatment installed around the world reflect the current confidence in the technology. Valued in USD 3.0 billion in 2019, the MBR global market is being pushed by stringent wastewater discharge regulations and increasing water stress in all regions of the globe. While they have been disregarded in the past for being costly, MBRs have become the choice for systems where the footprint is limited and high wastewater quality is a requirement. For being able to remove all suspended solids and pathogenic microorganisms, MBRs were implemented on a widescale in Europe to comply with the EU Bathing Water Directive. The ability to produce effluents that can be directly fed to reverse osmosis (RO) systems has favored the technology even further. For instance, the largest water reuse project in the southern hemisphere – the Brazilian venture Aquapolo – employs MBRs coupled with RO systems to treat sewage and deliver up to 100 MLD of process water for industries. Increasing public acceptance together with favorable governmental incentives for more environmental-friendly treatment solutions can prompt the application of MBRs for municipal and industrial uses even more in the next decades.

Notwithstanding, the more widespread adoption of MBRs over traditional treatment systems is still restrained by higher capital and operating costs, which remain higher than competing processes. Even with falling membrane costs, the technology is energy intensive and demands specialized workforce. Most of the extra energy costs are due to the phenomenon known as membrane fouling. Fouling describes the deposition of entities – in MBRs mainly colloidal and macromolecular matter – onto the membrane surface during operation. It is the most persistent problem in MBR processes, leading to reduction in process productivity, higher energy consumption, need of frequent membrane cleaning or even replacement. Fouling control strategies managed to partially overcome the problem and achieve stable operation throughout long time periods, yet cleaning procedures are unavoidable. Among these strategies are air scouring and flux control. Air scouring is the main method to prevent fouling in submerged MBRs and is the culprit of the high energy input required. On the other hand, flux control is an efficient way to prevent heavy fouling, although it incurs in the need for larger membrane areas and therefore higher capital investment. The trade-off between flux control and fouling prevention has been subject of several cost-benefit analyses, which are naturally influenced by factors such as membrane lifetime, costs and resistance to attachment of fouling agents.

Low flux operation in MBRs found support in the concept of critical flux. According to this theory, fouling will not occur if the process is run under a certain flux threshold, defined as the critical flux. This limit exists because, while the permeate drag force pushes particles towards the membrane, back transport mechanisms, explained through different transport phenomena, pulls the particles away from the membrane surface. Even though studies have empirically proven the concept, complex media formed by substances with different sizes and natures do not exhibit a well-defined critical flux, which is the case of activated sludge – the medium in MBR systems. However, operators of MBRs can make use of this concept to find flux ranges that minimize the deposition of most particles onto the membrane. In this context, the notion of sustainable flux emerged. The sustainable flux represents a limit for the flux below which the rate of deposition in a certain time span is considered acceptable. Hence, it is more linked to subjective analysis of the application field and time scale of operation rather than to a physical phenomenon of transition between non-deposition and deposition.

The complex relation between all factors affecting fouling urges manufacturers and plant designers to develop a profound understanding on how these factors interact with each other, so that total costs can be further minimized. This translates into a search for optimal module design, energy-saving aerators and tailor made membrane materials. This is a challenge for the research and development of products in view of the fact that lab-scale MBR systems rarely behave comparably to real plants. Causes for this are many, such as the need for activated sludge (composed of live microorganisms that digest pollutants), synthesis feed streams that mimic real wastewater composition, design of comparable geometries and usage of equivalent equipment, like pumps and aerators.

In this context, MICRODYN-NADIR GmbH, a membrane and MBR manufacturer based in Wiesbaden (Germany), operates an MBR pilot unit in a wastewater treatment plant. Recently acquired and renamed MANN+HUMMEL Water & Fluid Solutions GmbH, the company and its R&D department thus have the possibility to test membranes in real conditions, with municipal wastewater as feed. However, the pilot unit only operates with modules above XX m^2 of membrane area, which can only be assembled when a sufficient amount of membrane is synthetized in the production line. This is adequate for new products that are about to be launched in the market, but not for materials at development stage. Moreover, the fully automated pilot plant cannot be programed to follow specific filtration protocols, which hinders short-term investigations of membranes developed at small scale.

This work is therefore the result of the company's effort to develop a test method that enables the investigation of small membrane areas by means of elaborate filtration protocols. Smaller membrane areas can be readily cast in the lab and adapted to fit in smaller modular units. These modules can be submerged in the activated sludge already available at the pilot unit in such a way that conditions are extremely similar to the ones in real plants. Analyses on membrane characteristics such as resistance to fouling agents can therefore be undertaken. For this end, flux-step filtration trials were executed to search for parameters such as the critical and sustainable flux. It was expected that such parameters would reflect the differences in properties between different membrane materials.

Beyond serving the purpose of the delivering to the company a membrane investigation method within the scope of MBRs, this work cemented the knowledge in membrane science and engineering in the field of wastewater treatment acquired by the student throughout his pathway in the Erasmus Mundus Master in Membrane Engineering for a Sustainable World program. The activity allowed not only the direct application of concepts learned during the educational program, but an experience of cooperation at the heart of an industry strongly committed to science and innovation.

2. Literature Review

This literature review provides a general overview on the fundamental concepts related to membranes applied to wastewater treatment, with focus on their application in membrane bioreactors.

2.1. Membrane processes

A membrane is defined as a permselective interphase separating two phases, acting as a barrier to the transport of matter between the two phases (Mulder, 1996). In water and wastewater treatment, a membrane is a semipermeable material that allows the passage of water while hindering the passage of other components in the feed solution. The permeate consists of water and other compounds that may cross the membrane, whereas the retentate is composed of those species rejected by the membrane (Judd, 2006). The process is represented in Figure 2.1.

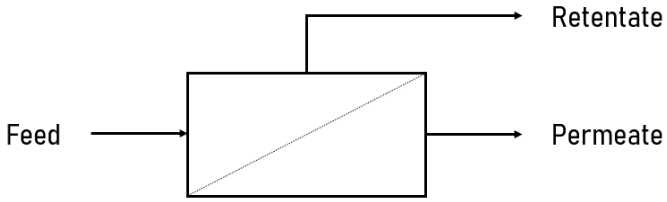

Figure 2.1. Schematic representation of a traditional membrane process (adapted from Mulder, 1996).

The four key membrane processes in which water forms the permeate are microfiltration (MF), ultrafiltration (UF), nanofiltration (NF) and reverse osmosis (RO). In these processes, a pressure difference is applied to force the feed through the membrane and generate water as the permeate. Accordingly, they are known as pressure-driven processes (Judd and Jefferson, 2003). Membranes used in MF and UF are similar in the sense that they are porous materials that rely on size exclusion to promote separation. On the other hand, NF and RO membranes are dense, with theoretical pore sizes as small as the range of thermal motion of the polymer chains of the membrane (Baker, 2004). Despite the similarities between these processes, the differences in pore sizes lead to very different behaviors and uses in industries. Figure 2.2 depicts the four processes and their range of application.

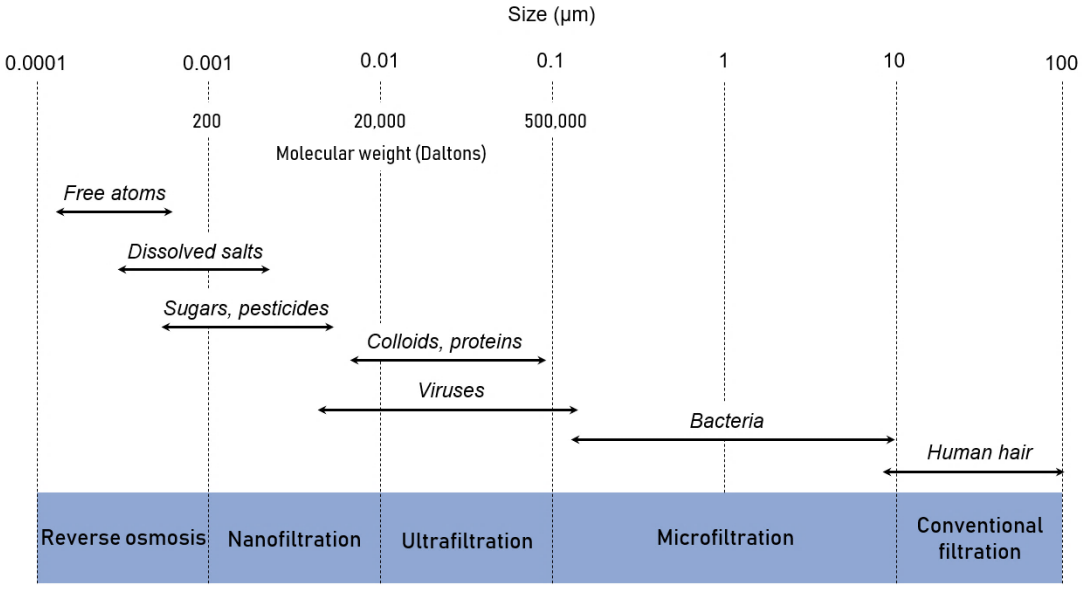

Figure 2.2. Overview on pressure-driven membrane processes (adapted from Judd and Jefferson, 2003).

The rejection or retention coefficient (R) is a measure of the ability of the membrane to retain a certain component from the feed solution, defined in Eq. 1 in terms of the concentrations in the feed (C_{feed}) and permeate ($C_{permeate}$). Rejection values range from 0 % (solute passes freely with the solvent through the membrane) to 100 % (solute is completely rejected) (Mulder, 1996).

$$R = 1 - \frac{C_{permeate}}{C_{feed}} \quad \text{(Eq. 1)}$$

The flow through the membrane, namely flux or permeation rate, is defined as the amount of permeate flowing per membrane area per time. In the above-mentioned operations, the flux (J) is quantified in terms of volume as the total flow (F) divided by the membrane area ($A_{membrane}$) (Eq. 2), with SI units of $m^3\ m^{-2}\ s^{-1}$ or the commonly adopted unit of $L\ m^{-2}\ h^{-1}$, nicknamed "LMH" (Judd and Jefferson, 2003).

$$J = \frac{F}{A_{membrane}} \quad \text{(Eq. 2)}$$

Transport across the membrane only occurs as a result of a driving force acting between the phases. The resulting permeation rate is mostly proportional to this driving force (Mulder, 1996). In pressure-driven membrane operations, the driving force is the pressure difference between both sides of the membrane, called transmembrane pressure (TMP). Here, the permeability (L_p) is defined in Eq. 3 as the ratio between the flux and the TMP (Judd, 2006):

$$L_p = \frac{J}{TMP} \quad \text{(Eq. 3)}$$

Nevertheless, the definition of permeability given by Darcy's law accounts for the film thickness and dynamic viscosity. The given definition of L_p corresponds to the water permeability, which already encompasses the film thickness and dynamic viscosity and therefore differs from the permeability as in Darcy's law. L_p is not an intrinsic property of the porous medium, but a parameter for a given membrane and a given fluid, i.e. water, at a given temperature (as it affects viscosity). This results in the need to normalize any permeability data to a defined reference temperature (Baker et al., 2010).

2.2. Membrane materials

Synthetic membranes can be made from a vast number of materials, yet the ones used in MBRs are either polymeric or ceramic. These materials must meet certain requirements in order to be suitable for the duty of membrane separation. First, they should have high surface porosity (% total surface pore cross-sectional area) and narrow pore size distribution to maximize throughput while having a selective degree of rejection. Then, the material must present mechanical resistance and structural integrity. Lastly, the membrane needs to withstand thermal changes and chemical attacks, since these are part of the regular cleaning routines performed in most membrane processes (Judd, 2006).

Membranes can be distinguished according to their morphology. While symmetric membranes have a homogeneous structure along their thickness, anisotropic membranes are made up of more layers. In the latter type, the thin active layer responsible for the separation sits on top of a more porous, thicker layer that ensures mechanical stability. This minimizes the total filtration resistance of the film, mostly dependent on the thickness of the upper and tighter layer. For this reason, this type of structure became ubiquitous in industries (Pinnekamp and Friedrich, 2006). Figure 2.3 illustrates a typical anisotropic membrane structure.

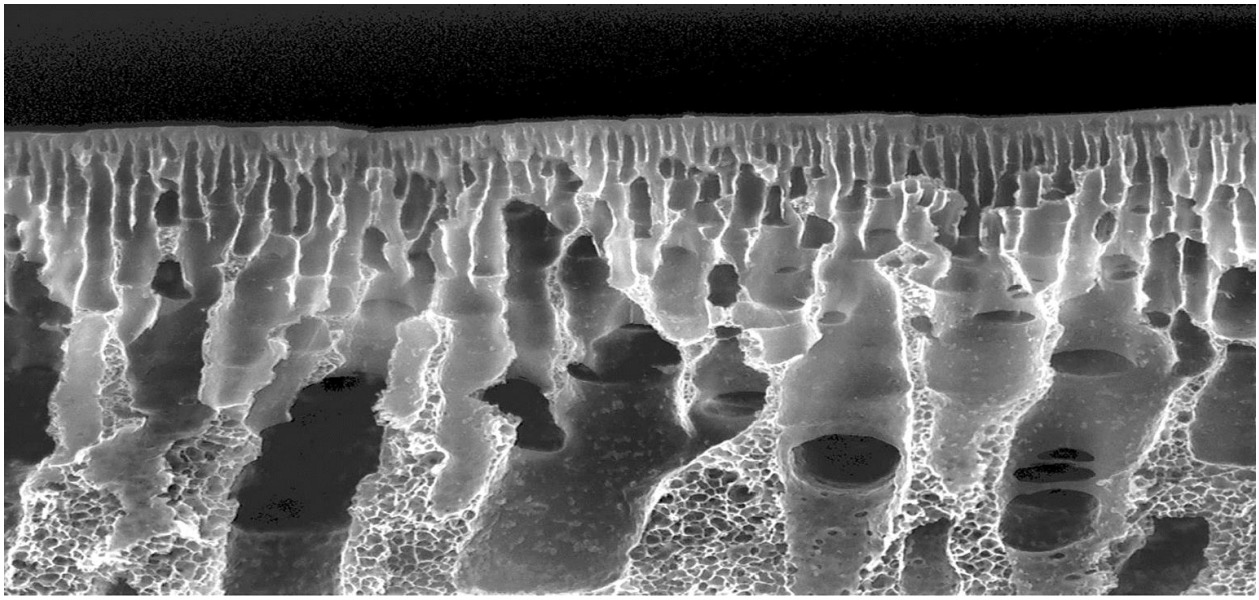

Figure 2.3. Cross-section of an asymmetric polyether membrane (Joshi et al., 2011).

Polymeric membranes dominate the water and wastewater field. This is the case because of their cheaper prices compared to ceramic materials and the possibility to select a specific polymer that suits the process characteristics (Pinnekamp and Friedrich, 2006). The most significant production method of these materials is phase inversion, a process in which the polymer is dissolved in a solvent, cast on a surface and then put in contact with another liquid that forces the precipitation of the polymer (Judd and Jefferson, 2003). The most prevalent polymers applied in MBR membranes are polyvinylidene difluoride (PVDF), accounting for almost half of all products, polyethersulfone (PES) and polyolefins: polyethylene (PE) and polypropylene (PP) (Judd, 2015). Their main disadvantage is their hydrophobicity, which make them prone to the adherence of hydrophobic matter from the feed, phenomenon known as fouling. For this reason, most films undergo surface modifications to produce more hydrophilic surfaces (Judd, 2006).

Ceramic membranes have the advantage of being stable at high temperatures and chemically inert. However, the investment costs are still much higher than those for polymeric membranes (Pinnekamp and Friedrich, 2006). Their application in MBRs is limited to niche markets such as high-strength industrial waste treatment and anaerobic degradation (Judd, 2006).

2.3. Membrane modules

Extensive membrane areas are usually required in industrial projects. The success of any membrane product is therefore bound to how efficient the packaging of large areas in a single unit is. This single package unit is called a module (Baker, 2004). The design of modules is based on two types of membrane configurations: flat and tubular. These geometries allow many possibilities for the construction of modules, the most relevant being (Judd and Jefferson, 2003):

- Plate-and-frame / flat sheet
- Spiral-wound
- Tubular
- Capillary
- Hollow fiber

The first two employ flat membranes while the others operate with tubular geometries, their main difference being the diameter. The choice of the best module type is linked to features like type of separation problem, ease of cleaning, ease of maintenance, ease of operation, compactness and possibility of replacement (Mulder, 1996). Moreover, the module should promote a high degree of turbulence on the feed side and at the same time keep a low energy expenditure (Yoon, 2015).

For MBR purposes, the only successful module types are plate-and-frame, tubular and hollow fiber. This is because the other modules do not allow proper cleaning or are prone to clogging (Judd, 2006).

Hollow fibers are the thinnest of the tubular membranes, with diameters ranging from 50 µm to 3 mm (Figure 2.4). They allow the assembly of compact modules with very large membrane areas, but have low fluxes compared to flat-sheet membranes of the same material. The fibers can be manufactured with the skin layer on the outside, inside or both. In MBRs, they only operate with outside-in filtration. This module type is the cheapest to manufacture but displays poor turbulence promotion for MBRs, since the width of membrane channels (space between fibers) is not well defined (Baker, 2004).

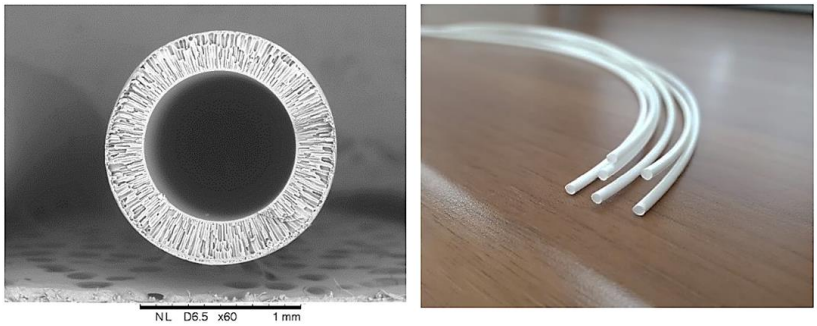

Figure 2.4. Cross-section (a) and general view (b) of a polysulfone hollow fiber membrane (Bazhenov et al., 2018).

Tubular (or multi-tubular) modules operate in the reverse way, i.e., inside-out, as their wider diameter allows the passage of the feed. This configuration is the most expensive and has the lowest packing densities, but corresponds to the most turbulent feed regimes. The tubes consist of a porous support covered with the membrane layer and are nested together in housings (Figure 2.5) (Baker, 2004).

Figure 2.5. Cross-section a multi-tubular membrane module (PCI Membranes, 2021).

Plate-and-frame or flat sheet modules extract the permeate from inside a membrane panel or “envelope” (outside-in filtration). The panels are made of two membrane sheets sealed on the sides and separated by a spacer, allowing the collection of permeate through specific channels (Figure 2.6). The original plate configuration uses a molded, rigid support onto which the sheets are attached, while the new flat sheet configuration is made up of thin flexible laminate sheets of 2 mm thickness. The

panels are loaded into a cassette that can hold many panels. Despite having higher costs compared to hollow fibers, flat sheet modules can promote a better degree of turbulence, since the flow channels between the plates are very well defined. However, most configurations do not allow backwashing, with notable exceptions such as the BIO-CEL® modules (Judd, 2006; The MBR Site, 2021a).

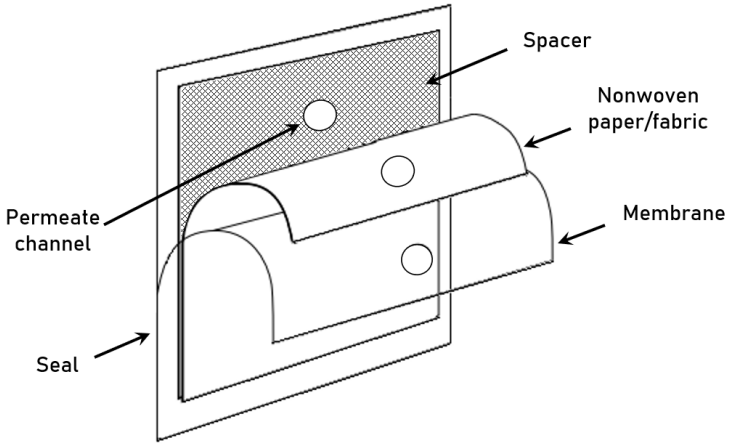

Figure 2.6. Typical flat sheet panel representation (adapted from Baker, 2004).

2.4. Operating modes

Membrane processes can be classified in two operating modes: dead-end and crossflow (Figure 2.7). In dead-end filtration, the feed flows perpendicularly to the membrane surface, leading to an accumulation of the retained material – the cake layer. The thickness of the cake increases during the operation and causes the permeate flow to decrease in time (Mulder, 1996). Usually, the module in dead-end mode is submitted to backwashing cycles to restore a reasonable permeate flow. Therefore, this type of operation is typically a discontinuous process (Melin and Rautenbach, 2007).

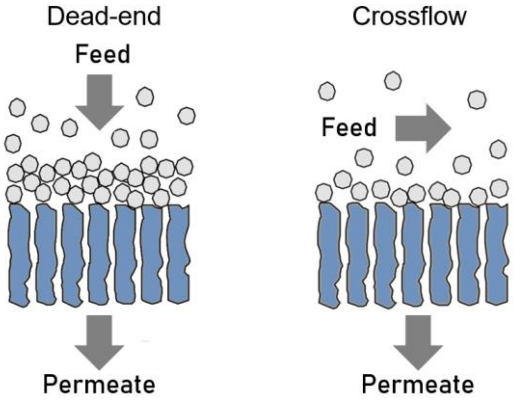

Figure 2.7. Representation of the two operating modes (adapted from Melin and Rautenbach, 2007).

In crossflow mode, there is a continuous flow parallel to the membrane, only a fraction of which is converted to permeate. The parallel flow induces shear forces on the membrane surface that removes part of the deposited material. This does not prevent the accumulation of suspended particles, but allows a certain degree of control over the cake layer formation (Pinnekamp and Friedrich, 2006). Ideally, a state of equilibrium is achieved when the rates of formation and removal of the cake layer are equal, making the permeate flow constant (sustainable flux). In reality, most systems require backwashing or some sort of cleaning after a filtration period. A disadvantage of this mode is the higher energy demand required by the pumps to generate the overflow (Melin and Rautenbach, 2007).

2.5. Fouling

The retention of species sets a major constraint on any membrane filtration process. The continuous accumulation of species at the membrane surface leads to an increase of the total hydraulic resistance, i.e. either a decrease of flux at constant pressure or an increase of pressure at constant flux (Figure 2.8). The phenomenon of deposition of material on the membrane surface and within the membrane structure is labeled fouling (Le-Clech et al., 2003; Judd, 2006). Another phenomenon responsible for flux decline is concentration polarization, intimately related to fouling and explained further ahead (Baker, 2004). Although inhibited to some extent, much attention is still given by industries and researchers to fouling and its control, as it remains as one of the major challenges for most membrane technologies (Meng et al., 2017).

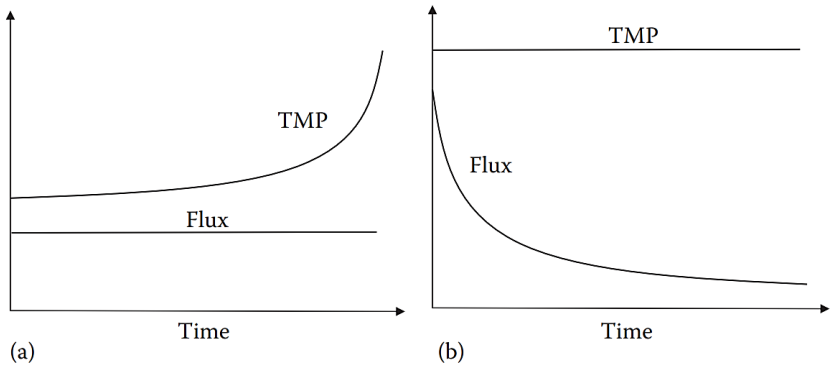

Figure 2.8. Fouling effects on flux and TMP at (a) constant flux and (b) constant TMP (Yoon, 2015).

No unified definition for fouling has been established. Authors use the term to cover most physicochemical and biological mechanisms of material deposition onto the membrane (Melin and Rautenbach, 2007). Fouling species (or foulants) can be macromolecules (proteins, polysaccharides), inorganics (scaling), colloids, particulate or biological matter (microorganisms) (Mulder, 1996). Fouling leads to filtration resistance that ultimately induces flux decline or pressure rise, which can be explained through the resistance in series model (Eq. 4). Considering no osmotic pressure effects:

$$J = \frac{TMP}{\eta \left(R_m + R_f\right)} \qquad \text{(Eq. 4)}$$

where η is the permeate viscosity, R_m the membrane hydraulic resistance and R_f the resistance due to fouling (and possibly concentration polarization) (Field et al., 1995). The hydraulic resistance of the membrane is generally considered fixed and can be determined with the pure water flux, as no fouling occurs. In this case, the flux is linearly proportional to the TMP (Judd and Jefferson, 2003). However, it has been shown that the “pure water” permeability is affected by the TMP and salt concentration. Pressure causes compaction of the membrane and additional resistance, specially in polymeric ones. Meanwhile, very low salt concentrations decrease the permeability, as the high zeta-potentials and thick double layers next to the membrane cause extra electro-viscous resistance to the flux (Huisman et al., 1997). On the other hand, the resistance at the interface depends on the amount of fouling, which increases with filtration time. Other resistances can be added to this model according to the specific mechanism that it aims to describe, such as resistance due to cake layer, reversible or irreversible fouling (Naessens et al., 2012). Figure 2.9 displays the behavior of the permeate flux in respect to the TMP considering the filtration of pure water and of a solution/dispersion.

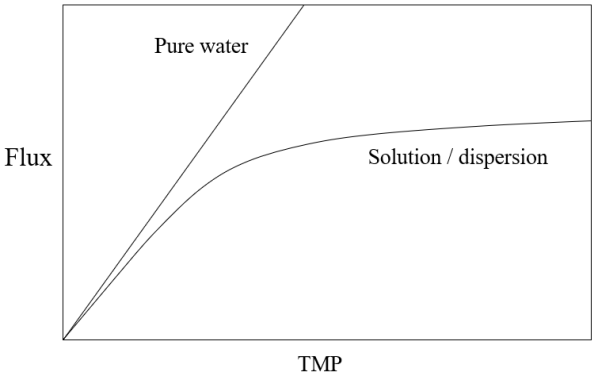

Figure 2.9. Effect of fouling on the permeate flux as function of TMP (adapted from Baker, 2004).

Fouling can be differentiated between reversible and irreversible. Normally, reversible fouling refers to material deposition that can be removed through physical cleaning, whereas irreversible fouling describes the accumulation of material only removable by chemical cleaning (Judd, 2006). However, this is subject of controversy, as no unified definition has been stablished. The most convenient terming is often applied according to how each system is operated and cleaned (Meng et al., 2009).

Different fouling mechanisms can be present according to the interactions between particles and the membrane (Figure 2.10) (Le-Clech et al., 2006; Baker, 2004; Visvanathan and Ben Aim, 1989):

a) Complete blocking (pore blocking): the particle blocks the pore entrance and stops the flow through it. It occurs when the diameter of the retained particle is in the range of the pore diameter.
b) Standard blocking (adsorption): particles can always be adsorbed by the membrane surface, even at zero TMP. When smaller than the pores, they can deposit on the internal pore walls (inner adsorption), leading to pore constriction and higher filtration resistance.
c) Intermediate blocking: some particles settle on each other while others deposit on the membrane, causing occlusion of pores by particle superimposition.
d) Cake layer: when the retained particles are larger than the pore size, they deposit on the membrane surface without blocking the pores, forming the so-called cake layer. The bigger the thickness of the cake layer, the more resistance to filtration it exhibits.
e) Gel-layer: solutes have much higher concentrations at the membrane surface than in the feed. At certain pressure values, macromolecular and colloidal solutes in close proximity can form a gel layer, which leads to a plateau in the flux (limiting flux) that cannot be exceeded.
f) Biofouling: microorganisms from the feed can lodge on the membrane surface and proliferate. They produce extracellular polymeric substances (EPS) to form a matrix in which they adhere, called biofilm. At a certain thickness, the biofilm causes extra resistance to filtration.

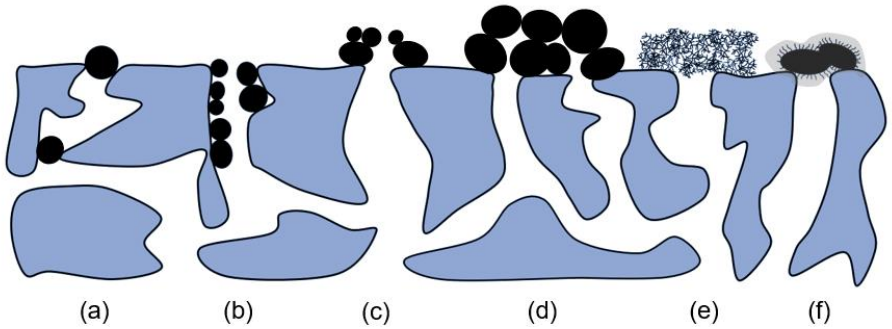

Figure 2.10. Fouling mechanisms in porous membranes: (a) complete blocking (internal and external), (b) standard blocking, (c) intermediate blocking, (d) cake layer, (e) gel-layer, (f) biofouling (adapted from Judd, 2006; Melin and Rautenbach, 2007).

Concentration polarization is the major reason behind fouling. It describes the occurrence of a concentration gradient at the boundary layer near the membrane surface during crossflow filtration. According to the thin film model, the boundary layer is a near-stagnant laminar film close the membrane surface, where the velocity of the liquid is virtually zero. This suggests that the only mode of transport through the thickness of the layer is diffusion. The boundary layer thickness is totally determined by the hydrodynamics of the system, with thinner films formed in more turbulent systems. Rejected components build up in this region, reaching concentrations way over the bulk value at a rate that increases exponentially with the flux. In pressure-driven processes, the water flux drags solutes in direction of the membrane while the concentration gradient pushes them back to the bulk through back-diffusion. At steady state operation, those forces balance each other and the concentration gradient becomes constant (Baker, 2004). Figure 2.11 portrays this phenomenon.

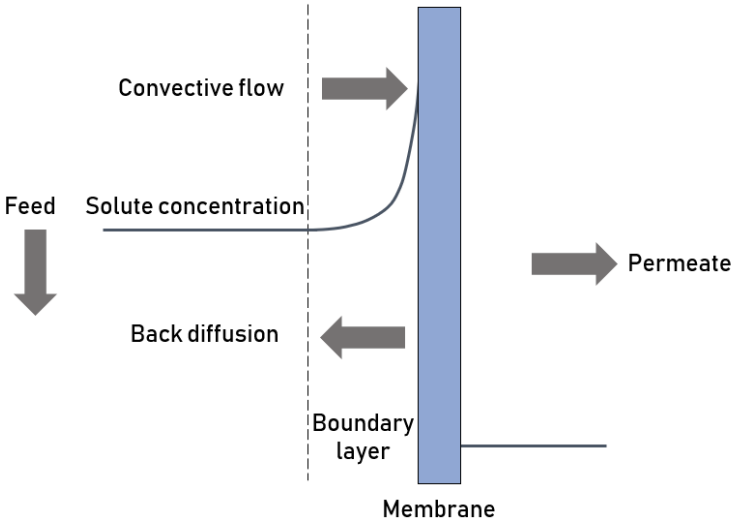

Figure 2.11. Representation of concentration polarization (adapted from Judd, 2006).

Nonetheless, it has been shown that back diffusion in the boundary layer is much more intense than that predicted by the thin film model, i.e. Brownian diffusion, which is referred as the “flux paradox”. Shear-induced diffusion and lateral migration are other back transport mechanisms that disperse particles away from the membrane and explain this effect (Li et al., 2000; Green and Belfort, 1980).

Concentration polarization affects essentially all membrane processes involving liquid phases. In RO and NF, it leads to an elevation of the osmotic pressure on the feed side, resulting in flux decline (Judd and Jefferson, 2003). In MF and UF, it can be very severe, as fluxes are large compared to diffusivities of the retained macromolecules and particles. The particles that build up at the interface are more prone to interact with each other and the membrane and promote fouling (Mulder, 1996).

2.6. Fouling control

Fouling control is essential for the success of membrane installations, as it aims at restoring the original flux obtained at the start of operation. Because of its complexity, many different methods are used in industries to prevent, control and remove fouling. First, membrane properties can play a role on how prone to fouling they are. As proteins and organics adsorb easily in hydrophobic surfaces, hydrophilic membranes should be preferred to avoid their adhesion. Then, pretreatment of the feed can also prevent a considerable amount of fouling in many systems, comprising pH adjustments, chlorination, adsorption onto active carbon and pre-filtration. Hydrodynamic conditions of the feed are also another decisive parameter. High flow velocities and turbulence (sometimes induced by

turbulence promoters) can lessen concentration polarization by reducing the boundary layer thickness and also help remove incipient fouling formation by scouring action. Cross flow velocities can also be provoked by air scouring in submerged membranes. Lastly and most importantly, cleaning routines are part of the essential maintenance of almost any membrane system. Two types of cleaning can be distinguished: physical (hydraulic or mechanical) and chemical (Mulder, 1996; Baker, 2004). Figure 2.12 presents the effect of a generic membrane cleaning on the flow at constant pressure.

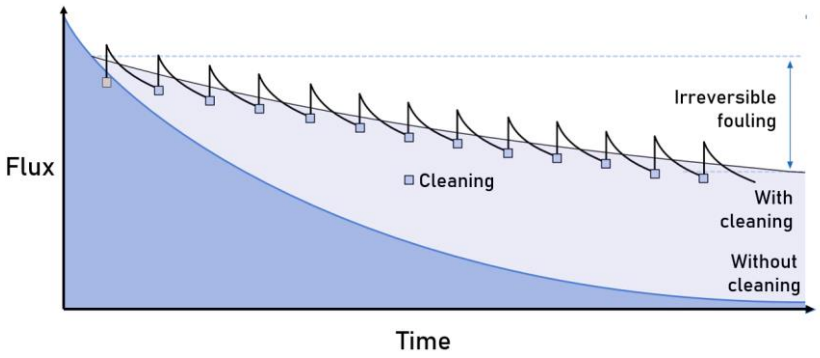

Figure 2.12. Effect of cleaning methods on the flow at constant pressure (adapted from Pinnekamp and Friedrich, 2006).

Hydraulic cleaning, also known as backwashing or backflushing, is a technique of physical cleaning in which permeate water is forced in the reverse direction through the membrane, lifting deposited materials from the surface. It must be done carefully to avoid membrane damage, being only used in modules that can withstand positive pressures in the permeate side, such as capillary and tubular. Whereas backwashing routines are advantageous to recover flux, they come at a cost, incurring in energy consumption, loss of product water and downtime (Judd and Jefferson, 2003; Baker, 2004).

Chemical cleaning is crucial to pressure-driven membrane processes. Purpose here is to remove foulants not removed during backwash and prevent future fouling. Many chemicals can be employed, acting for the dissolution of fouling agents, killing of microorganisms or complexation of species. Commonly applied chemicals include acids, alkali, detergents, complexing agents and disinfectants. Although having clear benefits, chemical cleaning is costly not only for the price of the agents themselves, but also for the disposal of the cleaning waste, shortening of the membrane lifetime, emptying of modules or tanks and downtime (Baker, 2004; Melin and Rautenbach, 2007).

Mechanical cleaning can be additionally executed. Submerged MBRs have been combined with scouring agents such as circulating granular media to remove cake layers (Meng et al., 2017). Else, sponge balls serve to gently scrap the membrane surface in tubular modules (Shim et al., 2008).

2.7. MBRs

Membrane bioreactor (MBR) is a term that describes a process where membranes are integrated within a biological reactor. Although also applied in different processes such as in bio-production, MBRs became universally known as a wastewater treatment method (Galinha et al., 2018). This biotreatment process removes suspended and dissolved organics from wastewater through biodegradation performed by living microorganisms. In MBRs, the membrane replaces the settling tank of the conventional activated sludge (CAS) system, retaining all biocatalyst and producing a final effluent with higher purity. Moreover, MBRs combine a more efficient biotreatment, smaller footprint due to less space required, reduced sludge production and better process reliability (Judd, 2006).

Aerobic (oxygen dependent) and anaerobic (oxygen independent) methods have been employed to treat domestic and industrial wastewater since the late nineteenth century. In such processes, microorganisms oxidate organic matter to derive energy and produce more biological cells, collectively called biomass. Organic matter is generally quantified as chemical or biochemical oxygen demand (COD or BOD), an indirect measurement of the oxygen required for oxidation of compounds. The other products generated during the digestion process can be H_2O, CO_2, CH_4 and inorganic nitrogen products, depending on the presence or absence of dissolved oxygen. In the CAS system, cells are supplied with oxygen through air bubbling. The cells aggregate into flocs due to the excretion of extracellular polymeric substances (EPS), remaining suspended in the medium – the mixed liquor. After the treatment, all biomass must be separated from the final effluent, which in CAS systems occurs by settling of the sludge in clarifiers. This clarification step is a limiting factor for the final effluent quality and total outlet flow rate. This is because the operation relies on the settling characteristic of the flocs, that depends on the residence time of the microorganisms (solid retention time, SRT), which in turn is coupled to the effluent hydraulic retention time (HRT). For this reason, CAS system commonly take up a lot of physical space (Metcalf & Eddy, 2003; Visvanathan and Ben Aim., 2000).

Membranes in MBRs overcome the issues related to clarifiers in CAS systems, not relying on the formation of microbial flocs. The operation is carried out using low-pressure MF or UF, with pore sizes ranging from 0.03 to 0.4 µm. Such pore size range enables total retention of flocs and nearly all suspended particles (individual microorganisms and inert solids), producing a highly purified effluent. Since all biomass is retained, MBRs can have very long SRT (up to infinite), regardless of the HRT, only dependent on the excess sludge purge rate. This allows higher biomass concentrations in the reactor, which increases the compactness of the system, apart from reducing total excess sludge production. Moreover, long SRT also favors slow growing organisms, such as nitrifying bacteria (Judd, 2015; Judd, 2006). The operating parameters HRT and SRT are defined in Eq. 5 and Eq. 6 below in terms of the reactor volume (V), the feedwater flow (F) and the purge volume per time (Galinha et al., 2018). Figure 2.13 displays a comparison between the CAS and MBR systems.

$$HRT = \frac{V}{F} \qquad \text{(Eq. 5)}$$

$$SRT = \frac{V}{Purge/time} \qquad \text{(Eq. 6)}$$

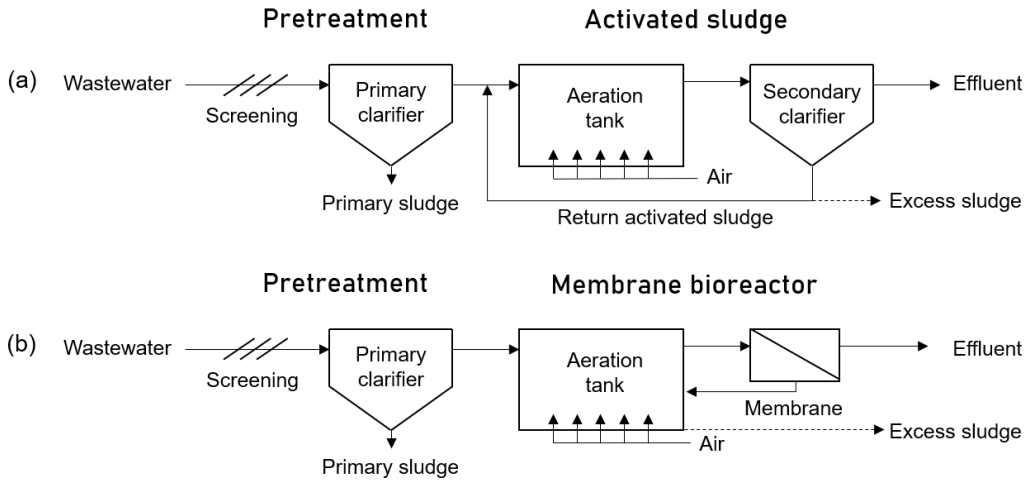

Figure 2.13. Typical wastewater treatment process schemes for the (a) conventional activated sludge (CAS) system and (b) membrane bioreactor (MBR) system (adapted from Ladewig and Al-Shaeli, 2016).

2.7.1. MBR configurations

Only crossflow filtration suits the separation of the activated sludge from wastewater by membranes. This is because the shear forces induced through the crossflow can control the cake layer formation and the occurrence of fouling. There are basically two possible MBR configurations: side-stream (or external) and submerged (or immersed), as shown in Figure 2.14 (Melin et al., 2006).

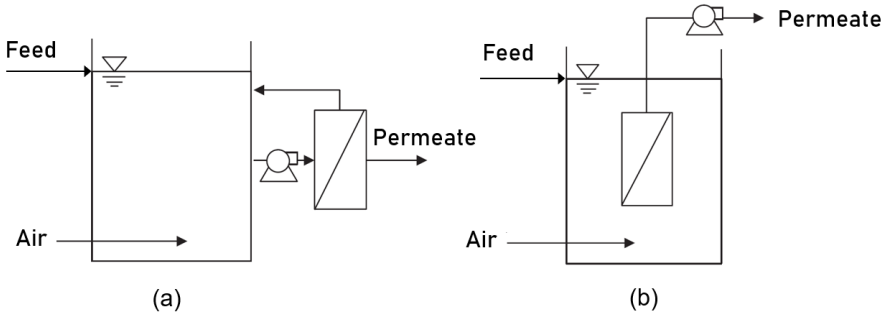

Figure 2.14. Scheme of MBR configurations: (a) side-stream and (b) submerged (adapted from Yoon, 2015).

Side-stream MBRs are commonly designed with tubular membranes. The mixed liquor – mixture of wastewater and biomass – is pumped into the modules in cross flow mode, with the retentate returning to the aeration tank (Pinnekamp and Friedrich, 2006). High crossflow velocities in the tubes ranging ensure fouling control and stable fluxes. However, there is a trade-off between maximizing the flux (by increasing the crossflow velocity and TMP) and restricting energy expenditure. Most often, side-stream MBRs are very energy intensive, operating at high fluxes (50 – 100 LMH) and TMPs of 3 – 6 bar, which leads to high fouling propensity. If developed, fouling in this configuration is more severe, as the high pressures cause compaction of the cake layer. Connecting modules in series is an attempt to draw as much permeate as possible, but longer channels lead to more pressure loss. In typical operating conditions, only 1 to 5 % of the pumped feed is recovered as permeate. Despite having clear advantages such as better module accessibility, easier maintenance and high reliability, the complex design of side-stream MBRs combined with their high capital and operating costs made them unpopular, remaining limited to some specific industrial uses (Judd, 2006; Yoon, 2015).

Submerged MBRs represent more than 99 % of all MBRs installed around the globe, being particularly successful for the aerobic treatment of domestic wastewaters. Reason for this is their lower energy demand: 0.1 – 0.2 kWh/m³ compared to 4 – 10 kWh/m³ in tubular modules, hence being the most economically viable for large-scale applications. Furthermore, the capital costs are much lower in this configuration since housed modules and high-pressure compatible plumbing are not a requirement. This allows investments in larger membrane areas, which in turn enables the operation at lower fluxes, which ultimately leads to a lower fouling potential. Usual flux values in submerged MBRs are of 15 to 35 LMH, with TMP as low as 50 to 500 mbar (Galinha et al., 2018; Yoon, 2015).

Membranes in submerged MBRs are basically configured as hollow fibers or flat sheets. Bundles of hollow fibers or panels of flat sheets are fit into open cassettes that are immersed in the mixed liquor. In both types, manufacture must be low cost, since the low flux operation demands large areas. Permeate extraction occurs under suction promoted by vacuum pumps, usually at constant flux. Common knowledge regards smaller pores (i.e., UF) as a safer barrier by rejecting smaller particles, despite having lower permeabilities than MF. UF also has the benefit of incurring more removable fouling, less likely to leave residual pore blocking or internal surface adsorption (Judd, 2006).

In a submerged MBR, crossflow is induced by air scouring (or air sparging). This method uses air bubbles to create an uprising intermittent two-phase flow (gas-liquid) along the membrane surface that creates tangential shear forces. This has proven to significantly improve the process performance by controlling fouling deposition and preventing channel clogging (Ladewig and Al-Shaeli, 2016). Besides, air scouring provides extra oxygen to microbes, keeps solids in suspension and improves external mass transfer conditions in the medium (Galinha et al., 2018).

K. Yamamoto and coworkers were the first to use direct membrane separation in activated sludge and take advantage of the existing biological aeration (Yamamoto et al., 1989). In the first designs, membranes were submerged directly in the aeration tank. However, maintenance procedures were difficult to perform in this setting. Consequently, a separate membrane tank in series with the aeration tank became a common solution (Figure 2.15). This also makes the system work like a plug flow reactor, where the aeration at the second stage helps oxidize contaminants not degraded at the first stage (Yoon, 2015). Many configurations with other compartments are possible, mostly used to achieve specific nutrient removal, like anoxic tanks to promote denitrification (Galinha et al., 2018).

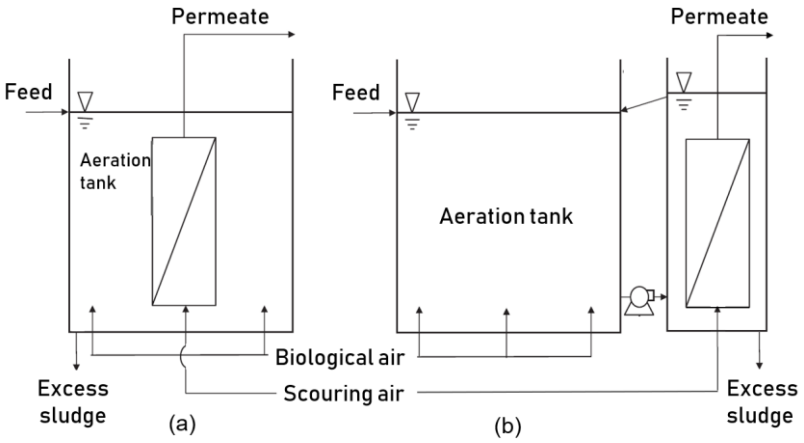

Figure 2.15. Submerged MBRs: (a) integrated and (b) separated membrane tank (adapted from Yoon, 2015).

The separate membrane tank emphasized the difference between biological air and scouring air. Maximizing oxygen transfer to the liquor requires high contact surface between phases, which is why fine air bubbles (2 – 5 mm in size) are employed as biological air. On the other hand, coarse bubbles (6 – 10 mm bubble size) are commonly recommended by manufacturers for scouring membranes, since they can induce higher turbulence and therefore shear stress (Judd, 2006). Nevertheless, conflicting results have arisen from studies (Yoon, 2015). Some of them showed that smaller bubbles are more effective for immersed flat sheets (Sofia et al., 2004), while others identified slug bubbling as a more effective and economic aeration mode (Wang et al., 2008). Although air scouring disrupts concentration polarization and fouling, the flux can only be improved up to a certain air flow threshold, above which operation is non-optimal (Cui et al., 2003).

2.7.2. Fouling in MBRs

Fouling is the most persistent problem in MBRs and remains the main obstacle for their widespread application. It reduces the process productivity, leads to higher energy consumption and demands frequent membrane cleaning or even replacement. Countless studies investigated the phenomenon in the last 20 years, but its complexity makes it a problem hard to overcome (Meng et al., 2017). Fouling is to be distinguished from clogging, which is the filling of the module channels with solidified sludge due to poor hydrodynamic conditions, commonly occurring in most MBR plants (Judd, 2006).

Many interconnecting factors influence the occurrence of fouling in MBRs, as portrayed in Figure 2.16. Aeration and cleaning are the main fouling control strategies. Operating parameters such as SRT, HRT, food to microorganism ratio (F/M) and dissolved oxygen (DO) do not influence fouling directly, but influence sludge properties that ultimately govern the generation of foulants (Meng et al., 2009).

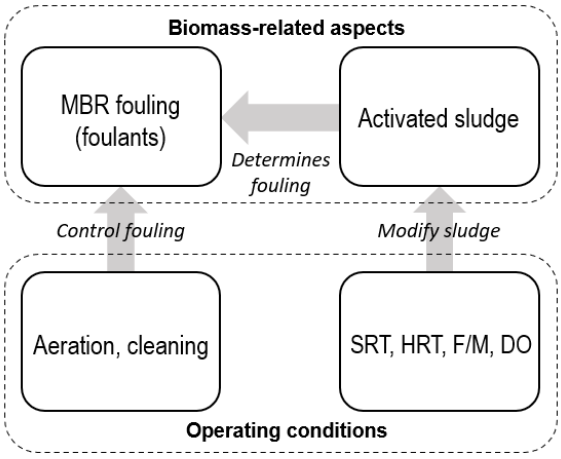

Figure 2.16. Factors affecting fouling in MBRs (adapted from Meng et al., 2009).

Fouling in MBRs is attributed mainly to small particles and macromolecules known as soluble microbial products (SMP) and extracellular polymeric substances (EPS), and not to the mixed liquor suspended solids (MLSS), as first thought. In fact, the concentration of MLSS – which are basically suspended microbial flocs – is a poor indicator of fouling potential as long as kept between 6 – 15 g/L. While EPS are the biopolymers that bind cell flocs, SMP are free biomolecules secreted by bacteria or debris of ruptured/hydrolyzed cells. A large portion of SMP is actually detached EPS (Yoon, 2015). Although the role of these substances in MBR fouling is not yet fully understood, fouling mechanisms have been proposed, including pore blocking, adhesion of foulants and gel layer formation. EPS and SMP also alter the sludge cake layer structure, raising its resistance several times (Lin et al., 2014). Biofilm formation in MBRs, also called bio-cake, is facilitated once SMP are deposited on the membrane surface. Small sludge flocs are typically the first colonizers. If attached, cells help increase even more the total EPS concentration at the surface, ensuring bio-cake stability (Meng et al., 2017).

Figure 2.17 depicts the spatial change in cake layer composition along time during an MBR operation. This change occurs as a result of permeate-induced deposition of SMP, release of biopolymers by dead cells and degradation of these biopolymers by live cells (Meng et al., 2017).

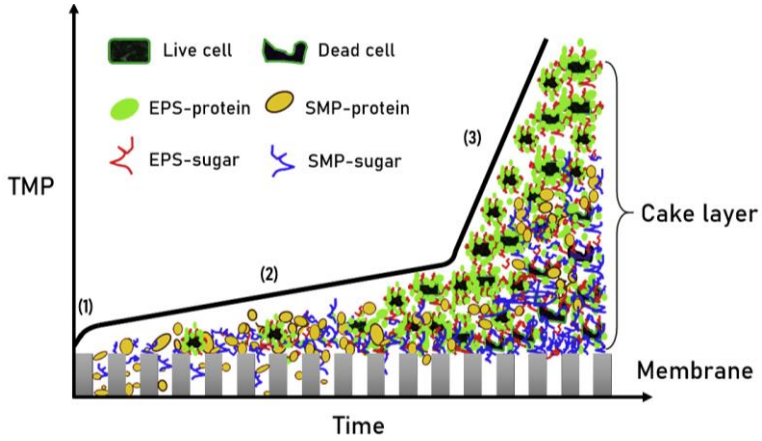

Figure 2.17. Spatial and temporal fouling development during TMP increase stages in MBR (Meng et al., 2017).

Figure 2.17 also shows the three stages of TMP increase during fouling development. The first stage, called conditioning fouling, takes place when biopolymers deposit onto the membrane surface and pores, being characterized by a short-term steep rise in the TMP. In stage 2, where slow fouling takes place, biomass particles attach to the surface already covered with SMP, causing a slow increase in TMP. Stage 3 is known as the TMP jump. According to the local flux effect model, inhomogeneous flux and air flow distributions make some regions more fouled than others, and the flux in less fouled areas increases locally very fast. This leads to exponential fouling in these areas, which is a self-accelerating effect that causes the TMP jump (Le-Clech et al., 2006; Meng et al., 2009).

Operating parameters as SRT, HRT and F/M are closely interconnected and affect fouling indirectly. F/M is a measurement of the amount of incoming food (COD/BOD) divided by the amount of biomass in the system (Le-Clech et al., 2006). High SRT (>20 days) – and therefore low F/M – has been shown to decrease fouling in MBRs (Drews, 2010). Some studies correlated the high SRT with lower SMP production, yet most observations pointed that the longer sludge age merely affects the quality/profile and not the quantity of SMP in the mixed liquor (Silva et al., 2016; Wu et al., 2013). Long SRTs also minimizes the undesirable production of excess sludge, but increases MLSS values. Above a certain threshold, MLSS can lead to clogging (Judd, 2006). Moreover, an excessive MLSS level also triggers fouling in MBRs, as it raises the liquor viscosity and blocks the bubbles' rising path, lowering the membrane scouring efficiency. Very high MLSS levels also lead to low oxygen transfer efficiencies (OTE), that in turn reduces DO and stress microorganisms (Yoon, 2015; Meng et al., 2017).

2.7.3. Fouling control in MBRs

Due to the complexity of fouling, a variety of approaches are necessary to decrease its impact. The main strategies include feedwater pretreatment, sustainable flux operation, aeration enhancement, modification of the mixed liquor and cleaning routines, briefly described ahead (Judd, 2006).

Feed pretreatment is crucial for MBRs to eliminate debris that might cause pore blocking or clogging. Clogging occurs almost inevitably, reducing treatment capacity, damaging membranes and incurring in onerous removal practices (The MBR Site, 2021a). Coarse screens used in CAS systems are insufficient for MBRs and must be narrowed down when plants are upgraded with MBRs (Judd, 2006).

Flux control in MBRs is key, since the fouling rate – a measure of the increase of pressure per time (Eq. 7) – has an exponential relation with the flux (Le-Clech et al., 2003). Limiting the flux reduces fouling but naturally provokes more demand for membrane area. The current trend is to operate submerged MBRs below the so-called critical (or sustainable) flux (Le-Clech et al., 2006).

$$Fouling\ rate = \frac{dTMP}{dt} \qquad \text{(Eq. 7)}$$

Different aeration strategies have been investigated to reduce fouling. Intermittent aeration is a promising method to control membrane fouling and simultaneously reduce energy consumption (Meng et al., 2017). Automatic aeration control is also of great interest for aeration optimization, enabling the system to react to fluctuations in the system's parameters (Meng et al., 2017).

Modification of the mixed liquor with additives is a technique that can improve filterability in MBRs. Additives such as cationic polyelectrolytes or alum act through adsorption of SMP, coagulation or crosslinking between floc/SMP (Drews, 2010). Adsorbents like powdered activated carbon or abrasive particles can also reduce fouling (Meng et al., 2017), but their use may be unpractical (Yoon, 2015).

Physical cleaning is a standard operating strategy to reduce fouling in MBRs. It includes backwashing and relaxation – when filtration is paused. Under relaxation, back transport of non-irreversibly attached foulants is boosted, especially when air scouring is maintained. (Le-Clech et al., 2006). Moreover, during the off time, the cake layer becomes looser and can be detached by the turbulence of the two-phase flow. Even with the pause, net fluxes are improved and further cleaning delayed. Relaxation typically takes 10 to 20 % of the cycle, commonly 9 min on and 1 min off. Meanwhile, the advantages of backwash are not so evident in MBRs, as it is poorly effective against the sticky cake layer formed by SMP/EPS. Nonetheless, it is still performed in many plants (Judd, 2006; Yoon, 2015).

Chemical cleaning is required when the effectiveness of physical procedures decreases. Chemically enhanced backwash, maintenance cleaning and intensive cleaning are applied with different frequencies: the first can be done daily, with chemicals being diluted in the backwashing water, the second on a weekly basis and helps reduce the frequency of the last, done once or twice a year, where the whole module stays immersed in cleaning solutions. Most employed chemicals are sodium hypochlorite and citric acid, with different protocols recommended by suppliers (Le-Clech et al., 2006).

2.7.4. Monitoring of MBRs

Monitoring of MBRs is directly linked to the attempt to reduce fouling and minimize operational costs. It involves the monitoring of the two processes: the biological reaction and the membrane filtration, which are closely related and whose performances affect one another (Galinha et al., 2018).

The biological process is often evaluated in terms of influent and effluent organic content. The most popular analytical method is the COD test, which takes only a few hours to complete, opposing to the 5 days required for BOD_5 analysis. MLSS is another important biological parameter, normally taken as the biomass concentration. However, one must bear in mind that not all suspended solids are viable or active microorganisms. Many other constituents may be analyzed to assess biological performance, such as ammonium, nitrate and phosphate (Galinha et al., 2018; Metcalf & Eddy, 2003).

The membrane operation uses the TMP as basic fouling indicator, as most MBRs operate under constant flux (Drews, 2010). Besides, the filterability of the mixed liquor is usually used to monitor fouling potential, with low values seen as an alert for upcoming fouling events. Various test methods have been developed, some of which are sludge filterability test (SFT), capillary suction time (CST) and sludge volume index (SVI) (Yoon, 2015; Alkmim et al., 2014). Although some studies correlated results to the fouling, others found inconsistent relations, proving them inadequate to forecast fouling behavior. Other approaches simulated MBR conditions more accurately, such as the Delft filtration and characterization method (DFCm) or the Berlin filtration method (BFM) (de la Torre et al., 2010).

2.7.5. Advantages and limitations of MBRs.

MBRs present clear advantages over traditional wastewater treatment methods, but display some limitations as well. The main advantages of MBRs are (The MBR Site, 2021; Judd, 2006):

- Excellent treated water quality, high enough to be discharged in sensitive receiving bodies.
- Absolute biomass retention, achieving almost complete effluent disinfection.
- High COD/BOD removal efficiency, due low F/M ratio
- Uncoupling of HRT and SRT.
- Small footprint (compactness) due to high levels of MLSS and no settling required.
- Low excess sludge production.

However, alongside these features, crucial issues hinder the performance and the broad diffusion of the technology. As the main shortcoming, fouling decreases the total yield of the processes, increases energy consumption and calls for frequent membrane cleaning routines and module replacement. Other limiting aspects are the occurrence of clogging in membrane channels, high energy demand and necessity of specialized workforce. In a survey conducted in 2015 among 186 MBR stakeholders (of which 85 % were practitioners rather than academics), when asked what the main technical issues in MBRs were, the participants ranked fouling, pretreatment, operator knowledge, energy demand and clogging as the most problematic aspects (Judd, 2015).

2.8. Critical flux and sustainable flux

The term “critical flux” has been vastly used in the membrane literature. It basically describes a limit for flux up to which no or negligible fouling occurs. The concept has been applied in many MF/UF systems, including MBRs, with the promise that subcritical operation would avoid flux reduction and frequent membrane cleaning. As it became relevant to determine the design flux, the idea evolved and gave origin to the notion of sustainable flux, which might find more utility in industries to identify the flux up to which the process is economically and environmentally viable (Bacchin et al., 2006).

2.8.1. Definitions

The first study to suggest a threshold for the flux below which “*fouling would not be expected to occur*” is attributed to Green and Belfort (1980). However, the definitions of critical flux (J_c) were only presented in the year of 1995. While studying transport phenomena close to the membrane surface, P. Bacchin and coworkers proposed a theoretical model for colloidal deposition considering surface interaction, diffusion and convection. It predicted a flux at which the repulsive forces are overcome, leading to coagulation on the surface. Below the critical flux, no fouling occurs (Bacchin et al., 1995).

The empirical definition was given in the same year by R. Field and colleagues, who defined critical flux as “*a flux below which a decline of flux with time does not occur; above it, fouling is observed*”. The authors stated that two forms of critical flux exist: the strong one and the weak one. The strong form corresponds to the flux at which the TMP deviates from the pure water one, being equivalent to a condition where no fouling occurs. The weak form assumes that on start-up a constant (and linear) flux-TMP relation is rapidly established and maintained until the critical flux is exceeded. The initial flux-TMP relation – below the one of pure water – occurs due to a rapid fouling (solute adsorption) at start-up (Field et al., 1995). The notions of strong and weak forms of critical flux prevailed as the main definitions in many studies (Bacchin et al., 2006). Both forms are portrayed in Figure 2.18.

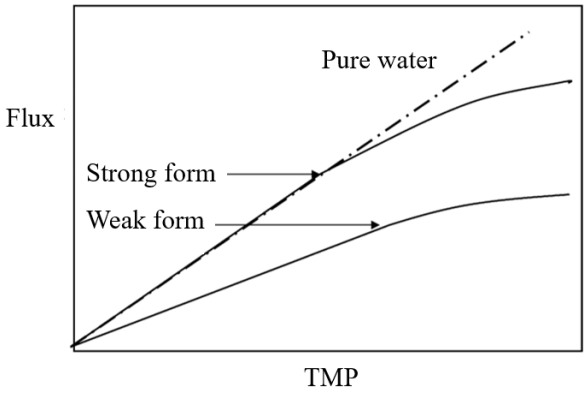

Figure 2.18. Strong and weak form of critical flux (adapted from Bacchin et al., 2006).

A decade later, Bacchin and Field reviewed the various concepts that had emerged for critical flux. Essentially, two categories of critical events can be distinguished. The first is the transition from a situation where the net flux of material towards the membrane is zero to a situation where this flux is positive. If adsorption is not present, this separates a complete non-deposition condition from a fouling condition and yields the definition of the *strong form of critical flux*. If adsorption occurs, this separates the steady-state adsorption condition from an additional deposition by convection and equates the *weak form of critical flux*. The second category of critical event is the transition between a system of dispersed solutes/particles close to the membrane to a system with aggregates on the membrane. This refers to an irreversible phase transition in the vicinity of the membrane, triggered above the critical flux, corresponding to the *critical flux for irreversibility*. (Bacchin et al., 2006).

The reason for the existence of a critical flux is connected to back transport mechanisms, namely surface interactions, lateral migration or shear induced diffusion. The former is of electrostatic nature, very relevant for colloids, while the latter two are hydrodynamic phenomena, significant for particles. These dispersive forces act in opposition to the drag force induced by the permeate flux (Figure 2.19) (Bacchin et al., 2006). First, diffusion at the boundary layer is much greater for particles above 1 μm than at first predicted by Brownian motion, being dependent on the amount of shear at the membrane, referred to as shear-induced diffusion (Romero and Davis, 1991). Brownian diffusion only becomes relevant for very small colloids (< 10 nm) (Bacchin et al., 2006). Then, lateral migration (or inertial lift) is a force that arises from the pressure difference that occurs when either side of a particle experiences a difference in fluid velocity (Green and Belfort, 1980). Lastly, surface interactions play a key role for particles under 10 μm, depending on the distance between entities, surface charge and ionic strength (Kwon and Vigneswaran, 1998). Surface interactions are also attributed to repulsion due to higher osmotic pressures closer to the membrane interface (Bacchin et al., 2006).

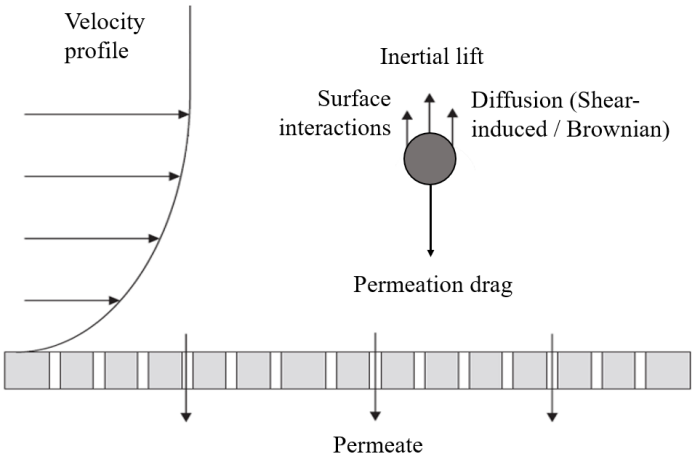

Figure 2.19. Balance of forces acting on a particle next to the membrane surface (adapted from Yoon, 2015).

Sustainable flux is in the meantime a fuzzy concept that emerged through analyses of the fouling rate, which is the rate of TMP rise in time when operating at constant flux. Operators realized that most systems did not allow operation at zero fouling, especially ones with complex feeds. In these cases, it is more appropriate to distinguish between low and high fouling rates. Significant differences have been found above and below certain defined fluxes that relate to the operational and economic sustainability of the whole process. The sustainable flux (J_{sus}) therefore would be the maximum flux that can be sustained for a defined period of time without incurring in a certain TMP rise, i.e. the need of membrane cleaning. It is not related to an event of criticality, but to subjective analyses of the application field and to the time scale of operation (Yoon, 2015; Bacchin et al., 2006).

2.8.2. Critical flux measurement

Different experimental methods have been used to estimate the critical flux. Most applied protocols involve flux-TMP measurements, more specifically flux-stepping methods. Other techniques are determination by mass balance and direct observation through the membrane (DOTM) (Drews, 2010).

Flux-step methods rely on constant flux stages that are incrementally increased one after the other, with the TMP being monitored. Every flux imposed should give a constant TMP below the critical flux. When the TMP increases inside a step, that flux is referred to as the critical flux. However, the total resistance (or permeability) should be calculated for every step to check if it has been constant, since a deviation might not always appear as a TMP rise within the step. If the flux-TMP relation until the critical flux is equal to the that of pure water, then the critical flux equates the strong form; if it differs, then the weak form. Above the critical flux, the TMP is expected to rise initially at a constant rate – the fouling rate – since the flux applied is constant. Yet, the fouling rate can increase during a step if the flux is maintained too long above the critical flux. Constant pressure tests are also a possibility: the decreasing fluxes lead to decreasing fouling rates and the system is self-regulated, achieving steady-state fluxes. However, this might not be feasible with complex suspensions or systems with unstable pressure. Moreover, pressure-step tests provide data useful for upscaling processes, but fail to deliver information on fouling rates as flux-step tests do (Le-Clech et al., 2006; Bacchin et al., 2006).

The hysteresis technique was widely used to determine critical flux, consisting of increasing flux steps followed by descending ones. Chen et al. (1997) used colloidal silica suspensions and reported a TMP hysteresis at the descending steps after the critical flux was exceeded, indicating that this flux (weak form) marked the transition from concentration polarization (and adsorption) to cake formation. The group also used intermittent steps (30 min on and 5 min off) to study cake removal at relaxation. Wu et al. (1999) used the procedure to identify the strong form as well as the weak form of critical flux for different model colloidal suspensions. The authors also proposed a second type of test, alternating increasing and decreasing steps and recording the TMP deviation for a same flux level. If deviation was zero, they presumed that no fouling had occurred at the higher step imposed.

Espinasse et al. (2002) developed further the alternative increasing/decreasing steps and proposed a method that allowed the quantification of fouling reversibility. The authors used constant pressure steps to determine the critical flux as well as to quantify irreversibility. Figure 2.20 illustrates their method: by comparing the steady-state fluxes of steps 1 and 4, one can deduce how reversible or not fouling caused in step 3 is (step 3 clearly shows fouling as it is far from the flux-pressure line of 1-2). For example, if the flux in step 4 is on point *a*, fouling is totally reversible; if the flux is on point *b*, fouling is 100 % irreversible. Therefore, their procedure makes it possible to ascribe a fraction of irreversibility to the fouling detected.

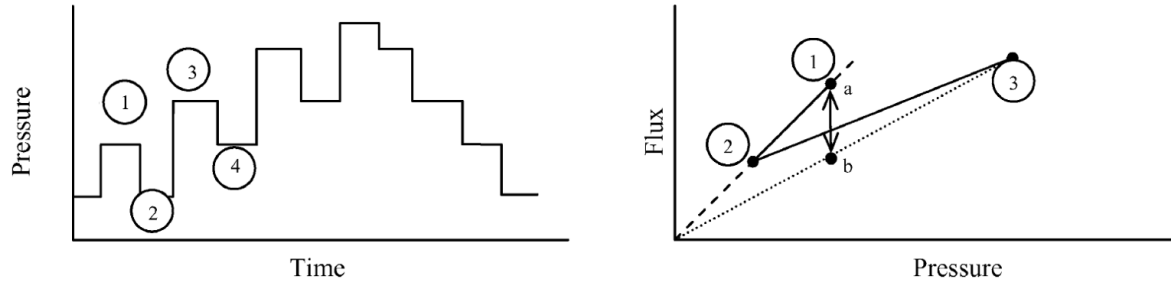

Figure 2.20. Pressure-step procedure used for determination of critical flux and its irreversibility (Espinasse et al., 2002).

The flux-step method was readily applied to MBRs. Bouhabila et al. (1998) used very long step durations (> 1 hour) in a submerged hollow fiber MBR and obtained increasing TMPs that later stabilized, which was associated with a sub-critical operation. Defrance and Jaffrin (1999) also obtained more or less stabilized TMPs below the critical flux. In disagreement with Field's definition, they admitted that fouling occurred even below the critical flux, but it changed dramatically when the critical flux was reached, leading to a steep TMP rise, possibly due to cake formation. This was supported by other studies (Tardieu et al., 1998; Madaeni et al., 1999; Cho and Fane, 2002).

Le-Clech et al. (2003) published a flux-step method that became standard for many MBR studies. Different step heights with different step durations were investigated for synthetic and real sewages, with a flux progression as shown in Figure 2.21. The rate of TMP increase dP/dt (the fouling rate) was calculated based on the difference between initial (30 s after start) and final TMPs for every step. In all trials, the fouling rate was never zero, even at low fluxes. Instead, the authors used other criteria to determine the critical flux. First, an arbitrary value for $dP/dt < 0.1$ mbar/min was used as threshold at which the flux causes "critical" fouling. Then, the critical point was suggested to be the flux after which dP/dt becomes exponential, as explained by the local flux model. Further, the critical flux was taken as the one after which the relation between the average TMP and the flux becomes nonlinear (similar to the weak form of critical flux). Another criterium for criticality was when $\Delta(dP/dt)/\Delta J$ – the second moment of TMP with respect to flux – displayed a discontinuity in its linear trend.

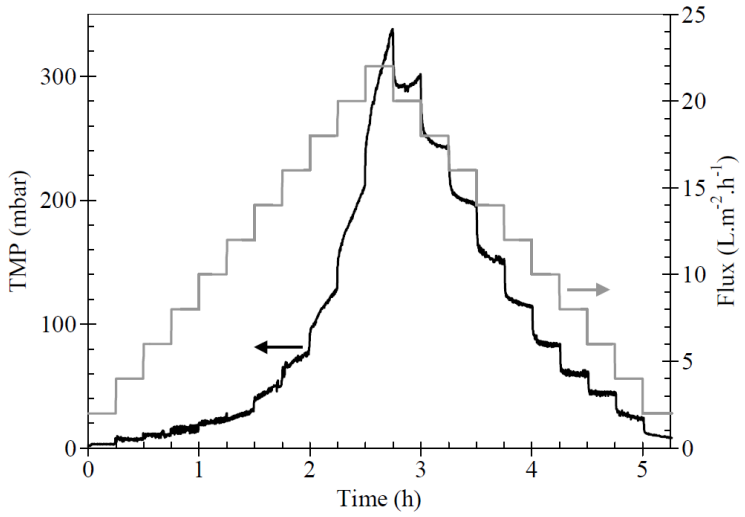

Figure 2.21. Flux-step method for critical flux determination using synthetic sewage (Le-Clech et al., 2003).

Zero fouling operation in MBRs is practically impossible, as it has been recognized by researchers. The critical flux in its strictest form is therefore unattainable. It has however been replaced by the flux at which changes in the system's behavior can be observed in flux-stepping experiments. The criteria for this change can be: (a) when dP/dt remains below an arbitrary limit, (b) when the average TMP and the flux remain on a linear trend, (c) when permeability decreases to e.g. 90 % of the initial one, (d) when dP/dt increases abruptly or (e) when $(dP/dt)/J$ displays a shift in trend (Drews, 2010; Guglielmi et al., 2007a; Diez et al., 2014). These criteria relate more to the idea of an acceptable permeability loss during operation, i.e. the notion of sustainable flux according to Bacchin et al. (2006). Other parameters relevant to the evaluation of flux-step trials are the initial TMP increase in respect to the previous step when a new flux is imposed (ΔTMP_0 or just ΔP_0) and the recovery factor ΔTMP, corresponding to the TMP difference between values at the same flux during descending and ascending phases (TMP hysteresis loop, as in Figure 2.22) (Guglielmi et al., 2007a).

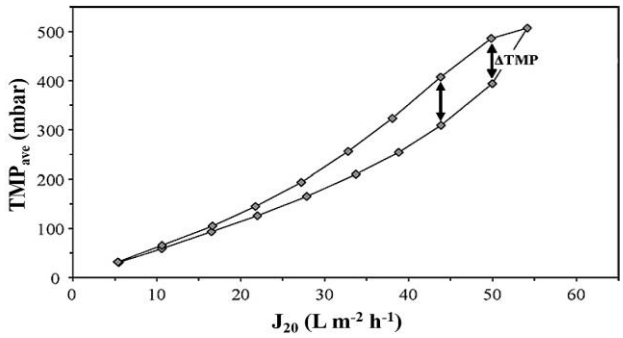

Figure 2.22. TMP hysteresis loop and recovery factor (Guglielmi et al., 2007a).

van der Marel et al. (2009) introduced an *improved flux-step method* to measure the irreversible fouling in MBRs. A reference low flux – at which fouling was supposed not to happen – was applied after each higher flux (Figure 2.23). This reference low flux was not an actual relaxation, but similarly promoted removal of reversible cake and allowed the measurement of a TMP at a reference level. Fouling caused at higher steps was considered reversible as long as the TMP at the lower steps stabilized at a same constant level. Otherwise, the critical flux for irreversibility had been exceeded. For instance, in Figure 2.23a, the critical flux for irreversibility was reached at the step F6. In practice, the authors computed the TMP rise for reference steps and used the criterium of 0.1 mbar/min.

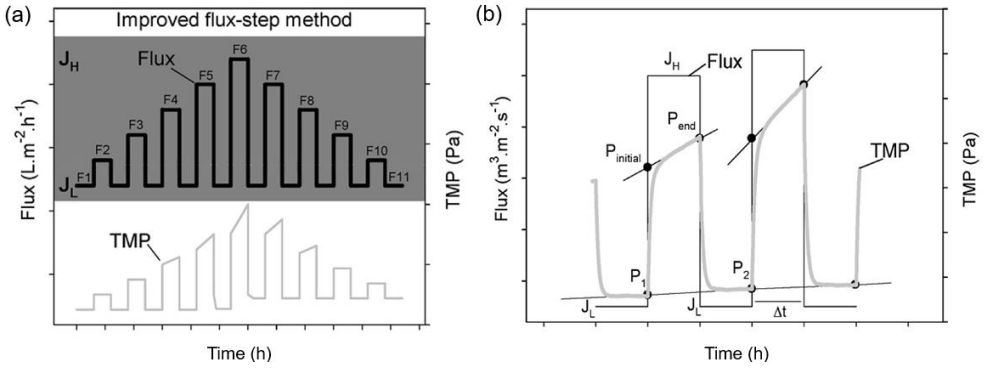

Figure 2.23. Improved flux-step method protocol and parameters (van der Marel et al., 2009).

van der Marel et al. (2009) also observed that the removal of fouling at the lower steps reduced the influence of fouling history. The common method yielded higher TMPs and fouling rate values, indicating that the fouling caused at initial steps had impact on the course of the trial. The fouling rate hysteresis for both methods thus differ, with the common method showing negative fouling rates at lower descending steps, as fouling removal in this phase is greater than supply (Figure 2.24).

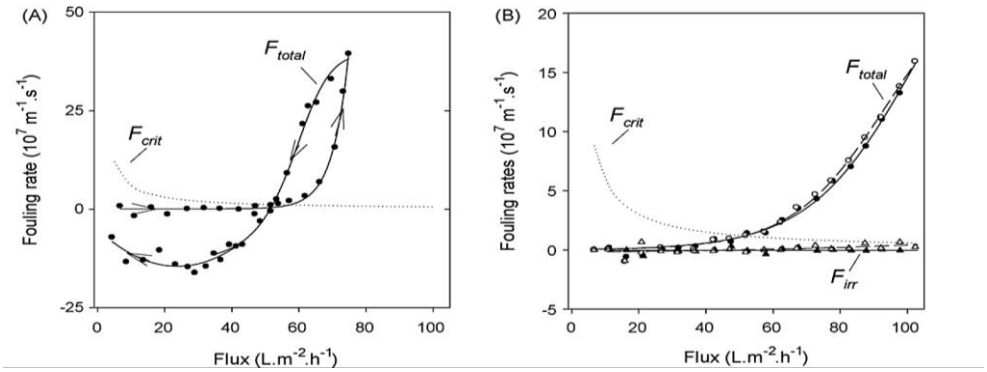

Figure 2.24. Fouling rate hysteresis for the (A) common and (B) improved flux-step methods (van der Marel et al., 2009).

de la Torre et al. (2009), inspired on the work by van der Marel et al., suggested another method mixing relaxation and lower steps. The group tested different protocols to evaluate irreversible fouling, aiming at bringing the method closer to real MBR filtration regimes, which includes total relaxation. Protocol II (Figure 2.25) operates with 5 min filtration and 2 min relaxation, while protocol III includes a 2 min low flux step of 5 LMH. The TMP at this pre-filtration step should give information about irreversible fouling remaining after relaxation. For total fouling, a limit of 0.2 mbar/min was chosen. However, de la Torre et al. did not detail results for the fouling during pre-steps. The average TMP for the common method was above the other two, but their fouling rates were unexpectedly comparable. The authors pointed out that, while the fouling history was cleaned by the pause, the sudden flux increment after the pause may have contributed to higher fouling. As observed by Chen et al. (1997), when high fluxes are imposed from zero, TMPs tend to be higher due to a chaotic cake formation.

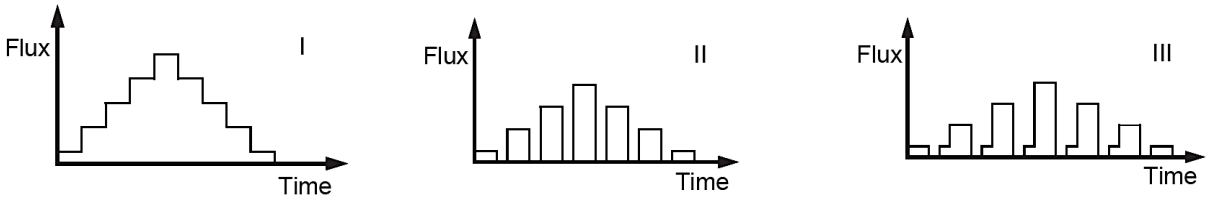

Figure 2.25. Flux-step methods: (I) common, (II) filtration/relaxation and (III) pre-step protocols (de la Torre et al., 2009).

Diez et al. (2014) proposed in their modified flux-step method for MBRs a pre-compression stage before each step to eliminate the effect of cake compression. Compressibility raises cake resistance and, as they claimed, can interfere in the TMP rise. However, results showed no difference in fouling rates between protocols with and without pre-compression (Figure 2.26a). In any case, their consideration zero cake compression allowed the determination of the critical flux by a model that distinguishes between deposition of non-settable fraction (free EPS and SMP) and sludge biosolids, as described ahead.

From Eq. 4, the fouling rate within a step can be described in terms of resistance increase rate:

$$\frac{dTMP}{dt} = \frac{d\left[J\eta\left(R_m + R_f\right)\right]}{dt} = J\eta\frac{dR_f}{dt} \qquad \text{(Eq. 8)}$$

Considering reversible fouling the main mechanism responsible for resistance increase and writing it in terms of the mass of material deposited per area (α) times its specific resistance (ω):

$$\frac{dR_f}{dt} = \frac{d(\alpha\omega)}{dt} = \alpha\frac{d\omega}{dt} + \omega\frac{d\alpha}{dt} \qquad \text{(Eq. 9)}$$

The change in specific resistance can be neglected once pre-compression is made or, as confirmed by the group, if compression and cake porosity reduction are insignificant. Below the critical flux, convection of non-settleable matter (macromolecules) is taken as the product of its concentration (c_{ns}) and the flux. Above the critical flux (J_c), biosolids from the mixed liquor deposit onto the membrane at a rate proportional to its concentration (c_{MLSS}) times the difference between the actual flux and the critical one. Attachment effectiveness factors (f_{ns} and f_{MLSS}) were considered as follows:

$$\frac{dR_f}{dt} = \alpha_{ns}\frac{d\omega_{ns}}{dt} = \alpha_{ns}c_{ns}f_{ns}J \qquad (J < J_c) \qquad \text{(Eq. 10)}$$

$$\frac{dR_f}{dt} = \alpha_{MLSS}\frac{d\omega_{MLSS}}{dt} = \alpha_{MLSS}c_{MLSS}f_{MLSS}(J - J_c) \qquad (J > J_c) \qquad \text{(Eq. 11)}$$

Fouling rates therefore can be written below and above the critical flux as:

$$\frac{dTMP}{dt} = \eta \alpha_{ns} c_{ns} f_{ns} J^2 \qquad (J < J_c) \qquad \text{(Eq. 12)}$$

$$\frac{dTMP}{dt} = \eta \alpha_{MLSS} c_{MLSS} f_{MLSS} (J - J_c) J \qquad (J > J_c) \qquad \text{(Eq. 13)}$$

By defining fouling capacities (k), and dividing the equation by J, linear expressions are obtained:

$$\frac{1}{J}\frac{dTMP}{dt} = k_{ns} J \qquad (J < J_c) \qquad \text{(Eq. 14)}$$

$$\frac{1}{J}\frac{dTMP}{dt} = k_{MLSS} (J - J_c) \qquad (J > J_c) \qquad \text{(Eq. 15)}$$

Hence, the representation of the *fouling rate normalized by the flux* should allow the identification of the critical flux, as portrayed in Figure 2.26b. This method resembles the determination through the shift in the second moment of TMP $\Delta(dP/dt)/\Delta J$, as described by Le-Clech et al. (2003).

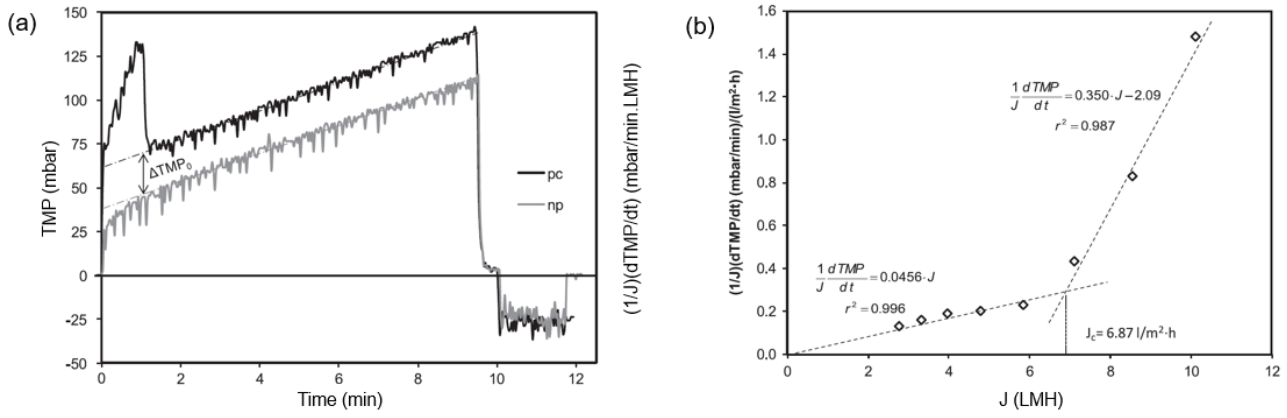

Figure 2.26. (a) TMP profiles showing similar fouling rates for a flux-step with pre-compression (pc) and without it (np) and (b) determination of the critical flux by plotting the fouling rate normalized by the flux (Diez et al., 2014).

Results for flux-step methods are strongly affected by experimental features. Suspension properties such as concentration and particle size are a decisive parameter. As expected, Higher MLSS levels have been related to lower critical flux values (Madaeni et al., 1999), a trend that was also observed for other suspensions (Kwon et al., 2000). The critical flux increases with increasing particle size, which can be explained by the lateral migration and surface interaction theories. This means that membrane fouling is generally more sensitive to deposition of smaller particles (Kwon et al., 2000). Hydrodynamic conditions also influence the critical flux, with higher crossflow velocities evidently yielding higher values for J_c (Espinasse et al., 2002). Le-Clech et al. (2003) showed that increasing step heights and step lengths led to lower critical fluxes, which was confirmed by Wu et al. (2008). This last study also showed that fouling history also shows a negative effect on the critical flux. Finally, membrane properties also play their role. Increasing pore sizes have led to lower critical flux values, but this could be due to local porosity effects (Wu et al., 1999). Higher porosity promotes a better distribution of the flux on the surface (lower local maximum flux) and thus increases the critical flux (Bacchin et al., 2006). Membrane materials affect surface charge and hydrophilicity, which, when increased, are expected to reduce fouling and increase critical fluxes. This effect, nonetheless, appears to be secondary when compared to morphological characteristics (Chan and Chen, 2004).

Mass Balance is another technique for determining the critical flux. By monitoring the concentration of particles in the outlet, Kwon et al. (2000) attributed any reduction in concentration to deposition (after adsorption was discounted) and thus measured the critical flux at which no deposition occurs. However, the critical flux measured by means of flux-TMP measurements was up to two times larger. Indeed, the mass balance technique does not provide information about reversibility of the deposit and is not applicable to macromolecules, which accumulate at the concentration polarization layer near the membrane. For this reason, mass balance is inadequate for MBRs (Bacchin et al., 2006).

Direct observation through the membrane (DOTM) is a visual technique that uses a microscope to observe cake formation on a transparent membrane. Li et al. (2000) used this method and show that the point of first deposition was not the point of a big change in resistant. Again, this technique only suits transparent membranes and larger size particles (around 10 μm), not fitting MBR purposes.

2.8.3. Sustainable flux measurement

Sustainable flux values can only be determined with long term trials. As pointed out by Bacchin et al. (2006), methods for measuring the critical flux only detect that the fouling rate is below a threshold of sensitivity for the set up and time scale used. Confirming this, Drews (2010) stated that it is more accurate to report an apparent sustainable flux when data are obtained from short term lab trials.

Howell et al. (2004) conducted long term trials above J_c with relaxation (15 min on, 15 s – 4 min off) and measured a *residual fouling rate*, defined as the increase in TMP at the beginning of each cycle. Figure 2.27 displays how the TMP at the MBR didn't restore its former value at the start of each step. According to their observations, residual fouling rates near the critical flux are proportional to the inverse of the gas flow velocity (u) and exponentially dependent on the flux applied, as Eq. 16 shows. This model can determine the TMP increase expected for a certain operation time, therefore enabling the establishment of a sustainability criterium, yet it does not predict when the TMP jump might occur.

$$\left(\frac{dTMP}{dt}\right)_{residual} = \frac{0.684}{u} e^{0.3893J} \qquad \text{(Eq. 16)}$$

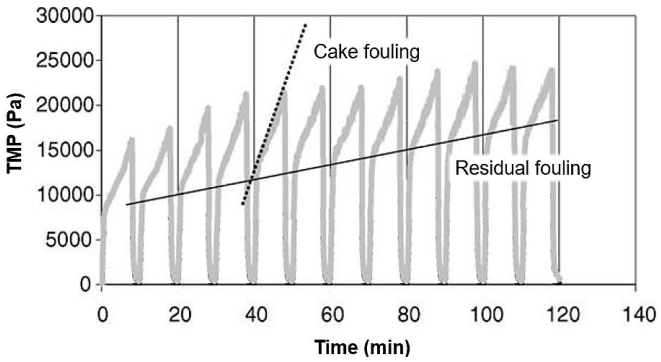

Figure 2.27. Intermittent permeation exhibiting cake and residual fouling rates (adapted from Howell et al., 2004).

The exponential relation between residual fouling rate and the flux had also been reported previously by Le-Clech et al. (2003), who observed residual fouling rates between 0.001 to 0.0007 mbar/min. Navaratna and Jegatheesan (2011) reported residual fouling rates below 0.002 mbar/min in an MBR employing a long flux-step protocol with relaxation, which they named *prolonged flux-step method*. Their routine included intermittent suction (12 min on, 3 min off) and step duration of 7 days, with the protocol taking over 60 days. Despite having the merit of imitating a real MBR operation, this method is rather unpractical as it demands a huge expense to carry out the long trial at constant conditions.

Another approach is to link the sustainable flux to the time needed until the event of TMP jump. Guglielmi et al. (2007a) determined the *time of sustainability* (t_{sus}) by performing long term trials and defining its value as the point where the TMP jump occurs. Figure 2.28 shows TMP profiles obtained when relaxation is employed for 1 every 10 min. When the applied flux was above the identified J_c of 30-31 LMH, t_{sus} was of 2 hours, while for fluxes below the critical one it ranged from ~ 90 to 200 h.

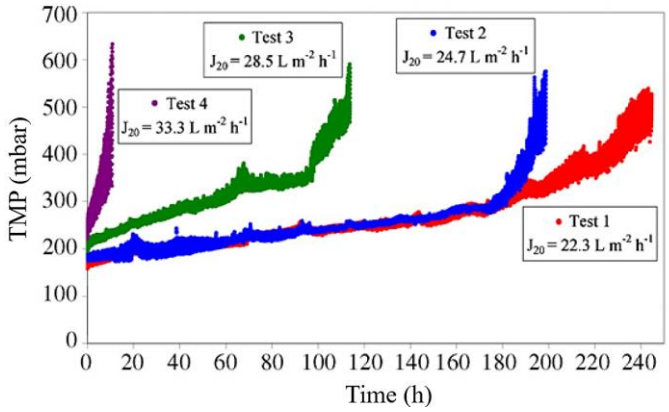

Figure 2.28. TMP profiles in long term trials showing TMP jumps at the sustainability time (Guglielmi et al., 2007a).

Guglielmi et al. (2007b) later proposed a model to predict when the TMP jump happens. It was based on the local flux concept, which explains the TMP jump: in nominally sub-critical operation, foulants (mainly EPS) cause a loss in permeable surface and increase the local flux above the critical one, leading to severe fouling (Cho and Fane, 2002). Guglielmi et al. (2007b) assumed that the kinetics of reduction in effective area is directly proportional to the flux of free EPS ($C_f Q$) and bound EPS ($C_b Q$):

$$\frac{dA}{dt} = -k(C_f Q)(C_b Q) \qquad \text{(Eq. 17)}$$

At constant total permeate flow, the local flux is inversely proportional to the effective permeable area:

$$Q = J(t)A(t) \qquad \text{(Eq. 18)}$$

Combining both expressions and integrating from the initial flux (J_0 at $t = 0$) up to the point where the local flux becomes critical (J_c at t_{sus}), Eq. 19 can be obtained:

$$t_{sus} = \frac{1}{kC_f C_b Q}\left(\frac{1}{J_0} - \frac{1}{J_c}\right) \qquad \text{(Eq. 19)}$$

To calibrate the parameters in the expression, two different experiments are required: a common flux-step method to determine J_c and a long term trial at sub-critical conditions to find the other constants. If an apparent resistance r is taken as the ratio between TMP and the flux during the first experiment, the slope of $1/TMP$ against t in the long term trial returns the constants looked for:

$$\frac{1}{TMP} = \frac{1}{TMP_0} - \left(\frac{kC_f C_b Q}{r}\right)t \qquad \text{(Eq. 20)}$$

Guglielmi et al. (2007b) predicted with good precision (errors below 15 %) the value obtained for t_{sus} in two reported long term trials. Navaratna and Jegatheesan (2011) also used the model and predicted sustainability times with errors below 10 %. Nevertheless, not all data fit the model and the studies recognized the susceptibility of the model to variabilities in MBR plants (MLSS levels, EPS content).

3. Context and Background

3.1. Context

This work results of a research and development project at MICRODYN-NADIR GmbH, a membrane manufacturer from Germany. With a wide range of products and over 50 years of activity, the company offers MF, UF, NF and RO solutions for different market segments. In its headquarters in Wiesbaden, MICRODYN-NADIR produces flat membranes and assembles the BIO-CEL® flat-sheet MBR series. In June 2021, the company was renamed MANN+HUMMEL Water & Fluid Solutions GmbH.

The inherent complexity of an MBR process makes it difficult to assess the performance of different membranes in lab-scale experiments. Laboratory tests normally struggle to operate under conditions that are similar to real MBR plants: they either lack real activated sludge media, operate with synthetic wastewater or even lack comparable geometries. For manufacturers such as MICRODYN-NADIR, this means that a potential new membrane can only be fully evaluated when a pilot plant with several square meters of membrane area is installed and operated, which is onerous for the production line.

The engineering team of the company hence recognized the need to develop a method that would operate in conditions as close as possible to a real MBR plant, but still possessing a small total area. This can be achieved by utilizing the resources available at the pilot unit that the company operates at the municipal wastewater treatment plant in Biebrich, Wiesbaden. The plant treats effluents from domestic sources and grants part of it to the mentioned pilot unit after primary treatment (screening). The small-scale method would not eliminate the necessity to evaluate a new product at pilot scale, but would indicate performance aspects such as fouling tendency by using actual activated sludge and domestic effluent. Smaller flat-sheet membranes can pass through the exact same procedure of XXXXXXXX and XXXXX used in the BIO-CEL® line, resulting in scaled-down membrane “envelopes”, with the advantage of enabling the use of membranes synthetized by casting in lab-scale.

The BIO-CEL® module (Figure 3.1) is produced with NADIR® UP150 membranes, a polyethersulfone (PES) ultrafiltration membrane. Although very well stablished in the MBR sector, the dynamics of the market force manufacturers to always seek improvement and develop new products with materials that outperform their current ones. For this reason, the development of a method to test novel membranes in an MBR environment is of high significance for MICRODYN-NADIR.

Figure 3.1. BIO-CEL® L-2 MBR module (MYCRODYN-NADIR, 2021).

3.2. Background

Previous efforts had already been carried out at the company in order to develop such a method. Among its achievements was the construction of a PVC frame to be submerged in the mixed liquor. The frame allows membrane XX × XX cm sheets to be affixed by the permeate collector and to be aerated by a perforated silicone air distributor (Figure 3.2).

Figure 3.2. PVC frame (a) unfinished (left) and completed (right), air distributor (b) and membrane sheet (c) (Wiese, 2021).

Trials conducted previously demonstrated several technical issues of the set up used at that time. First, it was verified that the peristaltic pump used for drawing permeate did not pump the same flowrate for a fixed rotation frequency at all configurations. The assumption that a peristaltic pump would deliver a constant flow for a certain frequency is not incorrect; peristaltic pumps are, after all, positive displacement pumps. This means that such a machine should deliver the same amount of liquid for each rotating cycle. However, the ideality of this behavior depends on the occlusion of the peristaltic pump. Occlusion is a measure of the amount of squeeze applied by the rollers to the tubing. Very high occlusion leads to more constant liquid displacement, but results in high flow pulsation and reduces the lifetime of the tubing (Treutel, 2009). Since the occlusion of the pump was not adjustable, calibration curves relating flow to rotation are inadequate, as displacement will differ according to the system's resistance. Fouling caused during trials clearly rose the resistance to suction, but the only solution at the time was to build calibration curves before and after each trial (Wiese, 2021).

Another problem in this earlier investigation was the difficulty to detect a constant pressure at rest. The pressure at rest relates to the size of the water column above or below the pressure transmitter. At this pressure, measured when filtration is stopped, the membrane does not experience any TMP difference, therefore equaling a state of equilibrium. This value should be always remain constant, since it relates to the geometry of the set up. However, trials had shown variable pressures at rest, even during the same trial. This was related to a possible accumulation of air in the suction hose, which would vary the vacuum sensed at the pressure transmitter. The installation of a deaerator tank was not able to help the system to overcome this issue, instead made the pressure more unstable. The problem was partially controlled when a shorter hose was used to connect the membrane to the pump, but instabilities were still observed in trials after this change (Wiese, 2021).

Generally, these trials laid the groundwork for the present project by constructing the architecture of the test rig and identifying its main issues. Nevertheless, the study lacked exhaustive test samples to deliver reproducible results for critical and sustainable fluxes as a means to compare membranes.

4. Materials and Methods

This section describes the set of materials, media, equipment, analytical techniques and methods used for the development of the work. At the end, the run of trials with varying parameters is listed.

4.1. Membranes

All membranes used in the experiments were produced with the same procedure and format. First, the production line casts the film on a non-woven polypropylene paper and then laminates the sheets with the spacer fabric. Squares of XX × XX cm were cut and sealed with ultrasonic sealing at all sides. A round hole was cut at the middle to allow the suction of permeate through a PVC permeate collector. XXXXXXX were additionally glued to the sides to stiffen the structure of the sheet, making its total area equal to XXX m². Figure 4.1 displays a sheet and the collector used.

Figure 4.1. Membrane sheet format used for trials and PVC permeate collector.

NADIR® UP150 membranes were used for almost all experiments. Made of PES, this UF membrane has a nominal MWCO of 150 kDa, nominal pore size of 0.04 µm and permeability above 285 LMH/bar (MICRODYN-NADIR, 2021a; 2021b). For the sake of comparison and validation of the method, another UF membrane made of PVDF (polyvinylidene fluoride) was used for later trials. This product is still in development, with pore size estimated at XXXX µm and permeability around XXX LMH/bar.

4.2. Media

Deionized water was the first medium used to assess the filtration performance of the set up. Next, bentonite suspensions were employed. Bentonite is a type of clay with particles bigger than the pores in UF, so that only cake layer formation is expected to occur. Bentonite (CERATOSIL®, from Clariant) was magnetically mixed for X hours with water to produce a masterbatch. The final desired concentration for the test was of XX g/L, calculated considering the XX % water content of the clay.

Activated sludge is currently used in the pilot unit at the wastewater treatment plant in Biebrich. After screening, domestic sewage is diverted to the unit. The pilot operates with two tanks: the aeration tank and the membrane tank. The aeration tank has around XX m³ of volume and is equipped with five aerators. Incoming effluent is fed into the aeration tank every time a level sensor indicates that the level is below a defined threshold. The mixed liquor is constantly pumped to the membrane tank, with X m³ of volume, from where it overflows back to aeration tank. The membrane tank lodges the membrane module currently being tested in the pilot by the company. The module carries its own aeration distributor. Permeate is drawn by a lobe pump at a 9 min on 1 min off cycle.

Figure 4.2. Schematic representation of the pilot unit coupled with the test rig used during trials.

The test rig used for method development was installed as shown in Figure 4.2, with the PVC frame submerged directly into the aeration tank. Aeration was supplied separately to the submerged set up. Since the membrane test rig was coupled to the pilot unit, many characteristics of the medium such as HRT and SRT were actually related to the operation of the pilot itself. The pairing of the two experimental set ups also leads to other issues, such as the influence of the tank's turbulence on the liquid flow around the tested membrane or the fluctuations of level in the aeration tank. These issues and their impact on the results are discussed in more detail further ahead.

4.3. Equipment

The pump used for drawing the permeate was a peristaltic pump XXXX (XXXX), with a pump head equipped with 4 rollers. The pressure transmitter was a XXXXXXXXXXX model (XXXXXXXXXXX). The flowmeter chosen was a XXXX model (XXXXX), a sensor that is externally attached to the hose and uses ultrasound to measure the liquid velocity. Temperature was measured with a digital temperature sensor (unknown manufacturer). All sensors were integrated with an EtherCAT coupler XXXXXX (XXXXX), therefore working as transmitters, with signals sent to a laptop (HP). Through the software XXXXXX all data could be graphically live visualized. Trials were programmed in a text file, whose execution generated a data file. The program also supported a feedback control system between the flowmeter and the pump to assure that the desired flowrate was being drawn. Figure 4.3 depicts a simple P&ID diagram for the test rig with the integrated sensors.

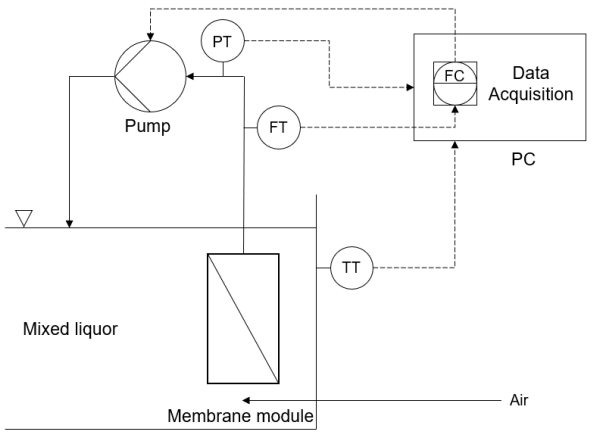

Figure 4.3. P&ID diagram of the test rig. PT, FT and TT are the pressure, flow and temperature transmitters, respectively.

4.4. Analytical methods

Sludge, permeate and influent parameters were monitored at least once a week during the execution of trials. The sludge parameters reported in this work are MLSS and CST. The COD of influent and effluent is also reported in order to assess the performance efficiency of the whole reactor.

MLSS represented the solids after drying a sample of filtered solids at 105 °C. A 50 mL of sludge sample is poured into a (pre-dried and pre-weighed) filter paper (Rotilabo 115A). After filtration of the sample under slight vacuum, the filter covered in sludge is put to dry in a analytical humidity scale. The difference in weights of the filter represents the amount of solids in the sample (APHA, 2017).

CST is measured with a filtration apparatus coupled with an automatic timer. Sludge is poured into a small reservoir, resting on a filter paper. Under the influence of the capillary suction of the paper, filtrate is drawn out of the sludge to saturate progressively a greater area of paper, causing the liquid front to advance outwards from the center. The rate at which water permeates through the filter paper varies depending on the condition of the sludge and the filterability of the cake formed on the filter paper. The CST is obtained from two electrodes placed at a standard distance. The time for the water front to pass between these two electrodes constitutes the CST (APHA, 2017).

COD was assessed using a test kit (HACH) for low range (1 – 60 mg/L COD). The test uses the reactor digestion method, where the vial with sample stays for 2 hours at 148 °C in the reactor and then has its COD assessed by a DR1900 spectrophotometer (HACH, 2021).

4.5. Testing protocols

Different protocols were adopted for the tests in order to evaluate the critical and sustainable fluxes. These protocols were named methods A, B, C and D, explained ahead in detail.

4.5.1. Method A

Method A was based on the original flux step method from Le-Clech et al. (2003), but with the inclusion of a relaxation phase (or pause) between steps, as described by de la Torre et al. (2009). This aims at bringing the method closer to a real submerged MBR operation. During relaxation, air scouring removes reversible fouling, allowing a flux step to be evaluated without the influence of (reversible) fouling caused in the previous step. The cycle consisted of 9 min of filtration and 1 min of pause. Steps started at 6 LMH, increased with a step height of 6 LMH up to 66 LMH and then descended again to 6 LMH, with total duration of 3.5 h. Figure 4.4 illustrates the course of the proposed protocol.

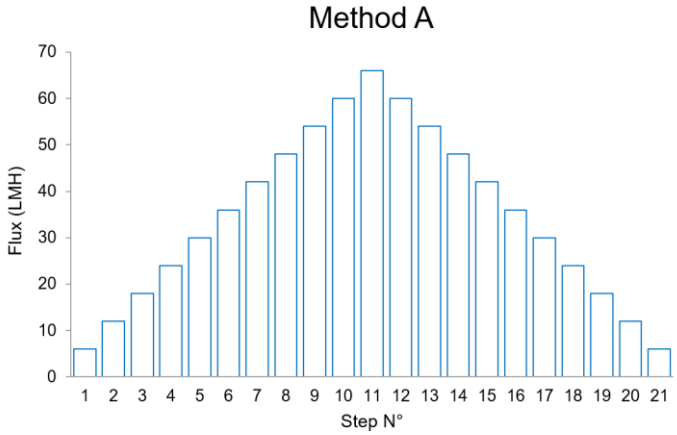

Figure 4.4. Representation of method A.

To evaluate the TMP rise within the step (fouling rate), two procedures were compared. The “slope” procedure calculated the slope of all TMP data in the step, excluding the first 60 s (stabilization time). The “end – start” procedure subtracted the average of the first 60 s (excluding the stabilization time) from the average of the last 60 s of the step, dividing the result by 7 min (time between the averages).

4.5.2. Method B

Method B was based on the improved method from van der Marel et al. (2009), which includes a lower intermediate step, called reference step, at which fouling supposedly does not take place. However, here relaxation between all steps was introduced, similarly to protocol III in Figure 2.25. The goal of introducing a low reference flux between the steps was to observe an increase in its TMP as a sign of irreversible fouling caused at the previous higher step. The cycle was kept as 9 min on, 1 min off, from 6 to 66 LMH, lasting 6.5 h. The reference step was defined at 6 LMH (Figure 4.5).

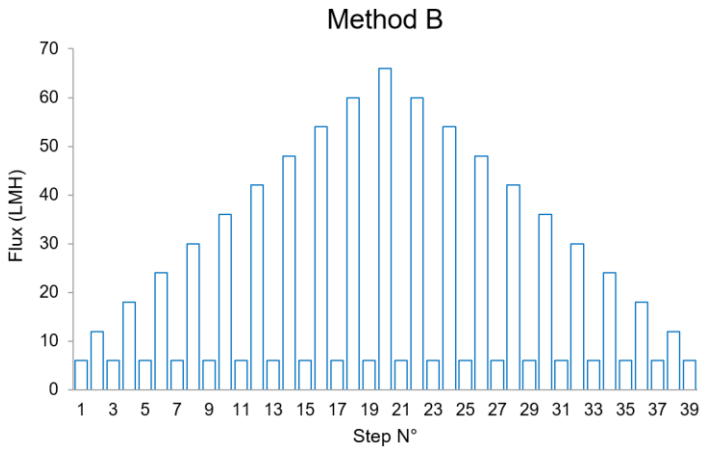

Figure 4.5. Representation of method B.

The fouling rate within a higher step must be differentiated from the fouling between reference steps. *Total fouling* describes fouling during a higher step, using the two procedures defined for method A. *Irreversible fouling* is the increase of TMP of reference steps in time. Here two procedures were used. The first calculated the average of the whole reference step (excluding the 60 s of stabilization) and subtracted it from the average of the next reference step, called “average – average”. The second procedure subtracted the average final TMP value of a refence step (average of the last 60 s) from the average final TMP of the following step, called “end – end”, similarly to van der Marel et al. (2009). The time considered for the fouling rate is the 9 min of the higher step, since the irreversible fouling perceived by these procedures is theoretically caused during the higher step. After observing that these two procedures did not yield reproducible results, another attempt was to plot the average TMP values of reference steps to obtain a curve with a certain slope that could then be interpreted.

4.5.3. Method C

Method C was built to evaluate the residual fouling rate at each flux. *Residual fouling*, as described in Figure 2.27, represents the slow increase of initial TMP at constant flux during intermittent operation (Howell et al., 2004), therefore differing from irreversible fouling as defined by van der Marel (2009). Inspired by Navaratna and Jegatheesan (2011), Method C used the values of Method A (6 to 66 LMH, 9 min on and 1 min off) and executed each step 7 times, with total duration of 24.5 hours (Figure 4.6).

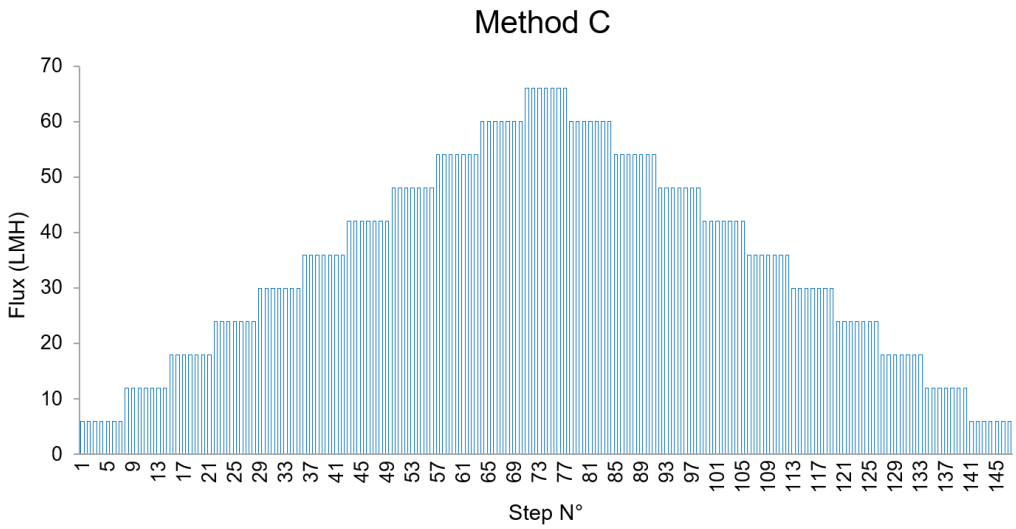

Figure 4.6. Representation of method C.

For all steps, the initial TMP was determined (average of the 60 s after stabilization time). Residual fouling was similarly assessed by the “slope” procedure and by the “end – start” procedure, the latter only considering the first and last initial TMP values of the block and the time between them (60 min).

4.5.4. Method D

After a few trails, it became clear that method C lacked reproducibility, apparently due to small number of repetitions of each step. To increase the total size of each block, only 5 flux values were chosen: 12, 24, 36, 48 and 60 LMH. Each step was executed a total of 21 times, following a pause of 30 min. The introduction of the pause had the purpose of letting aeration remove all removable fouling so that fouling caused at a certain flux level would have less influence on the following block. Furthermore, the descending phase was also dismissed in method D, since it was observed in method C that lower blocks had similar fouling rates compared to neighboring higher ones while descending. Figure 4.7 portrays the routine proposed for method D, which takes a total time of 19.5 hours to complete.

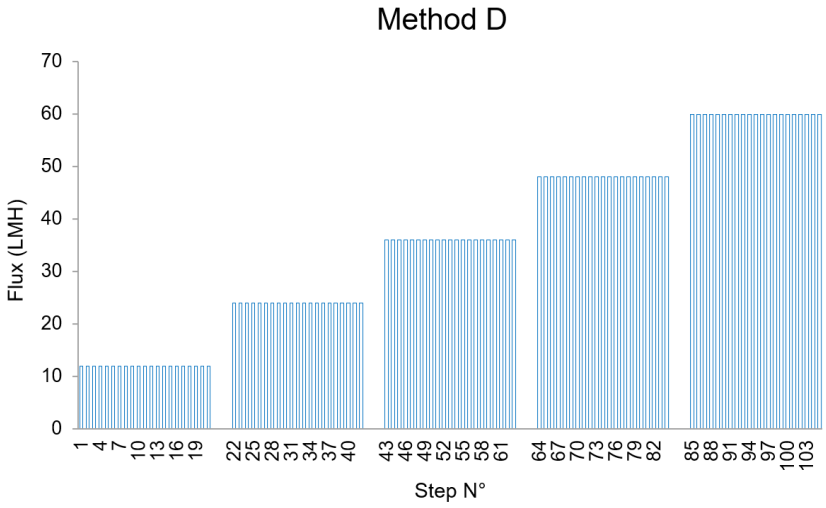

Figure 4.7. Representation of method D.

The evaluation of residual fouling rate was identical to method C: average initial TMP of steps were calculated and the “slope” together with the “end – start” procedures were applied for each step-block.

4.6. Temperature and pressure corrections

Results for permeability were normalized to a standard temperature of 20 °C (Eq. 21). This aims at correcting flux variations due to changes in viscosity, although it has been observed that only viscosity correction does not explain completely flux variations with temperature (Judd, 2006). The same equation can be applied for the normalization of the flux, in case this parameter is to be reported. Evidently, this correction should only be used once; either for the permeability or for the flux.

$$K_{20\,°C} = K_T \times 1.024^{(20-T)} \quad \text{(Eq. 21)}$$

The pressure at rest must be measured and discounted from the raw values obtained for the pressure. This was done by carrying out filtration and, after ensuring the hose suction side was free from air, ceasing the flow. The value of the pressure read by the transmitter relates to the water column below (or above) the device and corresponds to a zero TMP experienced by the membrane.

Moreover, also the pressure loss must be subtracted from the pressure readings. The pressure loss is the pressure lost due to friction between the liquid and the walls of the tubing, increasing at higher flow velocities. It was measured with the suction hose detached from the membrane, pulling water from a bucket. After subtracting the pressure at rest for the system, a calibration curve allowed the establishment of a relation between the flow in mL/min and the pressure loss. By this manner, Eq. 22 was applied for every pressure data point considering the reading of the flowmeter.

$$TMP = |P_{read}| - |P_{at\ rest}| - \left|P_{loss,(Q)}\right| \quad \text{(Eq. 22)}$$

4.7. Trial series

Corresponding to the three media used in the investigation, three trial series were developed. Trials in water and with bentonite suspension used method A, B and C, while trials in sludge included all four methods and additionally long term trials. Long term trials consisted of the repetition of the cycle (9 min filtration and 1 min relaxation) at a fixed defined flux during 1 – 2 days . The purpose here was to correlate the sustainable time with residual fouling rate obtained from methods C and D. Table 4.1 contains the number of repetitions of each method in each medium, detailed in the results section.

Table 4.1. Trials series and corresponding repetitions for each method.

Series	Method	Repetitions
Water	A	7
	B	5
	C	2
Bentonite	A	3
	B	3
	C	2
Sludge	A	23
	B	11
	C	2
	D	12
	Long term	2

4.8. Statistical analysis

Statistical analysis of data was carried out using student's t-test for the difference of the means, indicated in the text as p-value smaller than the significance value ($p < \alpha$), defined at $\alpha = 0.05$.

5. Pre-trials

Several experiments were carried out at the initial stage of the work in order to investigate the behavior of the system. Using pure water, different conditions and configurations were tested bearing in mind the issues that had been found previously. Initially, the pump was tested alone at different heights in respect to the water level in the tank, namely - 40, + 45 and + 230 cm, as shown in Figure 5.1.

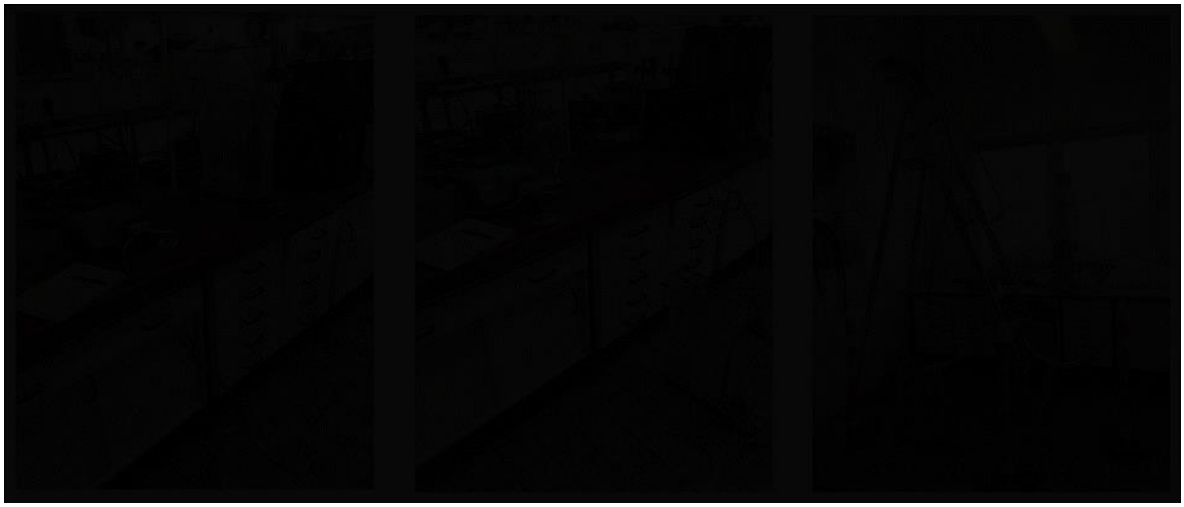

Figure 5.1. Pre-trials with the pump at varying height differences.

The results clearly indicated that the pump drew lower flowrates in those configurations with higher resistance. Then the membrane sheet was attached to the suction hose and flowrates compared. Figure 5.2 shows that the membrane represents an even greater resistance to the pump. However, the pump was still able to pump water at the setting similar to the pilot unit (height of + 230 cm).

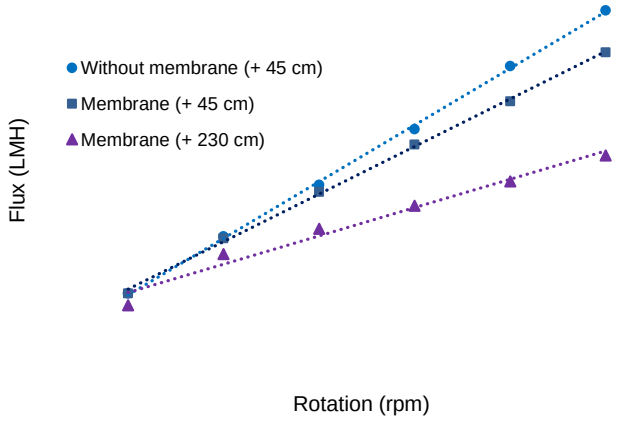

Figure 5.2. Differences in flux/flow for set ups without membrane and with it at varying height differences.

These observations emphasized the need of a flowmeter. The occurrence of fouling during a trial in sludge would also contribute to an increase in total resistance. Therefore, to guarantee constant flux operation, a closed-loop feedback system was necessary, so that the pump would adjust its rotation speed according to the course of the test. Real MBRs rarely operate with feedback systems, mainly because the pumps employed (typically lobe or gear) are less sensitive to small resistance increases.

While the chosen flowmeter was ordered, membrane filtration trials had the flux evaluated in terms of mass of water (weighing scale XXXX XXXXXXXXXX) collected at a certain chronometered time. Series of trials had setting with and without air bubbles, with and without height difference, using a protocol that would later become methods A and C. The goal here was to observe if the pump managed to work with air bubbles coming at the suction side and, further, to examine how to establish a constant pressure at rest during pauses. Figure 5.3 displays the set up for these configurations.

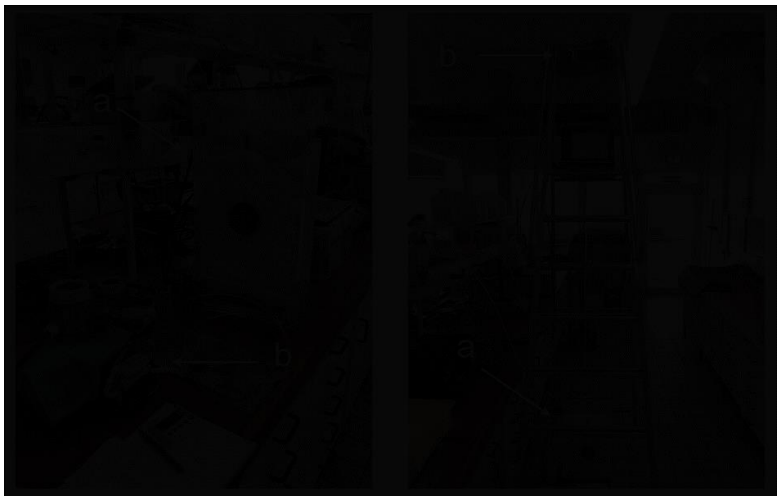

Figure 5.3. Set-up built in the lab for initial membrane filtration trials: without (left) and with (right) height difference. Membrane filtration tank (a) and peristaltic pump (b) are indicated.

It became clear that air bubbles always appear at the suction side. This can be explained by the fact that the water in the tank is saturated with air. The lower pressure at the suction side lowers the solubility of the dissolved gas, which then agglomerates into bubbles. The accumulation of gas before the pressure transmitter interrupts the water column and prevents the establishment of a constant pressure at rest. For this reason, it was defined that the suction hose should have no high sections before the pump; the pump must to be at the highest point (as in right side of Figure 5.3).

The integration of the flowmeter in the system required many adaptations in the software used so far. At first, the flowmeter was used to investigate the pulsation of the flow. Peristaltic pumps are known for producing pulsating flows that become more steady the more rollers the pump head has. At very short response times (which is the time the sensor takes to react and report each flowrate data point), the flowmeter showed evidence of this, as shown in Figure 5.4.

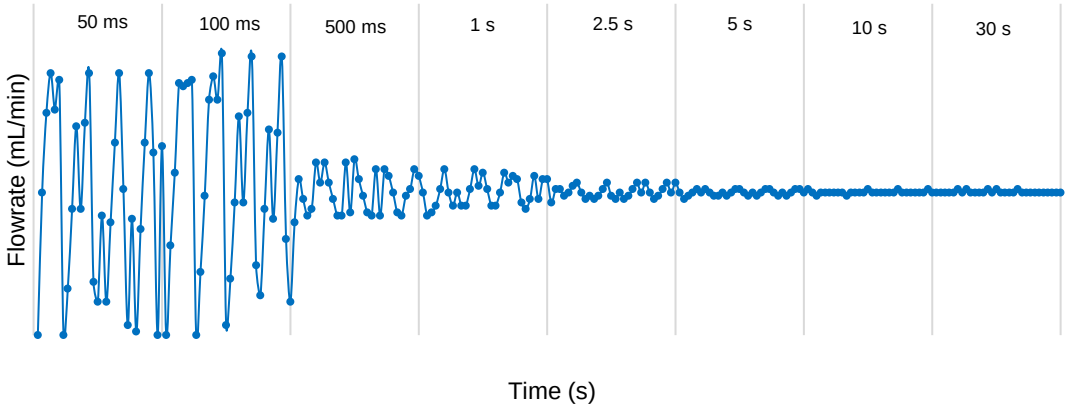

Figure 5.4. Flowrate reading at different sensor response times.

Shorter response times yield stronger fluctuations but correspond more accurately to the immediate flow value. On the other hand, longer response times have a better averaging capacity of the flow, despite incurring in delays in respect to current values. Since the reading was to be used in a control system, stronger fluctuations and long delays are undesired. Therefore, the response time chosen was of 5 s, which still had reasonable reaction to change (< 1 s). The fact that the peristaltic pump worked with pulsating flow was unavoidable. Figure 5.4 indicates that, when asked to draw 40 mL/min, the actual flux felt by the membrane oscillated between 0 and 80 mL/min. Although this can clearly be pointed out as an error source, several studies researching critical flux also used peristaltic pumps (Le-Clech et al., 2003; van der Marel et al., 2009).

The effect of the passage of bubbles through the flowmeter was also analyzed. At the chosen response time, even larger bubbles purposely introduced in the permeate side did not affect the values of the flowmeter. However, temperature had a significant effect. Changes in temperature alter the fluids viscosity, which in turn change the speed of the ultrasound waves used by the sensor. Calibration of the zero point thus had to be carried out at the start of each trial. Even so, the difference between the sensor's reading and the flow measured by weighing timed samples could reach 10 %.

The feedback control system installed was a PID controller, with architecture portrayed in Figure 5.5. Each of the controllers parameters (P, I and D) have to be tuned for the characteristics of each particular system. P stands for proportional gain; increased values give more proportional action in respect to the error and faster control. I corresponds to the integral gain; decreased values give more integral action in time and faster reaction. D is the derivative gain, which is not present in this set-up, as it may cause disturbances when dealing with noisy data.

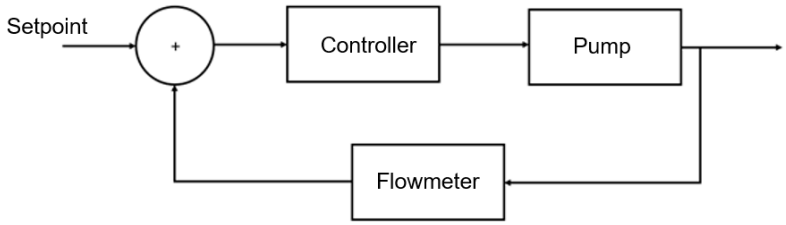

Figure 5.5. Representation of the feedback control system built in the set-up.

Three types of tunning were experimented: manual tuning, the Ziegler-Nichols tuning method – most known and well stablished method – and the SIMC (simplified internal mode control) tuning method, also of widespread acceptance. Manual tuning consists of trying different P and I pairs and recording the systems reaction to changes in the setpoint. The Ziegler-Nichols method, shortly ZN, requires the user to set I to zero and increase P until the system oscillates constantly. The P at which this happens is the ultimate gain (K_u) and the oscillation period is T_u. For a PI controller, $P = 0.45\ K_u$ and $I = 1.2\ T_u$. The SIMC method records the system's step response and, with the observed plant gain, dominant time constant and effective time delay, gives possible PI values for more or less aggressive tunning (Skogestag, 2001). Table 5.1 summarizes the findings for these both tunning methods.

Table 5.1. PI parameters according to ZN and SIMC tunning methods.

Parameter	ZN Method	SIMC method
P	0.315	0.135
I	0.100	0.108

Results from manual tuning indicated that P/I ratios above 1 and below 10 led to better responses. This was confirmed by testing the parameters from the tunning methods described above, as shown in Figure 5.6. Below this ratio the pump's reaction was too slow, while above it the response was too aggressive, causing overshooting. Overshooting was to be avoided since the aim of the flux-step method is to approach the flux level from lower values. A sluggish reaction was also unwanted, especially during pauses, as the pump has to achieve zero rpm to guarantee a 1 min relaxation pause.

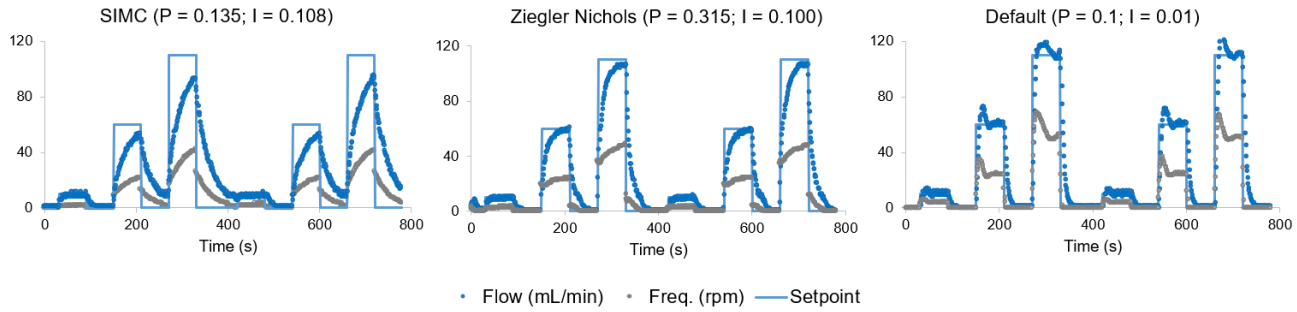

Figure 5.6. Tunning the control system: step tests with varying PI parameters proposed by different tunning methods: SIMC (sluggish response), ZN (good response) and default parameters from LabVIEW controller (aggressive response).

The ZN tunning was then considered the best fit for the system, but there was room for improvement, i.e. the controller could be faster. The refining of parameters was based on the experience with manual tunning. ZN parameters were then adjusted to yield a slightly more aggressive response, namely with decreased I, so that the final values used in experiments yielded P = 0.315 and I = 0.070.

6. Results and discussion

Results of each trial series (water, bentonite and sludge) are presented separately in this section. Their discussion as well as the evolution of the method development are done in parallel.

6.1. Water series

This series had the purpose to verify the stability of the set up and to assess permeabilities of sheets. The first trials in water still faced problems such as poor tuning (before refinement) and code errors. Nonetheless, results for permeabilities could still be taken into account. After solving these issues, graphs for the TMP evolution could be plotted for each method, as shown in Figure 6.1 for method A.

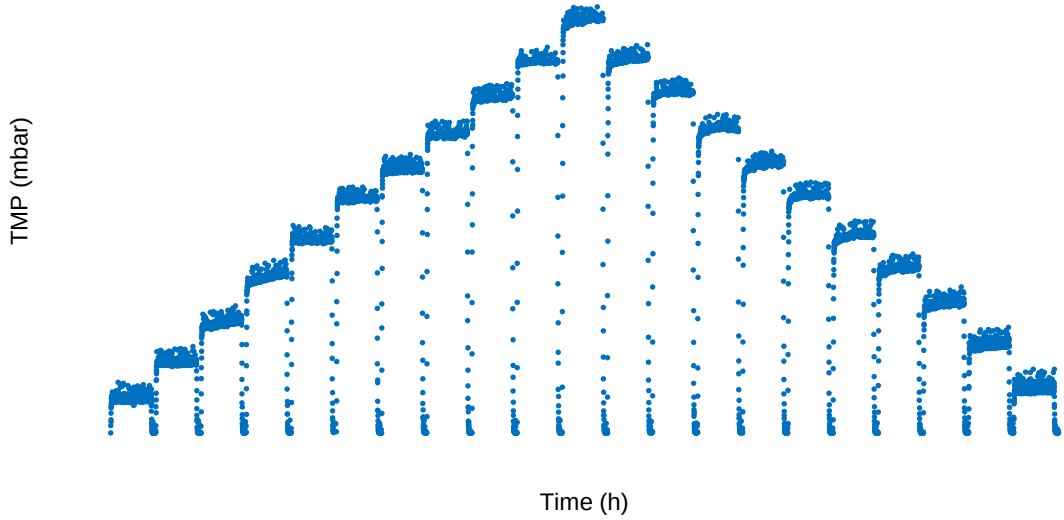

Figure 6.1. TMP development during trial with PES sheet in water using method A.

Figure 6.1 confirms that the pressure at rest was established during all relaxation pauses. This is seen through the concentration of data points around zero at every pause. However, the TMP appears to rise in several steps. Indeed, this phenomenon was observed in practically all trials with pure water. The TMP increase within a step is not expected to occur during water permeation and is an indicator of particles or impurities in the medium. In fact, suspended particles were observed through the transparent walls of the tank. The tank, previously used for mixed liquor, was rather hard to clean. The narrow width of the rectangular entrance (< 5 cm) did not allow a thorough cleaning at the bottom of the compartment which, even after washed with sodium hypochlorite, remained releasing particles. The presence of organic matter was confirmed when membranes left in the medium during 2 – 3 days were covered in a thin viscous slime. This is a sign of bacterial growth and was also pointed as a cause for the TMP rise. The tank was periodically washed with hypochlorite to minimize this effect.

Permeability values during the trials reflected this behavior. Figure 6.2 exemplifies the behavior of permeability and refers to the same trial shown in Figure 6.1. The decrease in permeability at the first steps can be correlated to the TMP rise verified. Furthermore, when comparing the first and last steps of the trial in both figures, the lower average permeability at the last step is linked to the higher average TMP at that step. This supports the interpretation that some deposition might have prevented constant TMP values when working with the referred tank. Temperature during trial was constant at 21.2 °C. The instabilities in permeability seen in Figure 6.2 are due to fluctuations in the flowrate.

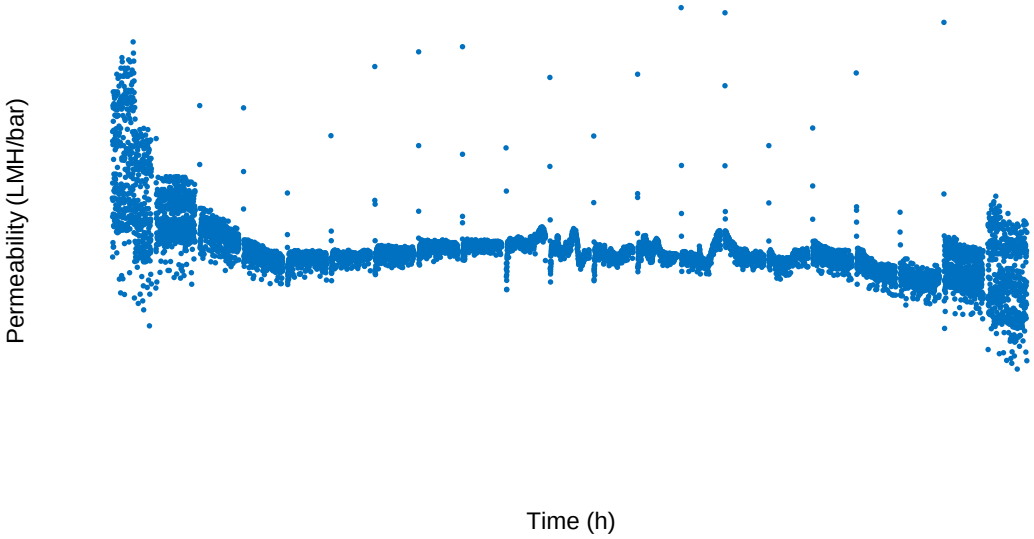

Figure 6.2. Membrane normalized permeability (20 °C) during trial in water with method A.

Trials with methods B and C also exhibited some fouling and instabilities, as seen in Appendix I. Nevertheless, the trials in water revealed that instruments and software were well integrated. Trials could last as long as desired, and programs could be written to combine more methods in sequence. Table 6.1 displays data regarding membranes' permeabilities during each trial, corrected for 20 °C. All trials had aeration set at v = 0.02 m/s. Membranes 1 and 2 were later used for the bentonite series, while membranes 4 and 5 were used for trials in sludge. After used for a first time and having their chemical preserving agents washed, all membranes were kept under water.

Table 6.1. Average normalized permeabilities (20 °C) during trials in water.

Trial N°	Sheet N°	Method	Permeability (LMH/bar)
1	PES 1	A	XXX
2	PES 1	C	XXX
3	PES 1	A	XXX
4	PES 1	A	XXX
5	PES 1	B	XXX
6	PES 2	A	XXX
7	PES 2	A	XXX
8	PES 2	B	XXX
9	PES 3	A	XXX
10	PES 3	C	XXX
11	PES 4	A	XXX
12	PES 4	B	XXX
13	PES 5	B	XXX
14	PES 5	B	XXX

To be able to compare permeability values delivered by the different methods, it had to be first verified if the permeabilities of each membrane was comparable. At a 95 % confidence level, only membranes 1, 4 and 5 did not exhibit statistically different permeabilities. Sheets of a same membrane material may differ due to inhomogeneities in manufacturing. As the sheets are cast on a XXX cm wide paper, the polymer layer may have varying thicknesses in that range, resulting in differences in permeability.

With the membranes with comparable permeability values, an analysis was be made regarding values given by each method (Figure 6.3). There was no statistical difference between average permeabilities of methods A and B ($p > 0.05$). As only one data point could be used for method C, no statical comparison was made, although the value is close to the average of the other two methods. Therefore, all three methods were considered equivalent in terms of reporting permeability.

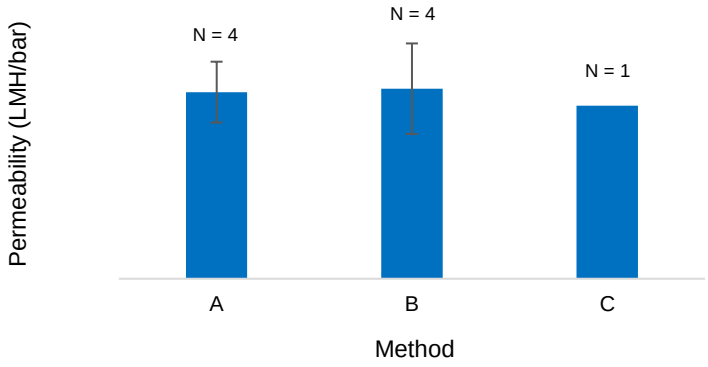

Figure 6.3. Average permeabilities obtained through methods A, B and C. N: N° of samples; error bars: SD.

6.2. Bentonite series

This series of trials had the purpose to observe how cake layer formation would reflect in the TMP. Trials with bentonite suspension directly showed TMP increases during flux steps, as expected. Methods A and B detected high (total) fouling rates, that increased with rising flux values. Additionally, method B gave results for irreversible fouling by the comparison between the low reference steps. Aeration was kept at a velocity of 0.02 m/s, which also prevented the particles of clay from settling at the bottom of the tank. Figure 6.4 portrays TMP data points during one of the trials using method B.

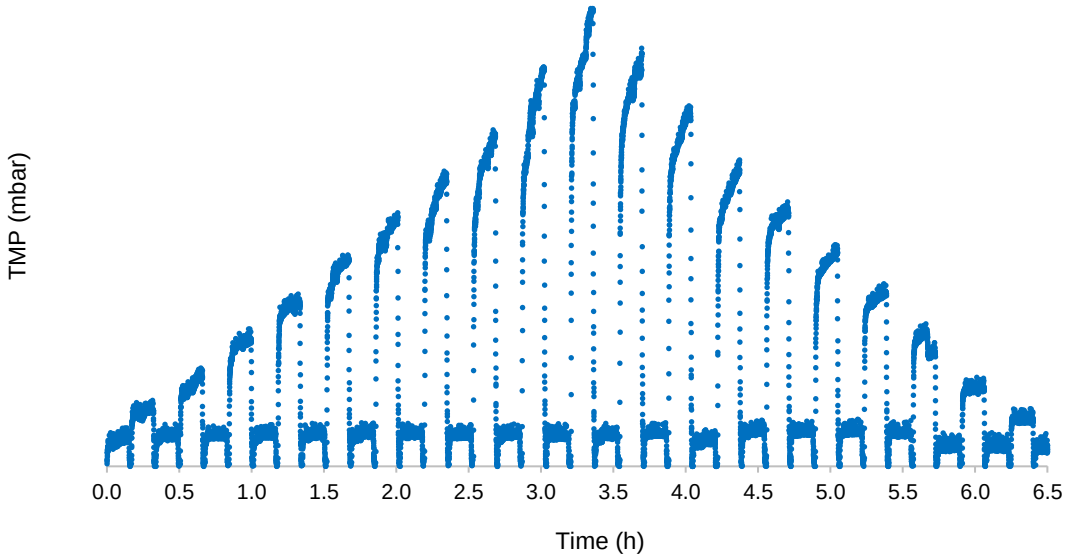

Figure 6.4. TMP development during trial in bentonite suspension (XX g/L) with aeration (v = 0.02 m/s) using method B.

During this and other trials using method B, TMP values at reference steps remained mostly stable, with some exceptions. Moreover, a comparison between reference steps reveals that TMP values were mostly constant. This could confirm the reversible character of fouling caused by bentonite, which has grain sizes bigger than the UF membrane pores and thus only forms reversible cake layers.

Fouling enabled a first evaluation of the different procedures proposed to calculate the fouling rate. Described in section 4.5, they comprise two calculation procedures to estimate total fouling in method A and B (slope and end-start) and two others to estimate irreversible fouling in method B (end-end and average-average). The results for fouling rates for the trial shown above are shown in Figure 6.5.

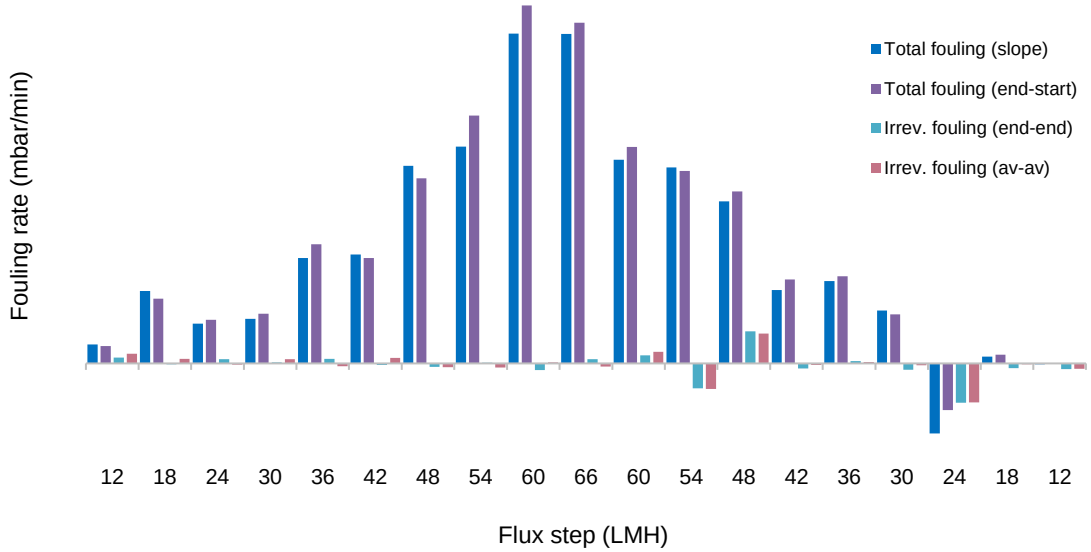

Figure 6.5. Fouling rates (total and irreversible) by different procedures for a trial in bentonite suspension using method B.

From the figure above, it is clear that higher fluxes induced higher total fouling. The two procedures used to estimate it seemed to deliver similar results, which was also observed in other trials, also for method A (Appendix IIa). Irreversible fouling remained close to zero in most steps, with some oscillations at a few descending steps, possibly corroborating for hypothesis of reversible deposit. Positive irreversible fouling values followed by negative ones (such as at the descending steps 60 to 54 or 48 to 24 LMH) can be an indicative of a deposition of particles that attached to the membrane, remained deposited on the surface for some time and then later were removed by air scouring action. Both procedures used to estimate irreversible fouling showed similar results in trials using method B. Considering this analysis, both procedures for both fouling types were to be tested in trials with sludge.

Critical fluxes were not calculated at this point. This is mainly because the various procedures proposed in the literature (zero fouling, threshold for fouling, change in fouling trends) would yield completely different findings with bentonite as with sludge. For instance, Figure 6.5 shows how fouling rates achieved values way above 1 mbar/min, while the most used threshold for fouling rate in sludge is 0.1 mbar/min. Indeed, the bentonite suspension does not mimic the behavior of sludge fouling or the viscosity of the mixed liquor. Therefore, the analysis of trials in bentonite suspension was confined to qualitative observations regarding the different procedures used to measure the fouling rate.

Method C was not able to deliver the expected results. A first trial exhibited many instabilities in the flux and TMP (Appendix IIb) while a second trial revealed continuous residual fouling (Figure 6.6). Residual fouling was not expected for bentonite suspension, as it should only cause reversible deposits onto the membrane. Since this trial exhibited remarkably low permeability, the hypothesis of biofilm formation was raised again. In fact, when the trial was ended, the membrane sheet was taken out of the tank and a thick viscous layer of clay, conceivably trapped in a biofilm, was verified.

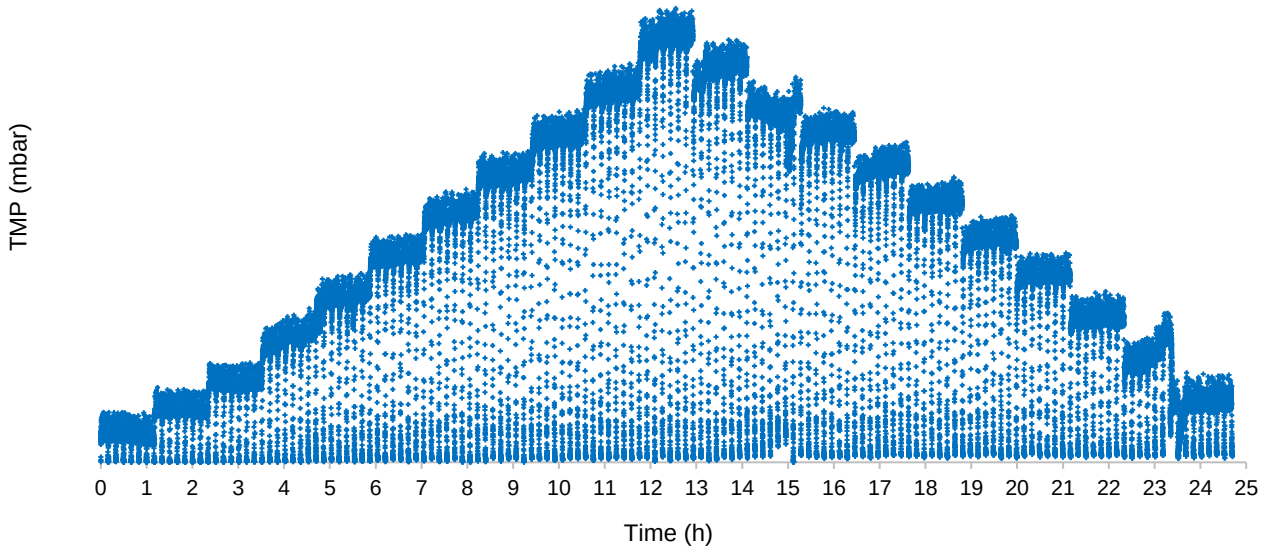

Figure 6.6. TMP during trial with bentonite suspension using method C displaying unexpected residual fouling.

Figure 6.7 confirms the irreversible deposition of bentonite. It also shows that the region right above the permeate collector is more prone to deposition. This is coherent with the trajectory of bubbles, which, when collide against the lower part of the collector, are forced to divert it, failing to efficiently scour the region above it. This phenomenon had already been observed by the technical team in the company. Due to time constraints and the schedule of the project, method C in bentonite suspension could not be repeated once again. Notwithstanding, it was to be tested in trials with sludge.

Figure 6.7. Membrane sheet covered with bentonite after the trial of Figure 6.6.

Permeabilities of the membranes used during bentonite trials are shown in Table 6.2. Since both membrane sheets had been used in the trials with water, they were soaked in a 500 ppm hypochlorite solution for 1 hour. The effect of cleaning can be seen in the higher permeability values in the first experiments with each membrane. The loss in permeability seen in following trials can be linked with the supposition of bentonite deposition combined with biological growth due to the presence of organic matter attached to the bottom of the tank. Less likely is the conjecture that bentonite was provoking pore blocking. Between trials, membranes were gently rinsed with water, which would not have eliminated such deposits. The analysis on the permeability values delivered by each method is pointless as values were subjected to the order in which methods were carried out. The influence of chemical cleaning combined with the gradual permeability decline also discredits any appraisal on

the average permeability value of the individual membrane sheets. The causes for the decline in permeability in these conditions was not further investigated, since the focus of the bentonite series was to observe fouling and to measure it with the proposed calculation procedures.

Table 6.2. Average normalized permeabilities (20 °C) during trials in bentonite suspension.

Trial N°	Sheet N°	Method	Permeability (LMH/bar)
15	PES 1	C	XXX
16	PES 1	A	XXX
17	PES 1	B	XXX
18	PES 1	C	XXX
19	PES 2	A	XXX
20	PES 2	B	XXX
21	PES 2	A	XXX
22	PES 2	B	XXX

6.3. Sludge series

Sludge trials consisted the main part of the work, in which the system parameters were put to the test. Fouling caused by activated sludge has unique properties and, as discussed in the literature review, depends highly on the biological state of the biomass. The results presented here must therefore be regarded under the consideration that the biology in the pilot unit was affected by different events, such as change in the main pilot module, chemical cleaning of the main module and fluctuations in HRT and SRT due to parallel trials with the main module. Furthermore, oscillations naturally occur in external conditions such as temperature and wastewater composition. A glance of the moment where membrane sheets are changed in the test rig is depicted in Figure 6.8.

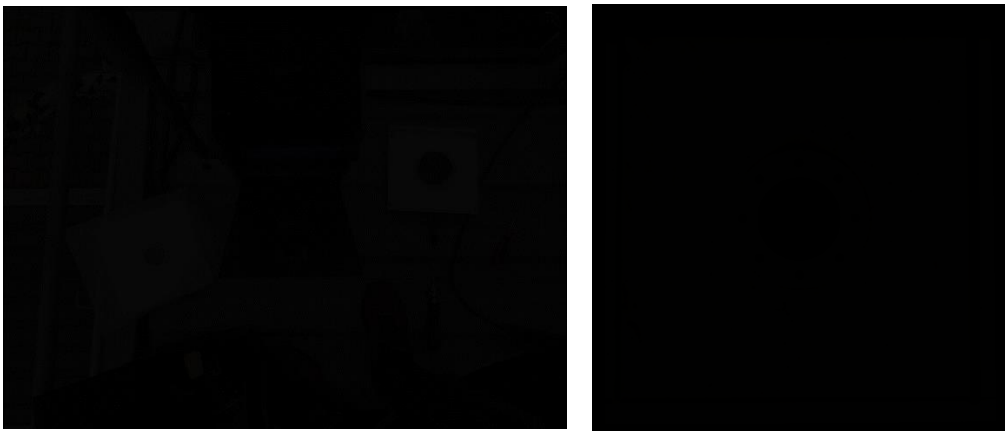

Figure 6.8. Change of membrane sheet in the test rig (left) and membrane sheet after a trial (right).

6.3.1. Choice of criterium for criticality

Filtration of activated sludge induced fouling in all trials. This could be clearly noted through rising TMP values at higher fluxes. Aeration was first set at 0.02 m/s, but was later reduced to 0.005 m/s, to induce higher fouling rates. As discussed before, the critical flux is the most adequate measurable quantity to assess the propensity to fouling of a membrane at given test conditions. However, different approaches can be used to investigate it. Here, three criteria were tested: the zero fouling approach, the shift in the normalized fouling rate approach and the threshold approach.

The zero fouling criterium was not a considered at first, as most studies report that zero fouling is not achievable in activated sludge. However, within the accuracy of the equipment, zero fouling was observed for lower steps in some trials. Figure 6.9 shows the course of the TMP for a method A trial. The quantification of the fouling rate was still carried out using the slope and end-start procedures. Fouling at each steps is portrayed in Figure 6.10a. It is clear that the system only noticed detectable fouling starting from 42 LMH and that before this point the fouling rate was mostly negative or zero. Therefore, within the precision and length of experiment, the critical flux is taken to be $J_c = 36\ LMH$. Whether this critical flux corresponds to the strong or weak form is difficult to say. This specific membrane sheet was not tested in pure water, so its water permeability is unknown. Since the permeability until the 36 LMH step remained constant, either forms of critical flux are thinkable.

Figure 6.10b displays the fouling curve for the slope procedure. Nearly no hysteresis was observed, indicating that fouling had similar values during ascending and descending phases of the method. Confirming the findings from van der Marel et al. (2009), this reinforces relaxation as an efficient way to remove cake layers formed during the steps, so that little residual fouling interferes in following steps. Both procedures to measure fouling deliver similar results, with some exceptions at low fluxes.

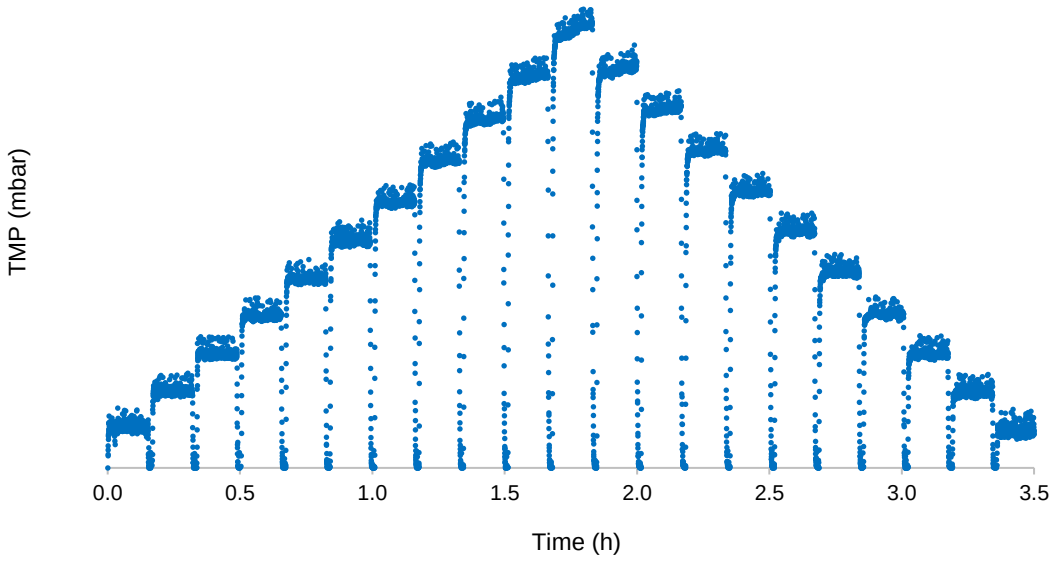

Figure 6.9. TMP development during a trial in sludge (aeration = 0.02 m/s) using method A.

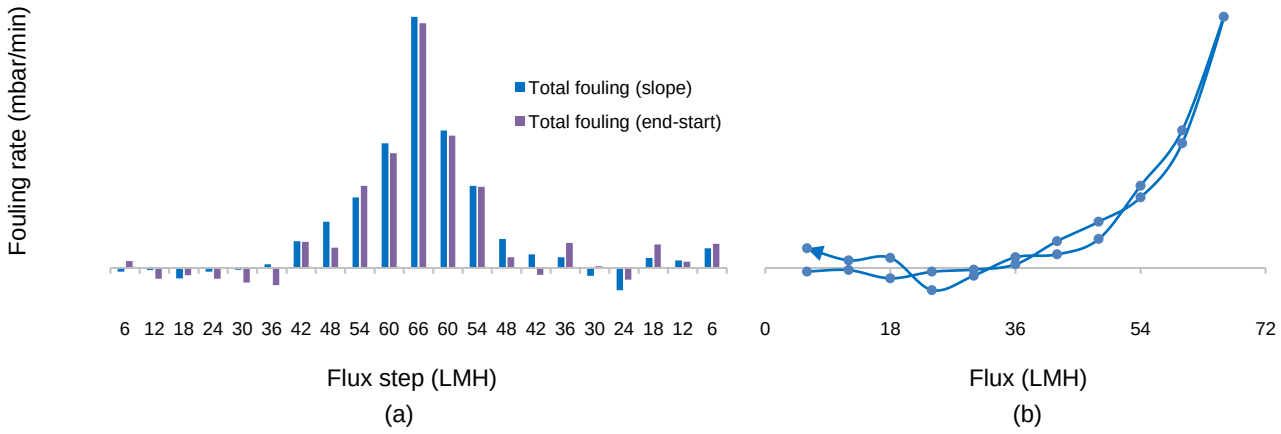

Figure 6.10. Fouling rate (a) at all steps according to both procedures and (b) hysteresis for the slope procedure.

Despite the result of the trial above, where the original definition of the critical flux could be applied, zero fouling at lower steps was not a reproducible situation. In most trials, fouling developed already at the first steps of the experiments. This lack of reproducibility might be a result from varying sludge properties. Indeed, in the trial above, MLSS equaled 6.5 g/L, which is among the lowest values recorded during experiments. Even though MLSS is not a decisive parameter for fouling, other indicators pointed at low fouling propensity. CST measured was at 13.7 s, a low value in comparison with other recorded values, indicating very good sludge filterability. Incoming wastewater COD was at 266.2 mg/L, also a low value (the average was around 400 mg/L), resulting in low levels of residual organic matter in the mixed liquor and therefore low fouling by soluble or particle COD.

Next, the shift in the fouling rate normalized by the flux was considered as a possible criterium for defining the critical flux. The normalization of the fouling rate had already been used in the study by van der Marel et al. (2009), but Diez et al. (2014) were the ones who developed a mathematical model relating the shift in $(dTMP/dt)/J$ to a change of species deposited onto the membrane, as described in the literature review in Eq. 14 and 15. Figure 6.11a shows the TMP development of a trial with method A, while Figure 6.11b portrays the fouling rate of ascending steps divided by each corresponding flux (here calculated with the slope procedure). The shift in the trend is very noticeable: around 42 LMH, fouling increases at a higher rate. According to the model by Diez et al., this relates to a situation of direct sludge fouling onto the membrane, while before this point fouling was due to the non-settable fraction (free EPS/SMP). The interception of the two regression lines characterizes this transition, therefore marking critical flux, here then calculated as $J_c = 39\ LMH$.

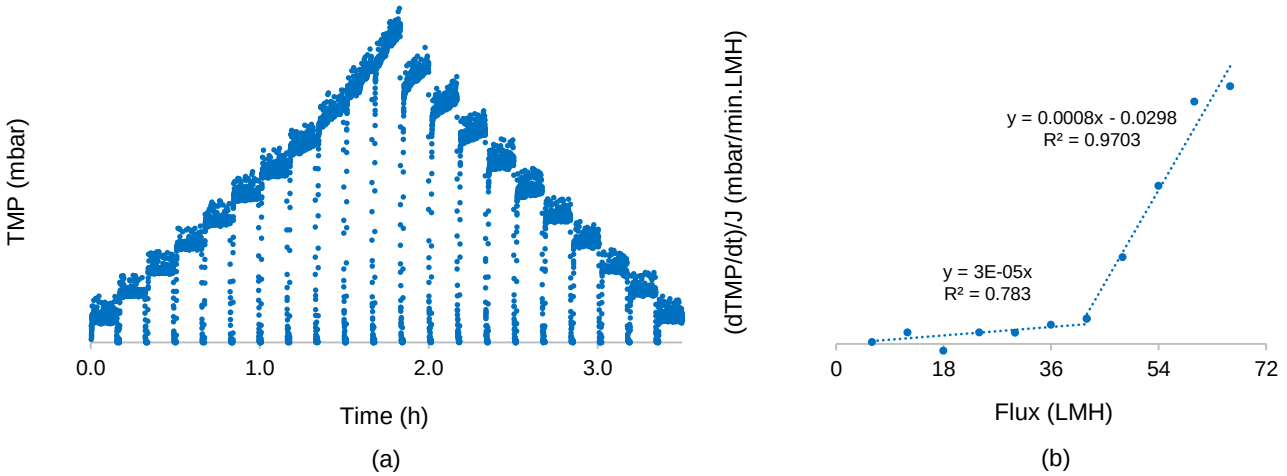

Figure 6.11. Trial with method A (aeration 0.02 m/s): (a) TMP and (b) fouling rate normalized by the flux (slope procedure).

Nonetheless, only a few trials exhibited fouling rates that adjusted well to the model proposed. The trial above was the only one with the UP150 membrane that had this behavior, interestingly right the one that had a surprisingly high permeability of XXX LMH/bar. Reason for this high value was unclear, possibly linked to a hypochlorite contamination of the water bath where the sheet was being kept. The good fit for this model was also seen in some trials with the UF PVDF membrane, which naturally display higher permeability. Most results for (dTMP/dt)/J, however, appeared to fit an ever-growing curve. Under the light of the model, this can indicate that both non-settable fraction and biosolids participate together in the deposition, even that at different rates for each flux level, so that no clear shift in fouling rate can be observed. As a consequence, the method by Diez et al. (2014) could not be applied as standardized criterium for the determination of the critical flux in trial in activated sludge.

The choice for threshold criterium seemed obvious at this point. All trials had varying fouling rates that started at low values and increased up to high values, making the election of an appropriate threshold the best approach for all trials. This has been applied by numerous studies (Le-Clech et al, 2003; van der Marel et al., 2009; de la Torre et al., 2009), with the most used value being of 0.1 mbar/min. Accordingly, this value was also applied in this work. However, this came into conflict with the operating mode of the pilot unit. The operation of the feed pump is intermittent: the pump works when the level of the aeration tank reaches a defined lower limit and stops after it reaches a higher limit. The resulting level fluctuations affect the TMP perceived by the pressure transmitter in the test setup. A dropping tank level increases the water column between the pressure sensor and the tank level, which creates more hydrostatic vacuum and lowers the absolute pressure perceived. Since the pump only runs at a fixed speed, the solution was to set the upper and lower limits as close as possible, with a difference of 1 cm. Notwithstanding, this equals to a 1 mbar variation, 10 times the threshold used in studies. With filtration flowrates between 1 and 2 m³/h and a surface area of 7.5 m² in the aeration tank, the 1 cm variation took between 4.5 to 2 minutes to be filtered by the main module, triggering again the feeding pump, which in turn required around 1 minute to fill up the volume again. As a result, 1 mbar oscillations were expected at this time interval in the TMP results of the test rig.

This consideration immediately disqualified the “end-start” procedure to calculate fouling rates. Reason here is that, in case that the start or the end of the flux step falls exactly at the moment of lowest or highest level, the rate of fouling will be strongly misjudged. On the other hand, the “slope” procedure is way less sensitive to these fluctuations, as the slope calculation compensates “ups” and “downs” that occur within the step. The slope procedure was thereupon adopted as the standard one. Figure 6.12a shows the TMP oscillations during the first hour of a trial with the UF PVDF membrane, which, for having higher permeability, results in lower TMP values that make fluctuations more visible. Figure 6.12b compares both procedures for the assessment of fouling during the whole trial and underlines how the slope procedure is more stable compared to the “end-start” one.

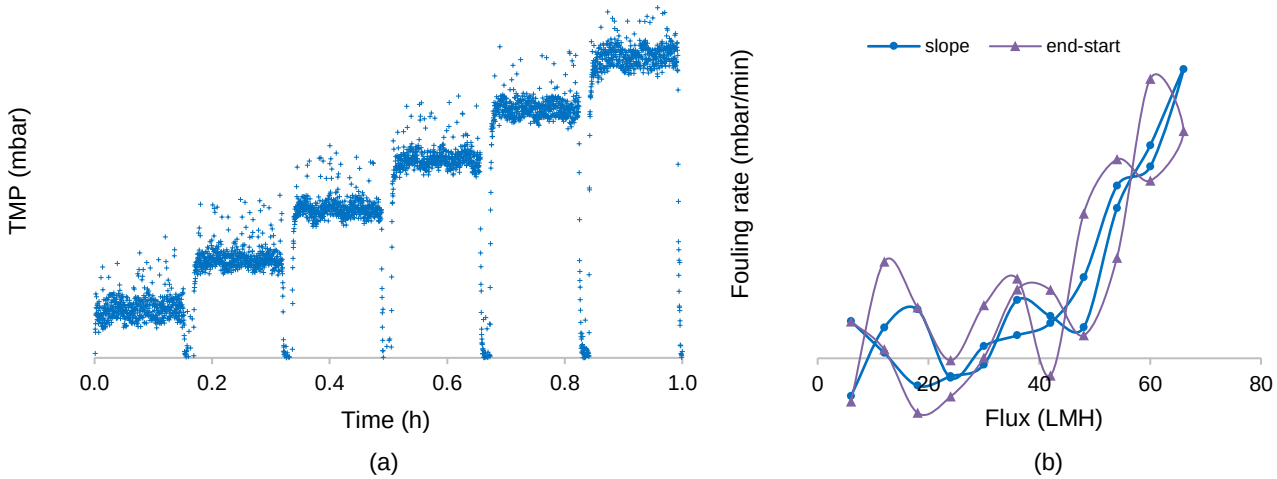

Figure 6.12. Oscillations of level causing (a) visible TMP fluctuations and (b) instabilities with the “end-start” procedure.

Furthermore, it was necessary to define that the critical flux was not the one with fouling rate immediately below 0.1 mbar/min neither the one right above this threshold, but the interpolation between these points. Even though this assumes a linear relation between fouling and flux (which is not true, as fouling rate increases exponentially with the flux), this is a way to correct the value of Jc in situations where it is about to be exceeded or has just been exceeded at a certain flux level.

6.3.2. Comparison between methods A and B

Methods A and B had, in theory, the same ability to report the critical flux. Both methods comprise rising steps from 6 to 66 LMH, followed by descending steps. The advantage of method B is allegedly the parallel investigation of irreversible fouling through the reference low steps in between every higher step. First, an analysis was made regarding the permeabilities that resulted from both methods. Then, an evaluation was carried out to determine whether both methods delivered comparable results for the critical flux. Method B could theoretically induce more fouling during the reference steps and due to longer trial duration – even though this was not expected – and end up delivering lower values for the critical flux. Following, an assessment on the irreversible fouling rate was carried out to determine whether method B presented reproducible results for this parameter. The course of TMP using both methods is displayed in in the graphs of Appendix III.

Table 6.3 lists the sequence of trials conducted with methods A and B using different membranes. Critical fluxes were also corrected to 20°C to allow direct comparison of results. Average temperatures during trials are reported even so. Membranes 4 and 5 had already been used in the lab and revealed unusually high permeabilities. As discussed above, this was possibly due to a hypochlorite contamination of the water bath where the sheets were kept between trials. Even though their reported values for Jc was comparable to the other experiments, trials with these sheets were discontinued and not taken into account in the analysis. Table 6.3 also reports the irreversible fouling rates resulted from method B. Its measurement procedure and applicability will be discussed in detail ahead.

Table 6.3. Average normalized permeabilities (20 °C), normalized critical fluxes (20 °C) and irreversible fouling rates for trials with sludge using methods A and B at different conditions of temperature (aeration 0.005 m/s).

Trial N°	Sheet N°	Method	Permeability (LMH/bar)	Jc (LMH)	Irrev. fouling (mbar/min)	Av. Temp. (°C)
23	PES 4	A	XXX	XX		16.2
24	PES 4	B	XXX	XX	XX	16.9
25	PES 5	A	XXX	XX		16.7
26	PES 5	B	XXX	XX	XX	17.3
27	PES 6	A	XXX	XX		17.7
28	PES 6	B	XXX	XX	XX	18.6
29	PES 6	A	XXX	XX		19.5
30	PES 6	B	XXX	XX	XX	20.6
31	PES 6	A	XXX	XX		19.5
32	PES 6	B	XXX	XX	XX	20.8
33	PES 7	A	XXX	XX		20.2
34	PES 7	B	XXX	XX	XX	21.2
35	PES 7	A	XXX	XX		20.0
36	PES 7	B	XXX	XX	XX	20.3
37	PES 7	A	XXX	XX		20.2
38	PES 7	B	XXX	XX	XX	21.1
39	PES 8	A	XXX	XX		22.0
40	PES 8	B	XXX	XX	XX	22.6
41	PES 8	A	XXX	XX		22.1
42	PES 8	B	XXX	XX	XX	22.0
43	PES 8	A	XXX	XX		23.0
44	PES 8	B	XXX	XX	XX	22.6

Permeabilities of each sheet had a falling tendency, as evidenced in Figure 6.13a. This is logical as trials performed in sequence lead to increasing resistances. Values among sheets were quite similar, although sheet 7 had significant lower average permeability compared to sheet 8 ($p < 0.05$). This, however, did not reflect on the results for the critical flux, as depicted in Figure 6.13b, which not only did not have a falling trend during trials but also had comparable values among sheets ($p > 0.05$). The higher temperatures during trials with sheet 8 (around 2 °C above those with sheet 7) could be a reason for its higher permeability, although this effect was not seen in sheet 6, with temperatures around 1°C below the ones with sheet 7. Even though permeabilities have been normalized at 20 °C, viscosity correction is insufficient to compensate variations in permeability, a well-known effect. Explanations to this, according to Le-Clech et al. (2006), are that (1) at lower temperatures, the more viscous mixed liquor reduces shear stress caused by aeration; (2) deflocculation is favored at lower temperatures, which releases foulants (EPS); (3) back diffusion is less intense at lower temperatures and (4) COD biodegradation is slower at lower temperatures, resulting in higher COD residual levels.

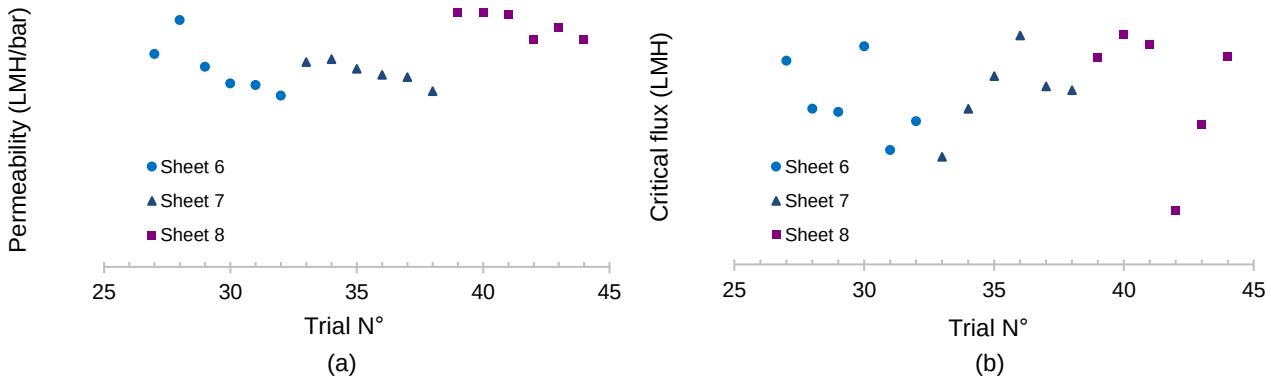

Figure 6.13. Permeability (a) and critical flux (b) normalized values (20 °C) for sheets 6,7 and 8 using methods A and B.

Since critical fluxes leveled among sheets, a comparison between methods A and B was possible. The results for Jc obtained from methods A and B are compared separately for each sheet in Figure 6.14, although the comparison of global averages is also feasible: method A estimated an average Jc of $XX \pm X$ LMH, while method B had an average of $XX \pm X$ LMH. This reassures that method B, adapted from van der Marel et al. (2009), is just as capable to investigate the critical flux as method A, here an adapted version of the protocol proposed by Le-Clech et al (2003). If method B is able to produce meaningful values for the irreversible fouling rate, it will show advantages over method A.

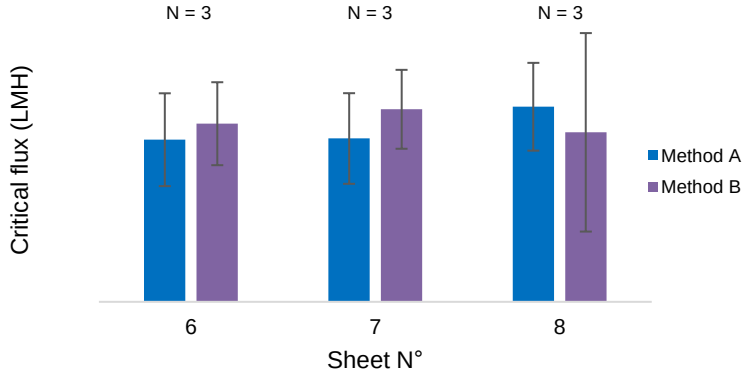

Figure 6.14. Comparison of critical fluxes (20°C) between methods A and B for sheets 6, 7 and 8. Error bars: SD.

Irreversible fouling rates were not well assessed neither by the “average-average” nor “end-end” procedures. The first compared averaged TMP values of reference steps, while the second compared final values (average of the last 60 s) of each reference step, under the assumption that the first half of the step could impart instabilities. However, instabilities were ubiquitous in all trials with method B. Irreversible fouling rates oscillated between positive and negative values that lacked a clear outcome.

In view of this fact, another assessment procedure was proposed: to plot the TMP average values of each reference step and find the slope of the line that best fits the points. This was then considered as the irreversible fouling rate, which only had one fixed value for each trial, as reported in Table 6.3. Strikingly, three of the trials resulted in negative irreversible fouling rates. Two trials of sheet 8 (20 and 22) have their average TMP of reference steps plotted in Figure 6.15, the second one showing the negative trend. Moreover, positive irreversible fouling rates varied strongly, ranging from XX to XX mbar/min. Reasons for this finding are hard to find without looking for explanations beyond the scope of the membrane, since a constant flux should result in at least a constant reference TMP, but not a dropping one. Hence, a possible reason could have been changes in the metabolism of biomass, maybe adapting to new conditions such as concentration or composition of wastewater.

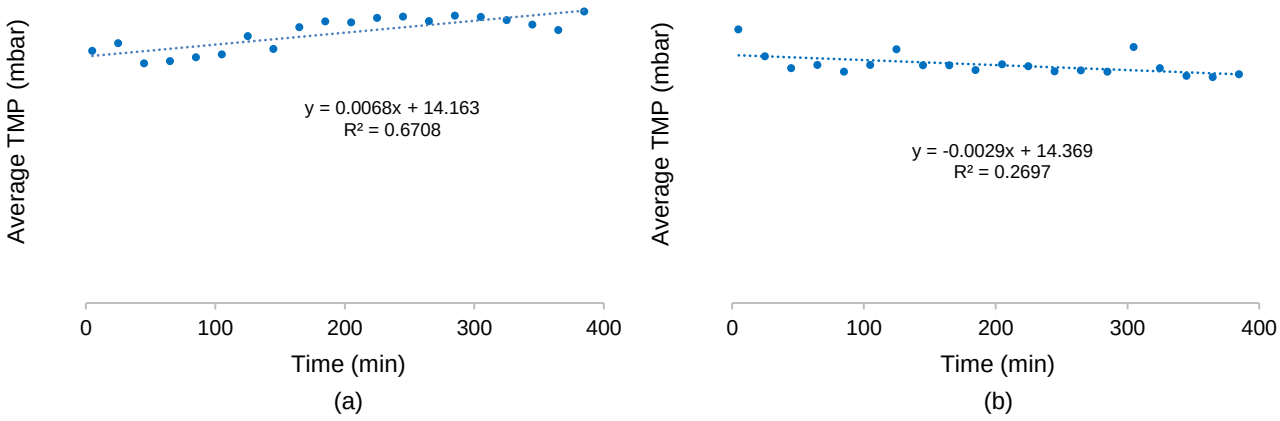

Figure 6.15. Rising (a) and falling (b) average TMP values for reference steps in trials 42 and 44 using method B.

van der Marel et al. (2009) also found a negative value for the irreversible fouling rate when they quantified the TMP difference between the last and first reference step. Explanations were not given. Since the TMP of reference steps appeared more sensible to external conditions than to a continual fouling process, method B was dismissed. This was unfortunate, as method B was thought to deliver results on the irreversible fouling rate additionally to the value of critical flux at a relatively short time.

In a final analysis, method A remained as the main tool to determine the critical flux. It requires less time to run compared to method B, with trials of 3.5 hours, and was able to deliver reproducible results for the critical flux. The step size of 6 LMH together with the step range (6 to 66 LMH) were also appropriate for the experimental accuracy desired. Moreover, the hysteresis curve could help identify residual fouling not removed during relaxation, even though this was not observed in this work.

Mixed liquor characteristics and COD levels during trials with methods A and B are listed in Table 6.4. MLSS remained within the typical MBR biomass concentration range (usually 6 – 15 g/L). CST indicated good sludge filterability compared to values in the record, from XX top XX s. Permeate COD concentrations (measured with samples collected from the main pilot module) oscillated together with incoming wastewater COD levels, so that organic matter removal efficiencies were of XX – XX %.

Table 6.4. Mixed liquor characteristics and COD levels during trials with methods A and B.

Sheet N°	MLSS (g/L)	CST (s)	COD_{feed} (mg/L)	$COD_{permeate}$ (mg/L)	COD removal (%)
PES 4 / 5	XX	XX	XX	XX	XX
PES 6	XX	XX	XX	XX	XX
PES 7	XX	XX	XX	XX	XX
PES 8	XX	XX	XX	XX	XX

6.3.3. Comparison between methods C and D

Method C was built to follow the same fluxes performed during method A, but repeating each flux step seven times, which was called a “step-block”. The number of repetitions was set so that the method could be executed within one day, lasting 24.5 hours. This number of steps was expected to deliver meaningful results for the residual fouling rates at each step-block. The first trial was very unstable: above the 42 LMH step-block, the TMP oscillated strongly. The reason for this behavior was unclear. A second trial, meanwhile, ran very smoothly, as shown in Figure 6.16

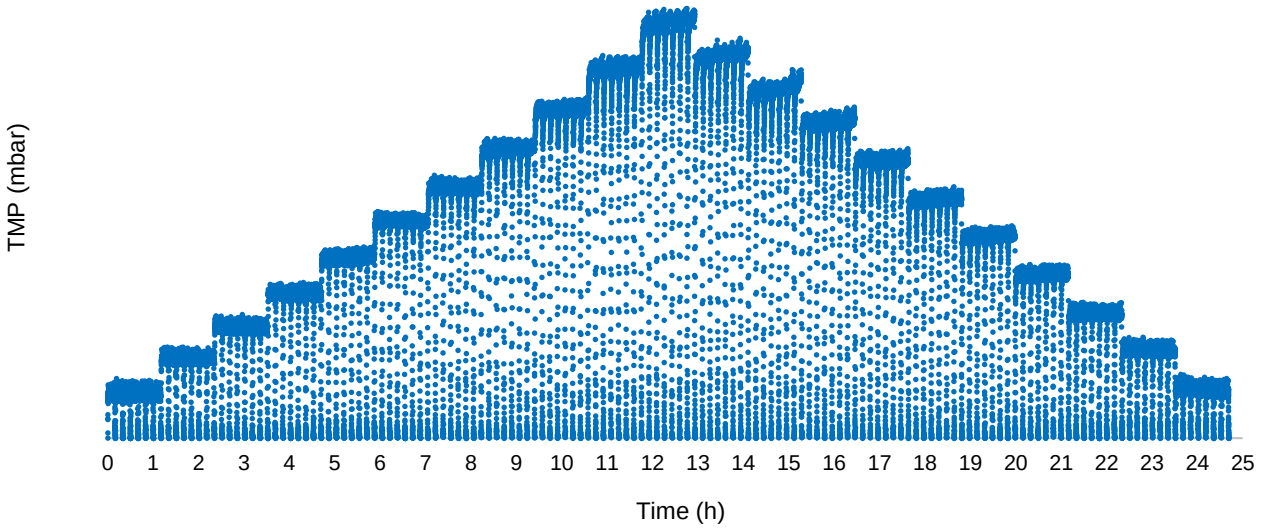

Figure 6.16. TMP development during trial with sludge using method C (aeration v = 0.005 m/s).

Nevertheless, residual fouling rates did not follow a consistent trend. Calculations were performed with two procedures, with both considering only the initial TMP of each steps (which is the average of the 60 s after the first 60 s of stabilization). The slope procedure measured the slope of the seven points for each block, while the end-start procedure took only considered the last and first data points of the block. Figure 6.17 confirms the uneven behavior of residual fouling, even in a trial such as the one above, where TMP within blocks appeared very stable. It seemed that the duration of each block was insufficient to detect a representative rise in the TMP, reason why method D was created.

Method D had the same aim as method C, but instead of going through all 11 steps, only 5 flux levels were chosen: 12, 24, 36, 48 and 60 LMH. The descending phase was also eliminated, since an eventual hysteresis would not have a direct interpretation and since longer step-blocks would have a major influence on descending blocks. To avoid influence of fouling between blocks, 30 minutes of aeration was introduced between them, although this certainly could not fully avoid interferences. Each cycle repeated 21 times, so that each step-block lasted 3.5 h, with the trial lasting 19.5 hours.

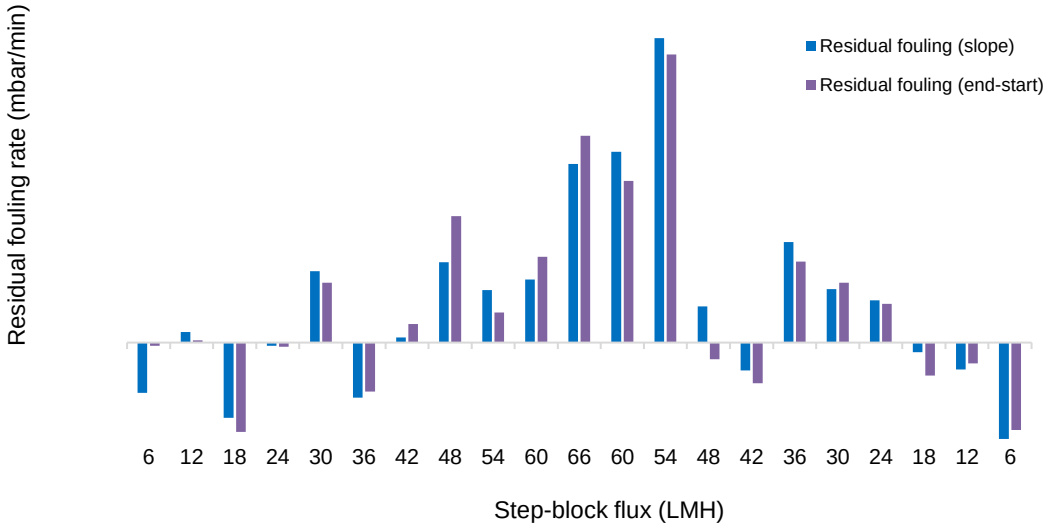

Figure 6.17. Residual fouling rates for trial in sludge (aeration 0.005 m/s) using method C according to two procedures.

The longer duration of step-blocks in method D yielded much more stable residual fouling rates throughout each step-block, as portrayed in Figure 6.18 below. Rising residual fouling rates were observed with rising flux levels. This is expected since, at higher fluxes, EPS and sludge biosolids are dragged to the membrane surface at a higher rate, which increases the probability of irreversible attachment onto the membrane that is not scoured by aeration during the relation time. The successful outcome with method D suspended further attempts with method C, that was then dismissed.

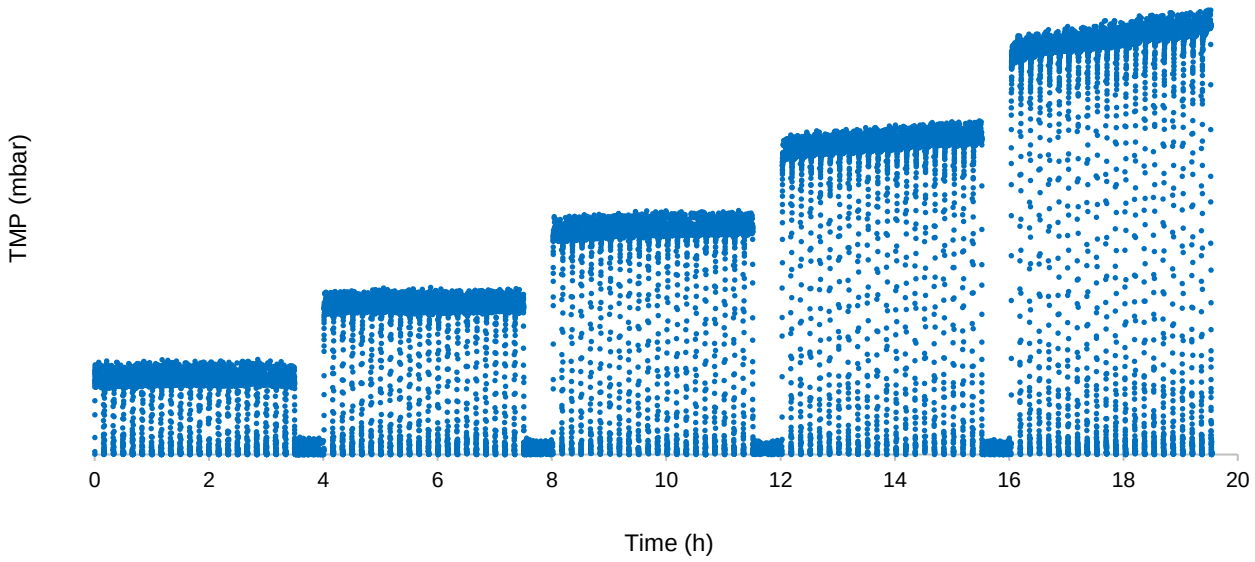

Figure 6.18. TMP development during trial in sludge (aeration 0.005 m/s) using method D.

At the last step-block in Figure 6.18, the difference between total and residual fouling becomes clear. While the former describes the TMP rise withing the 9 min of filtration of each cycle, the latter equates the TMP slope of several cycles performed in a row. It is that residual fouling is much lower than total fouling. This fact confirms relaxation as an efficient method to prevent steep TMP rises. Residual fouling rates were calculated only using the slope procedure, since the effect of fluctuating level invalidated the end-start procedure, as discussed before. Results are shown in Figure 6.19.

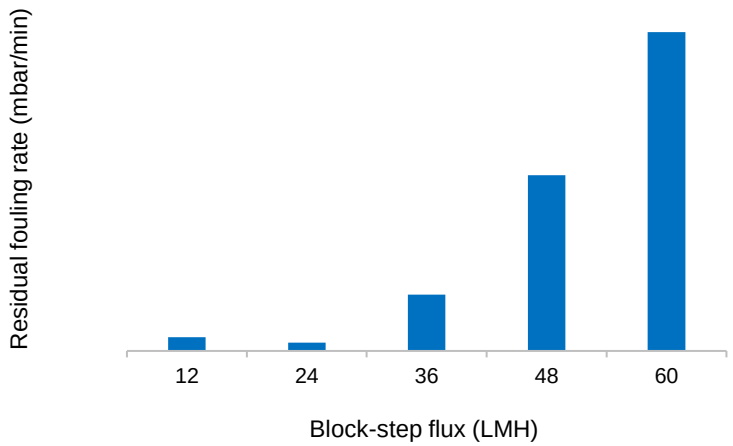

Figure 6.19. Residual fouling rates for the trial of Figure 6.18 according to the slope procedure.

Similarly to what was done for total fouling, a threshold for the residual fouling rate was defined in order to obtain a value for the sustainable flux. This was arbitrarily defined as equivalent to a TMP increase of 100 mbar per week, or 0.00992 mbar/min, rounded up to 0.01 mbar/min. A 100 mbar increase in the week was considered reasonable, although it might be a high increase for real cases. For instance, if this membrane with permeability of ~ XXX LMH/bar operated at ~ XX LMH, an initial TMP of 100 mbar would double within a week at this threshold value. Nevertheless, the choice of this arbitrary limit, once equally used for all trials, would deliver comparable results between them. Moreover, trials had residual fouling rates of 0 – XX mbar/min, so this threshold suited the results. For the trial above, $J_{sus} = XX\ LMH$, interpolated between the XX and XX LMH step-blocks (slope).

Another parameter that could be obtained from trials using method D was the rate of increase of residual fouling in respect to the flux. According to Howell et al. (2004), residual fouling rates near the critical flux at constant aeration are exponentially dependent on the flux applied, as shown in Eq. 16. The exponential regression of the data revealed a good fit of the model ($R^2 = 0.92$). Eq. 23 shows the expression obtained for this trial, where the exponential coefficient can be understood as parameter that governs the rate of increase of residual fouling in respect to the flux.

$$\left(\frac{dTMP}{dt}\right)_{residual} = 0.0004 \times e^{0.0834\,J} \qquad \text{(Eq. 23)}$$

These two values obtained with method D – namely J_{sus} and the exponential coefficient – may serve as relevant parameters in the comparison of two membranes with different filtering properties. Together with the critical flux, obtained with method A, they might form a robust tool to characterize membrane performance in MBRs. Despite being subjected to conditions of the mixed liquor that are hard to control, it is expected that these parameters reflect the good or bad resistance of membranes against fouling. To this end, methods A and D were combined in a single protocol, that executed method A, introduced a 30 min pause to then execute method D. This would make sure that both methods were carried out under similar conditions of sludge. The total duration of the method, hereinafter referred to as method AD, amounts to 23.5 hours, therefore performable within one day. The slope procedure was defined as standard for both total and residual fouling rates. An excel tool was created to receive the raw data from the merged method, perform all calculations and plot graphs. Whether the results of such investigation would correspond to actual differences between membranes of different materials had to be the be subject of a validation procedure, which is presented next.

6.3.4. Validation of final method with different membranes

The final protocol composed of methods A and D combined was performed three times for two PES (UP150) and two PVDF membrane sheets. First, a comparison between the permeabilities of the different membranes was made. Then, an analysis on the results for critical flux was carried out, followed by an evaluation on the differences of sustainable fluxes. Lastly, an investigation regarding the residual fouling exponential coefficient was undertaken between the different sheets.

Table 6.5 lists the sequence of trials conducted with the four membrane sheets using the AD method. Sheets 9 and 10 follow the numeration started previously, since they are UP150 sheets. The UF membranes of PVDF are indicated as so. Trials 60, 62 and 68 exhibited very erratic fouling curves during the execution of Method D, which will be discussed ahead, and for this reason parameters were not included in the table. Trial 61 also resulted in illogical TMP developments that did not reflect the flux imposed at each step, hence not able to produce results for the critical flux. Graphs for Methods A and D for the PVDF membrane are shown in Appendix IV.

Table 6.5. Average normalized permeabilities (20 °C), critical fluxes (20 °C), sustainable fluxes (20 °C) and residual fouling exponential coefficients for trials with PES and PVDF membranes (aeration 0.005 m/s) using methods A and D.

Trial N°	Sheet N°	Method	Permeability (LMH/bar)	J_c (LMH)	J_{sus} (LMH)	Exp. coef. (LMH^{-1})	R^2	Av. Temp. (°C)
45	PES 9	A	XX	XX	XX	XX	XX	23.1
46	PES 9	D	XX	XX	XX	XX	XX	23.8
47	PES 9	A	XX	XX	XX	XX	XX	23.6
48	PES 9	D	XX	XX	XX	XX	XX	23.9
49	PES 9	A	XX	XX	XX	XX	XX	23.2
50	PES 9	D	XX	XX	XX	XX	XX	23.0
51	PVDF 1	A	XX	XX	XX	XX	XX	22.6
52	PVDF 1	D	XX	XX	XX	XX	XX	21.2
53	PVDF 1	A	XX	XX	XX	XX	XX	21.2
54	PVDF 1	D	XX	XX	XX	XX	XX	21.1
55	PVDF 1	A	XX	XX	XX	XX	XX	22.0
56	PVDF 1	D	XX	XX	XX	XX	XX	21.3
57	PES 10	A	XX	XX	XX	XX	XX	22.4
58	PES 10	D	XX	XX	XX	XX	XX	21.9
59	PES 10	A	XX	XX	XX	XX	XX	22.2
60	PES 10	D	XX	XX	XX	XX	XX	21.9
61	PES 10	A	XX	XX	XX	XX	XX	22.7
62	PES 10	D	XX	XX	XX	XX	XX	21.8
63	PVDF 2	A	XX	XX	XX	XX	XX	21.8
64	PVDF 2	D	XX	XX	XX	XX	XX	21.6
65	PVDF 2	A	XX	XX	XX	XX	XX	21.6
66	PVDF 2	D	XX	XX	XX	XX	XX	21.0
67	PVDF 2	A	XX	XX	XX	XX	XX	22.4
68	PVDF 2	D	XX	XX	XX	XX	XX	22.1

The higher permeabilities of PVDF membrane sheets is the most noticeable difference at first glance, but they were still well below the XX LMH/bar measured in the lab. This measurement, however, was performed with the unlaminated sheet in a stirred cell, which likely explains the higher lab value. As shown in Figure 6.20, permeabilities of all sheets had a falling trend between successive trials. This

was expected since no chemical cleaning was performed in between trials. Chemical cleaning was not considered due to time constraints, as each AD trial took almost 24 hours to complete and a cleaning between each of them – typically lasting a half hour – would drag out following trials. However, this allowed an analysis on the decline of permeability. Sheets of PVDF presented a much steep permeability decrease than those of PES. This might indicate a tendency for higher residual fouling rates and therefore lower sustainable fluxes for PVDF, but Table 6.5 appears to show the opposite effect. This will be discussed in detail during the analysis regarding the sustainable flux.

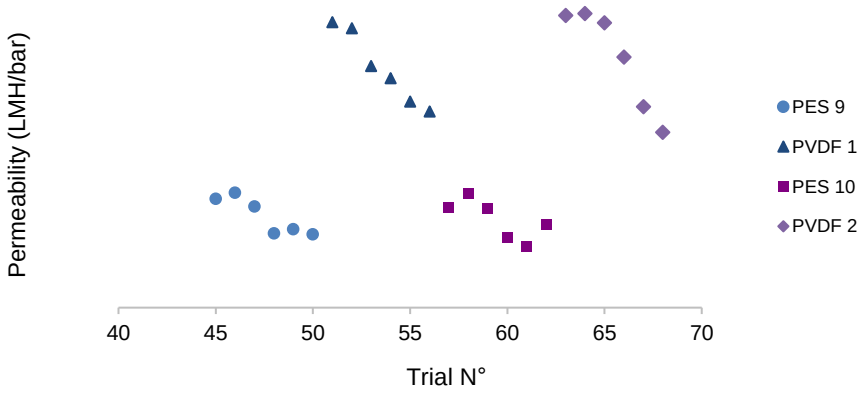

Figure 6.20. Permeability of four membrane sheets during sequence of trials using method AD.

The comparable analysis between critical fluxes showed that this parameter did not manifest the same differences observed for permeabilities. Average critical fluxes for PVDF sheets were only marginally superior to those of PES. In fact, only the second PVDF sheet had critical fluxes significantly above those of the other two PES membranes ($p < 0.05$). The other three sheets presented no significant difference in J_c, implying that the critical flux reflected poorly the differences between the materials.

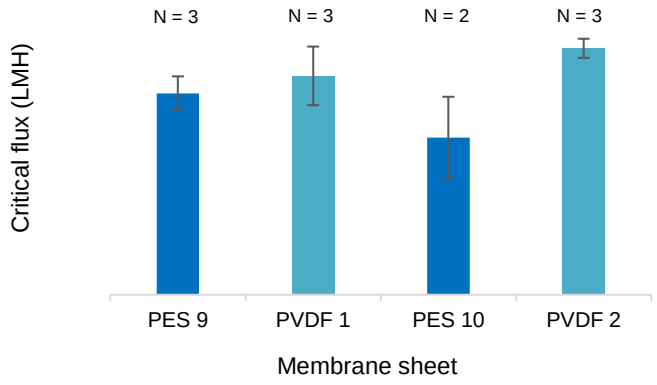

Figure 6.21. Comparison between critical fluxes for PES and PVDF membrane sheets. Error bars: SD.

Bacchin et al. (2006) observed that, in most studies, initial permeability and material hydrophilicity had little effect on the critical flux value. Much more relevant is the surface porosity and morphology. Higher porosity will lead to a better distribution of the permeate flux through the porous surface and thus to lower local fluxes, which results in higher global critical fluxes. Furthermore, Bromley et al. (2002) showed that the critical flux for latex particles can be five-fold higher for microfilters with slotted pores than for circular pores, again revealing the impact of local surface structure on the critical flux.

Surface porosity does not directly relate to pore size; it measures the percentage of superficial area covered by pores. Morphological analysis of the two membranes revealed that both had similar surface porosities: XX and XX % for the PES and PVDF materials, respectively. If the slightly higher critical fluxes observed for the PVDF are due to this small porosity difference is hard to evaluate, especially when dealing mixed liquor, a medium that changes constantly due to external factors.

Sustainable flux values, on the other hand, showed significant difference between PES and PVDF membranes. Both PVDF membranes presented significantly higher J_{sus} compared to PES sheet N° 9 ($p < 0.05$). Statistical comparison with the PES sheet N° 10 was not possible, as only one result was available. Yet, its sustainable flux remained in the range of the other PES sheet, possibly confirming the findings. This indicates that the PVDF membrane was less prone to suffer from residual fouling. Since residual fouling is caused by the irreversible attachment of species – irreversible here meaning that the deposit is not removed during the relaxation pause – these results point to the fact that this PVDF membrane leads to less irreversible fouling. This can be linked to a lower affinity of molecules and suspended matter to the membrane surface, which in turn can be caused by surface charge, surface topography or chemical affinity. Figure 6.22 sums up the sustainable flux average values.

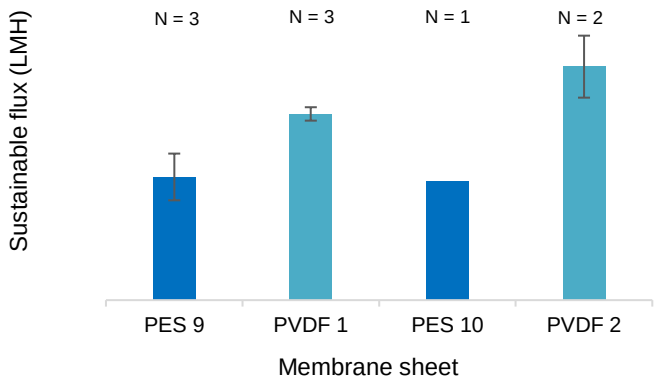

Figure 6.22. Comparison between sustainable fluxes for PES and PVDF membrane sheets. Error bars: SD.

This outcome seems to contradict the steep permeability decrease observed for PVDF membranes in Figure 6.20. After all, higher sustainable fluxes should be the result of lower residual fouling rates and thus correspond to mild permeability declines. However, the apparent conflict is solved when more attention is drawn to the TMP values: for having much higher permeability, PVDF membranes result in much lower TMPs during trials. A certain low amount of fouling (i.e., TMP increase over time) will be proportionally much more significant to this material than to PES, that operates at higher TMPs. Thus, even at lower residual fouling rates, PVDF sheets experienced a stronger permeability decline compared to PES sheets. Operators should be aware this when setting chemical cleanings every time permeability drops a certain percentage, as it will not necessarily coincide to a sharp TMP increase.

A comparison between sustainable and critical fluxes for each sheet can be made by combining Figure 6.21 and 6.22. Figure 6.23 provides this contrast between the two materials investigated: while the sustainable flux is principally below the critical one for PES sheets, it is at the same level or even above the critical flux of PVDF sheets. This means that the PES membranes achieved the threshold for residual fouling rate of 0.01 mbar/min at a flux lower than the critical one, defined at 0.1 mbar/min. Meanwhile, the PVDF material imparted the ability for the membrane to operate even above the critical flux and still not surpass the defined threshold for the sustainable flux.

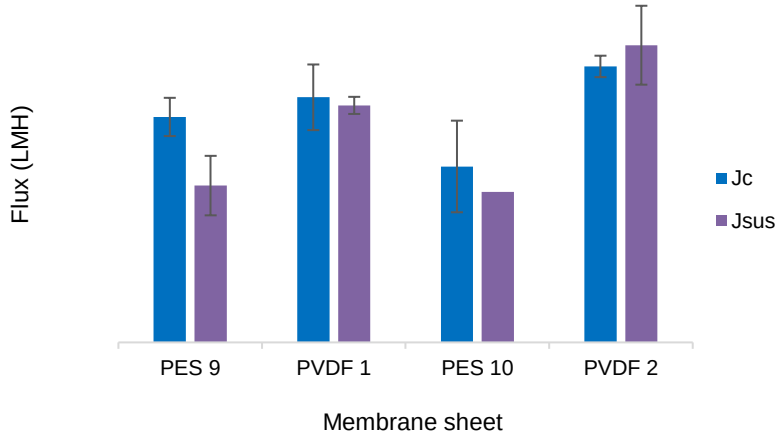

Figure 6.23. Comparison between critical and sustainable fluxes for PES and PVDF membrane sheets. Error bars: SD.

Residual fouling behaviors during trials 60, 62 and 68 were unexpectedly irregular. As depicted in Figure 6.24, trial 62 had an increasing TMP at the first block-steps, which later turned into decreasing TMP values at higher steps. This was also observed in the other referred trials. No explanation for such unusual manifestation can be given apart from changes in the biology or feed stream: flocculation, deflocculation, EPS release, sudden drop/rise in COD content, sudden death of bacteria due to toxic substances or even rainfall are a few factors that affect the sludge and fouling in MBRs.

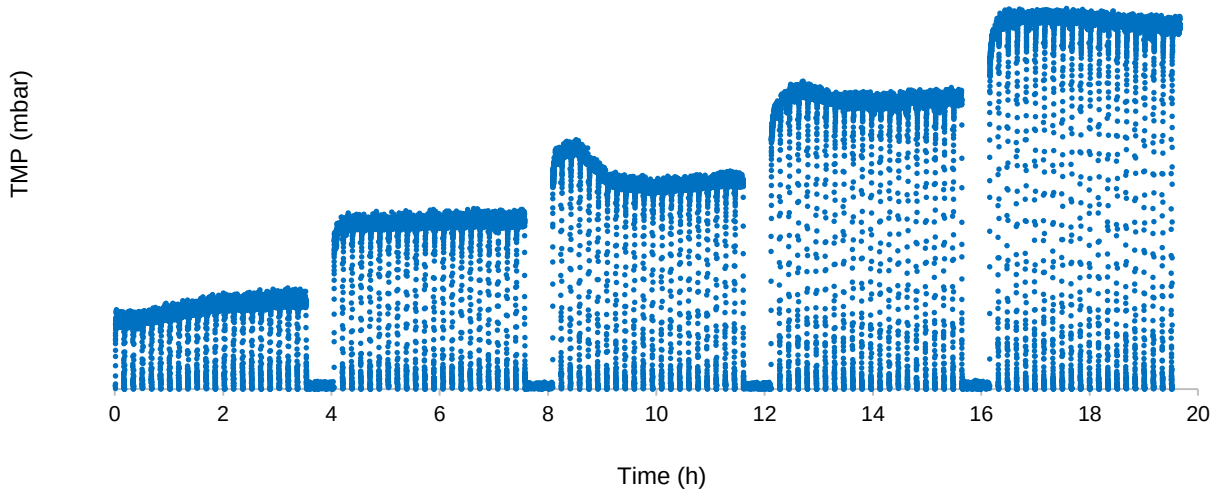

Figure 6.24 Unusual TMP development during execution of method D (trial 62).

The strong dependence of the method on stable conditions of mixed liquor, wastewater composition and external circumstances (temperature, precipitation) is certainly a weakness to be overcome. Since fluctuations in these parameters are inherent to real MBR plants, comparison between membranes should be carried out simultaneously, with sheets operated at the same time.

Exponential coefficients for residual fouling rates varied independently from the membrane tested (Figure 6.25). Ranging from XXX to XXX LMH^{-1}, their values are likely more dependent on conditions of mixed liquor rather than on membrane material type, at least in view of these results. Higher exponential coefficients express an increasing affinity of the membrane to irreversible foulants with increasing fluxes, signaling that the material becomes more susceptible to the sorption of

macromolecules and/or colloids at higher fluxes. Higher flux and TMP values promote more contact at the membrane interface, which can lead to more effective deposition and attachment of the species. Although being well below the value of 0.3893 LMH^{-1} found by Howell et al. (2004), the good fit of the data in the model represented by R^2 above 0.9 for all trials in Table 6.5 proves that residual fouling does have an exponential increase with the flux. Nevertheless, these authors applied their model and constants in data obtained previously and observed a poor fit. The researches pointed out that this outcome emphasizes the dependence of fouling behavior on the history of membrane use and that, even though such series of trials can be well modelled, such modelling is not yet predictive.

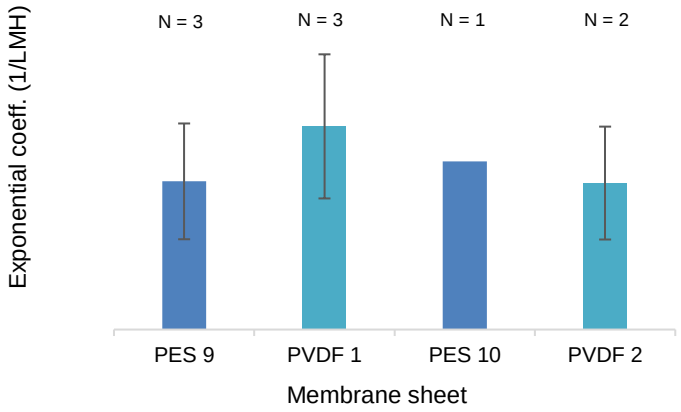

Figure 6.25. Exponential coefficient for residual fouling in respect to the flux for different membrane sheets. Error bars: SD.

The analysis of sludge characteristics was not as frequent for this series of trials as it had been for the other trials, as seen in Table 6.6. Values for MLSS and CST remained, nevertheless, in the same range as in previous analysis, as well as those for COD and removal rates. No indication of unusual biological activity could be translated by these results, as it would have been expected due to results of trials 60, 61, 62 and 68. In fact, as observed by Meng et al. (2017), fouling behaviors are hard to explain based on MLSS levels, and its occurrence is much more linked to presence of EPS and MSP. Other authors went on to say that not only the concentration but also the nature of these substances, determined by parameters such as SRT, F/M and wastewater composition, play a key role in fouling (Silva et al., 2016; Wu et al., 2013). Indeed, during the referred trials, tests with different flux levels were carried out in the main module. Moreover, the purge time of sludge varied vastly during all trials, as an attempt to control MLSS levels in the tanks. This equated in SRT varying from XX to XX days and F/M fluctuating between XX and XX kg kg^{-1} day^{-1}, factors which might likely have led to variations in the profiles of EPS and SMP released by microorganisms. Since no analysis on the EPS/SMP content of the mixed liquor was conducted, this hypothesis could not be confirmed.

Table 6.6. Mixed liquor characteristics and COD levels and removal during trials with method AD.

Sheet N°	**MLSS (g/L)**	**CST (s)**	**COD_{feed} (mg/L)**	**$COD_{permeate}$ (mg/L)**	**COD removal (%)**
PES 9	XX	XX	XX	XX	XX
PVDF 1	XX	XX	XX	XX	XX
PES 10	XX	XX	XX	XX	XX
PVDF 2	XX	XX	XX	XX	XX

6.3.5. Long term trials

Long term trials were scheduled to verify the model for the sustainability time, as defined in Eq. 19. However, only two trials were successfully executed during the period of testing. One trial was interrupted due to a power cut at the station, another had a code error and yet another was halted when the computer restarted itself. Of the two long term trials carried out, the first presented irregular alternating decreasing and increasing TMP values, similarly to the trial represented in Figure 6.24. The other trial ran during 45 hours, with the PVDF sheet N° 1 at 42 LMH, following the standard cycle of 9 min of filtration and 1 min of relaxation. Data for the TMP is presented in Figure 6.26 as the average of 20 values for every 20 s interval, excluding data collected during relaxation.

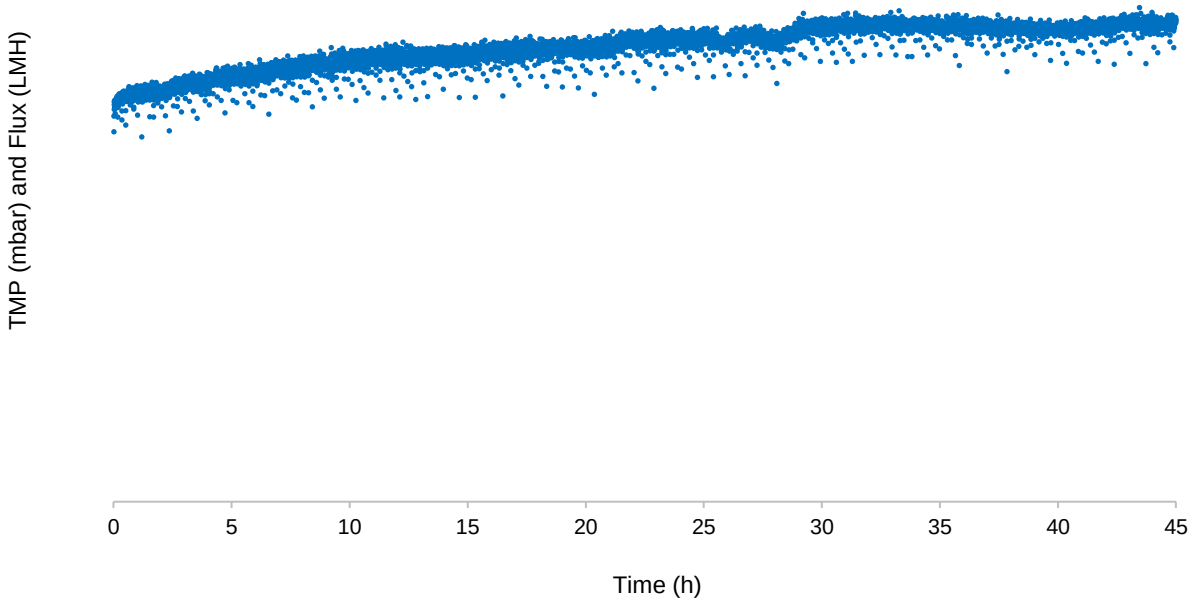

Figure 6.26. TMP development during long term trial in sludge at 42 LMH (aeration 0.005 m/s) with PVDF sheet.

As shown, no TMP jump occurred, even with the flux being as high as 42 LMH, which is close to the critical flux measured for this membrane sheet right before the long term trial started, of 42.3 LMH. For this reason, no sustainability time could be defined and no verification of the model was possible. Using method A to obtain the critical flux and method D to obtain values for the residual fouling rate from any of the block-steps of is enough to predict the moment of TMP jump. This prediction, however, makes sense for filtration below the critical flux, as it predicts a sustainability time of zero when the permeate flux equals the critical one. For this trial, the flux was only marginally below the critical one. Strikingly, with the residual fouling rates of all block-steps of method D, predicted sustainability times ranged from 360 to 7583 hours. The trial certainly lasted shorter than that and, since no TMP jump was observed, this could imply that the model is correct. Nevertheless, this is not a trustworthy result, and any investigation on why such a small difference between the applied flux and the critical flux resulted in the prediction of such long sustainability times is merely speculative. Here it should be reminded that this critical flux is the one defined by the arbitrary threshold value of 0.1 mbar/min, and that the actual value for the local critical flux – concept in which this model is based – may be different.

7. Conclusions and perspectives

The work accomplished the implementation of an integrated filtration test setup in an MBR pilot unit with the objective to execute programed trials using membrane sheets submerged in activated sludge. Problems in previous attempts such as variable flowrates or unsteady pressure at rest were solved with the installation of a flowmeter and a suitable configuration of the system's geometry, respectively. The peristaltic pump was well operated through a feedback control system coupled with the flowmeter.

Pre-trials confirmed that the flowrate drawn by the pump varied according to the system's resistance. They also proved the good tuning of the controller's PI parameters by the Ziegler-Nichols method. Further, trials in water estimated an average permeability for the PES membrane at XXX LMH/bar, and revealed that the flux-step methods called A, B and C could be equally executed for this end. Bentonite suspension was used to investigate the TMP rise within steps of these methods and enabled the computation of the fouling rate by different calculation procedures.

Activated sludge caused different fouling behaviors with the methods tested. The criterium to define the critical flux that suited these different behaviors was the fouling rate threshold of 0.1 mbar/min, which was applied in methods A and B. The adequate procedure to determine the fouling rate was identified as the slope of TMP data points in respect to the time, that was able to compensate for the oscillations in the aeration tank level. Method B was dismissed for not yielding meaningful results for the irreversible fouling rate. Method A was elected as an appropriate tool to evaluate the critical flux, and the lack of a fouling rate hysteresis attested the efficiency of the relaxation to remove fouling. Method C was unable to give insight on the residual fouling rate, being then adapted and molded into method D, that showed that the residual fouling rate increased exponentially with the applied flux. The sustainable flux could then be set as the one that induced residual fouling rates of 0.01 mbar/min. The final method, nicknamed AD, is formed of a common flux step method (A), with step duration of 9 min of filtration and 1 min of pause, starting at 6 LMH, ascending up to 66 LMH with increments of 6 LMH and then descending the same steps. After a 30 min pause, a prolonged flux step method (D) is executed, following the same cycle of 9 min on – 1 min off, but repeating each of the defined steps (12, 24, 36, 48 and 60 LMH) 21 times, with a 30 min pause in between every so-called block-step.

The validation of this combined protocol was performed comparing results obtained for membranes of two different materials: PES and PVDF. The outcome of this investigation revealed that, although the initial permeability of PVDF was three-fold higher as that of PES, their critical fluxes did not differ. Neither their distinct chemical nature nor different pore sizes (0.04 and XXX µm for PES and PVDF, respectively) led to significant difference in the critical flux. This parameter seemed to be dependent, in this case, more on the properties of the medium rather than on the membrane characteristics. This suggests that the drag force promoted by permeate suction is the governing factor for cake build up. Nonetheless, clear differences between both materials were verified in results for the sustainable flux. PVDF sheets had lower residual fouling rates that resulted in higher sustainable fluxes. This implies that PVDF was less susceptible to the irreversible attachment of species – irreversible in the sense that deposition remains attached after 1 min relaxation at the aeration rate of 0.005 m/s – than PES. The better performance of PVDF membranes in this study might highlight its advantage over PES and explain its prevalence among MBR products, but characteristics such as membrane lifetime, cleanability and resistance to chemicals must still be taken into account for a full evaluation.

Despite the achievements of the method development, the filtration set up and the method itself can still undergo improvement efforts. The main limitation observed during trials was the high dependence of results on the characteristics of the mixed liquor, which became evident when negative residual fouling rates were registered in several trials. This can only be overcome if the test rig is expanded into a setup with two separate peristaltic pumps, two flowrates and two pressure transmitters that operate filtration tests in two membrane sheets simultaneously. This will allow the membrane sheets to be tested in the exact same conditions and therefore produce more substantial, comparable results. Even during anomalous fouling events, caused by varying wastewater composition, temperature changes or oscillating SRT and F/M, the sheets will react together and reflect their different attributes. Changes in step height and duration can also be undertaken according to the membranes tested. Furthermore, the filtration setup might as well be used for investigations regarding differences in the aeration rate on both critical and sustainable fluxes or even to assess the mixed liquor filterability.

Finally, the development of this project reassured the advantages of low flux operation in MBRs. Residual fouling rates of 0.08 mbar/min – the average recorded at 60 LMH – correspond to TMP rises of 800 mbar in a week (at the tested aeration rate) and would be prohibitive to any MBR plant. If restricting the permeate flux leads to an increase in the required membrane area, it reduces energy consumption due to aeration and lowers costs related to chemical cleaning. First, this is more environmentally beneficial. Second, it yields a more easily controlled operation, free from sudden fouling events such as multi-layered fouling and TMP jumps. Furthermore, it also increases the membrane lifetime, as frequent cleaning procedures affect its structure and intense aeration threatens its physical integrity. Lastly, it tends to be more economically attractive, since membrane prices have dropped in the last years. In summary, low flux operation in MBRs aims at the development of a more sustainable and viable membrane technology for wastewater treatment purposes in the future.

8. Appendix

I) Water series, PES membrane

a) Method B (trial N° 13)

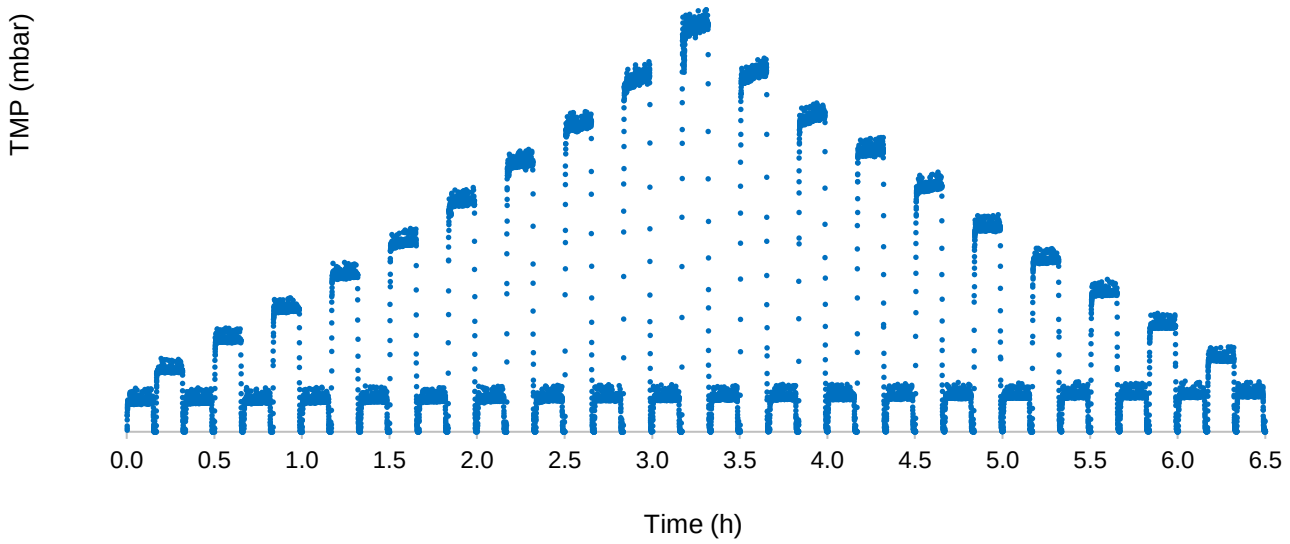

b) Method C (trial N° 2)

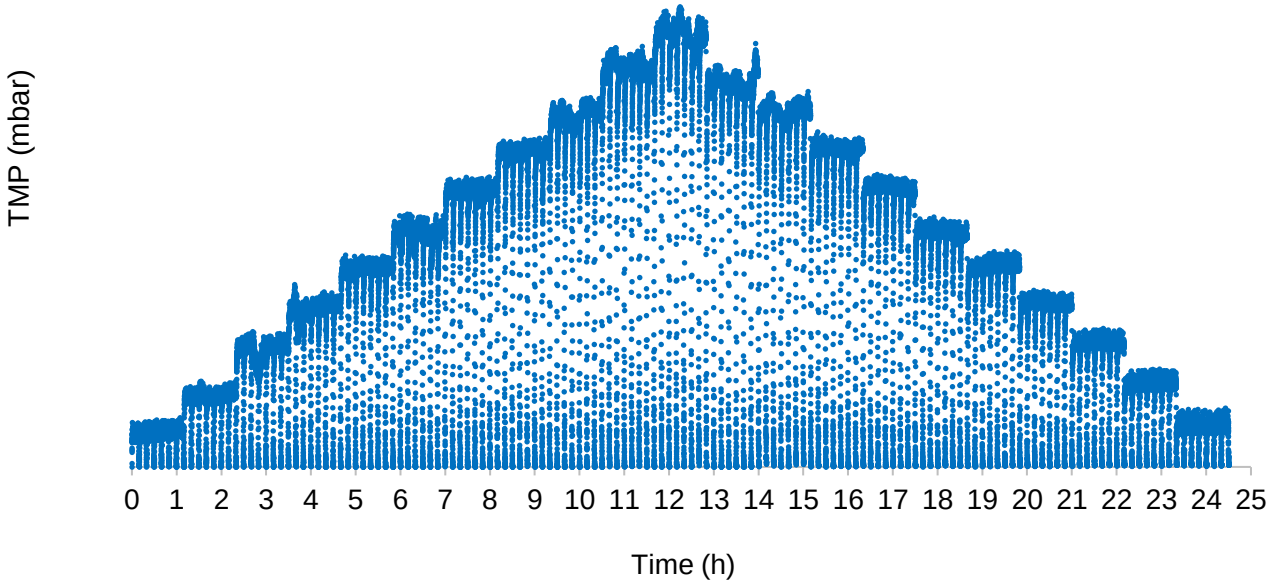

II) Bentonite series, PES membrane

a) Method A (trial N° 19)

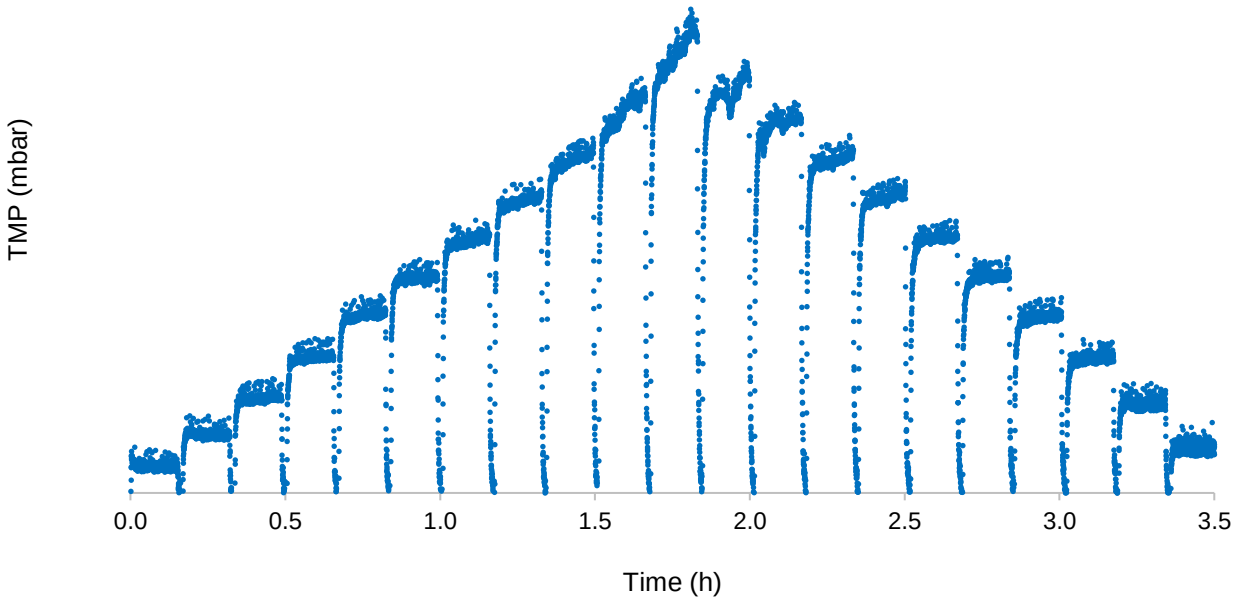

b) Method C (trial N° 15)

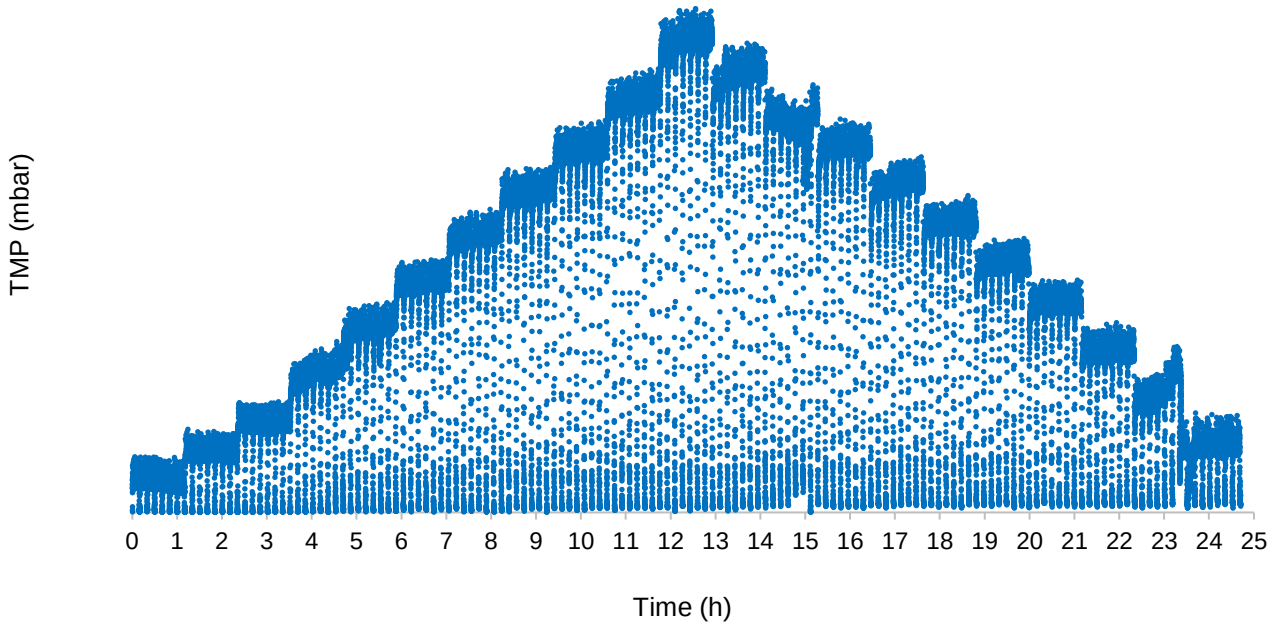

III) Sludge series, PES membrane

a) Method A (Trial N° 37)

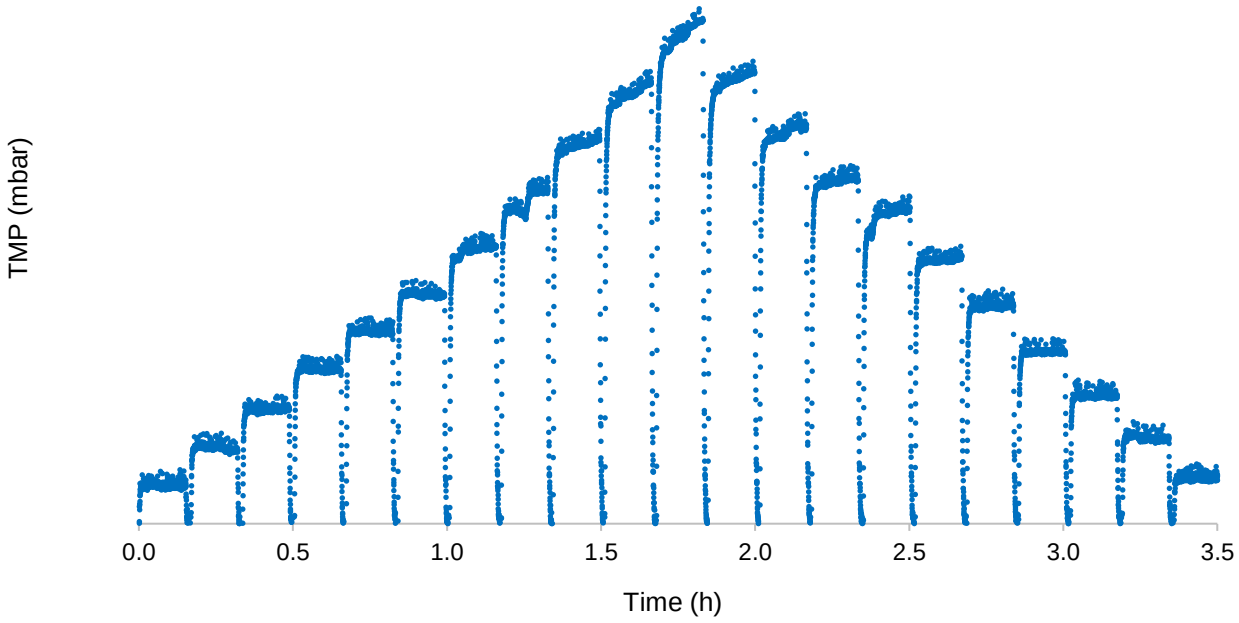

b) Method B (trial N° 26)

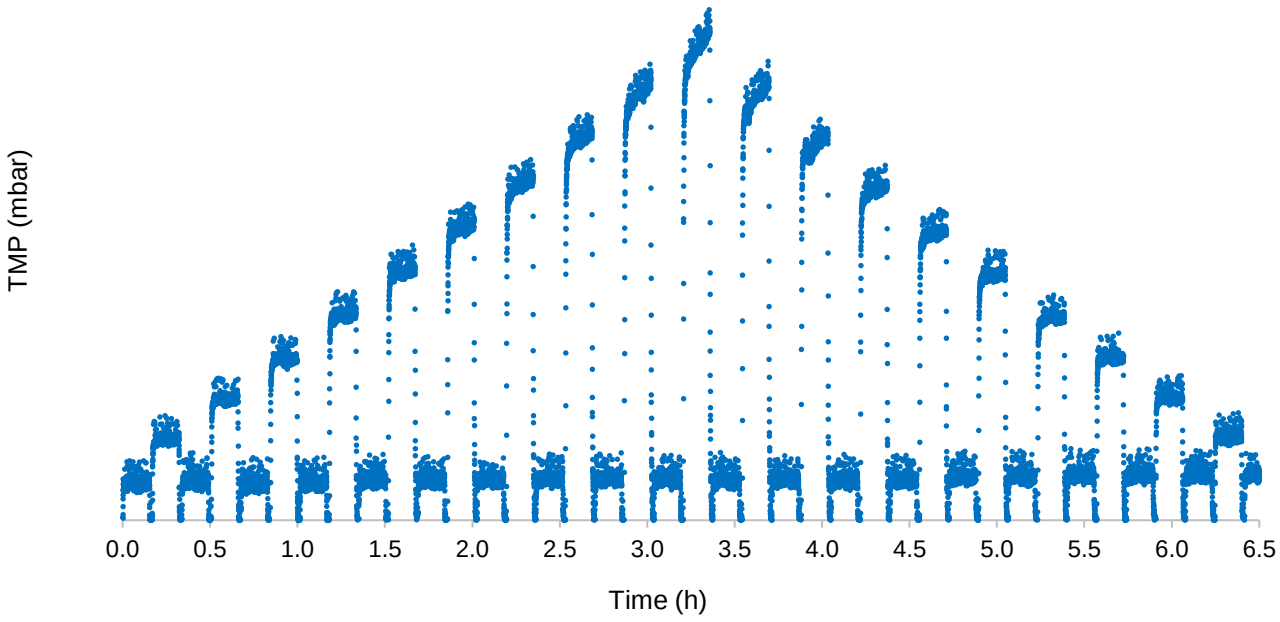

IV) Sludge series, PVDF membrane

a) Method A (trial 55)

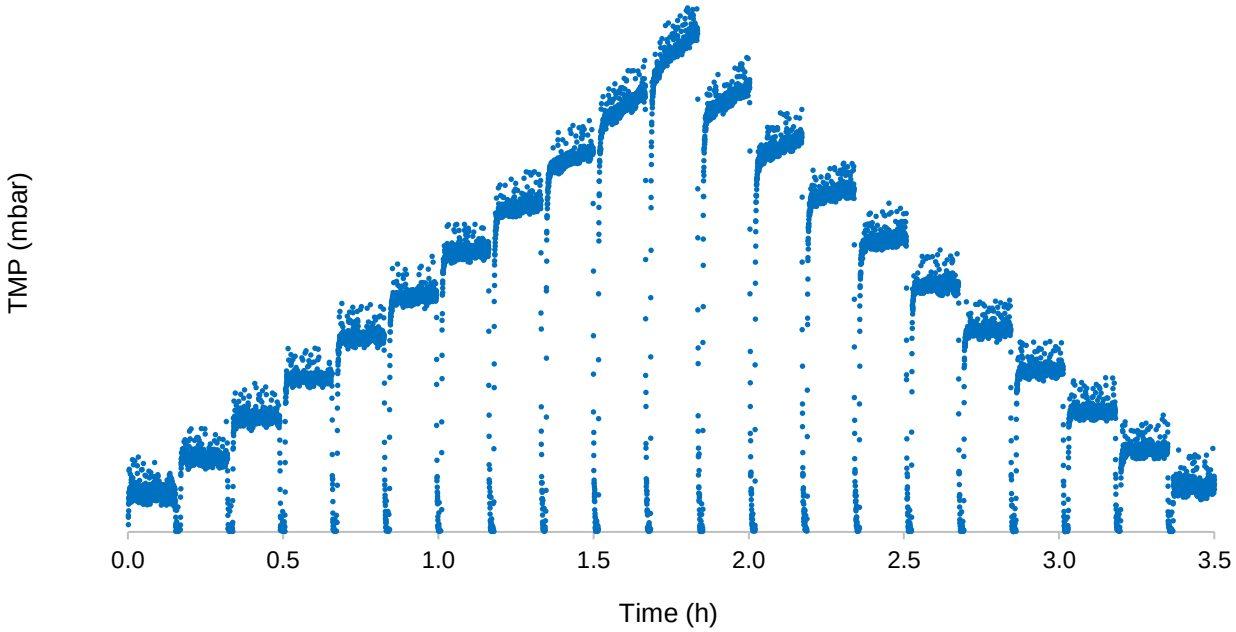

b) Method D (trial 56)

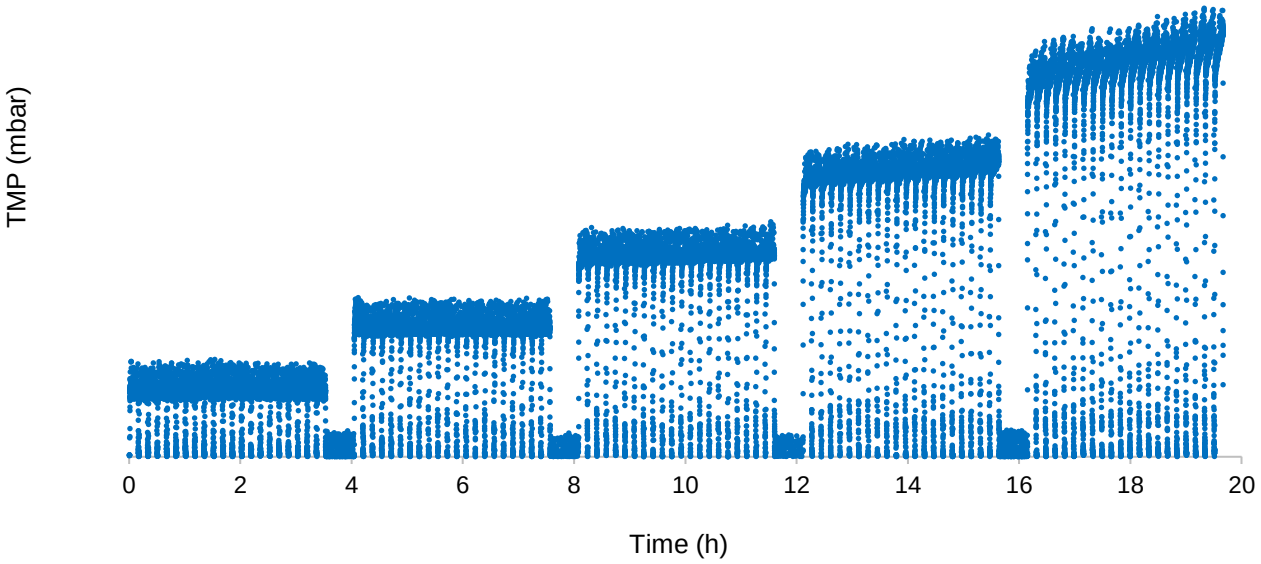

9. References

ALKMIM, A. R.; COSTA, P. R.; AMARAL, M. C. S.; NETA, L. S. F.; RICCI, B. C.; OLIVEIRA, S. M. A. C.; CERQUEIRA, A. C.; SANTIAGO, V. M. J. (2014). The application of filterability as a parameter to evaluate the biological sludge quality in an MBR treating refinery effluent. Desalination and Water Treatment, 53, 1-10. https://doi.org/10.1080/19443994.2014.943055.

APHA (2017). Standard methods for the examination of water and wastewater, 23rd ed. American Public Health Association. Washington, DC.

BACCHIN, P.; AIMAR, P.; SANCHEZ, V. (1995). Model for colloidal fouling of membranes. AIChE Journal, 41, 368-377. https://doi.org/10.1002/aic.690410218.

BACCHIN, P.; AIMAR, P.; FIELD, R. W. (2006). Critical and sustainable fluxes: theory, experiments and applications. Journal of Membrane Science, 281, 42–69. https://doi.org/10.1016/j.memsci.2006.04.014.

BAKER, R. W. (2004). Membrane Technology and Applications, 2nd Edition. John Wiley & Sons, Ltd. ISBN: 0-470-85445-6.

BAKER, R. W.; WIJMANS, J. G.; HUANG, Y. (2010). Permeability, permeance and selectivity: A preferred way of reporting pervaporation performance data. Journal of Membrane Science, 348, 346–352. https://doi.org/10.1016/j.memsci.2009.11.022.

BAZHENOV, S. D.; BILDYUKEVICH, A. V.; VOLKOV, A. V. (2018). Gas-Liquid Hollow Fiber Membrane Contactors for Different Applications. Fibers, 6(4), 76. https://doi.org/10.3390/fib6040076.

BOUHABILA, E. H.; BEN AÏM, R.; BUISSON, H. (1998). Microfiltration of activated sludge using submerged membrane with air bubbling (application to wastewater treatment). Desalination, 118 (1–3), 315-322. https://doi.org/10.1016/S0011-9164(98)00156-8.

BROMLEY, A. J.; HOLDICH, R. G.; CUMMING, I. W. (2002) Particulate fouling of surface microfilters with slotted and circular pore geometry. Journal of Membrane Science,196, 27-37. https://doi.org/10.1016/S0376-7388(01)00573-7.

CHAN, R.; CHEN, V. (2001) The effects of electrolyte concentration and pH on protein aggregation and deposition: critical flux and constant flux membrane filtration. Journal of Membrane Science, 185, 177–192. https://doi.org/10.1016/S0376-7388(00)00645-1.

CHO, B. D; FANE, A. G. (2002). Fouling transients in nominally sub-critical flux operation of a membrane bioreactor. Journal of Membrane Science, 209, 391-403. https://doi.org/10.1016/S0376-7388(02)00321-6.

CUI, Z.F.; CHANG, S.; FANE, A. G. (2003). The use of gas bubbling to enhance membrane processes. Journal of Membrane Science, 221(1–2), 1-35. https://doi.org/10.1016/S0376-7388(03)00246-1.

DEFRANCE, L.; JAFFRIN, M. (1999). Comparison between filtrations at fixed transmembrane pressure and fixed permeate flux: application to membrane bioreactor used for wastewater treatment. Journal of Membrane Science 152, 203-210. https://doi.org/10.1016/S0376-7388(98)00220-8.

DIEZ, V.; EZQUERRA, D.; CABEZAS, J.; GARCÍA, A.; RAMOS, C. (2014). A modified method for evaluation of critical flux, fouling rate and in situ determination of resistance and compressibility in MBR under different fouling conditions. Journal of Membrane Science, 453, 1-11. https://doi.org/10.1016/j.memsci.2013.10.055.

ESPINASSE, B.; BACCHIN, P.; AIMAR, P. (2002). On an experimental method to measure critical flux in ultrafiltration. Desalination. 146. 91-96. https://doi.org/10.1016/S0011-9164(02)00495-2.

FANE, A. G.; YEO, A.; LAW, A.; PARAMESHWARAN, K.; WICAKSANA, F.; CHEN, V. (2005). Low pressure membrane processes ~ doing more with less energy. Desalination, 185, 1–3, 59-165. https://doi.org/10.1016/j.desal.2005.04.039.

FIELD, R. W; WU, D.; HOWELL, J. A.; GUPTA, B. B. (1995). Critical flux concept for microfiltration fouling. Journal of Membrane Science, 100, 259-272. https://doi.org/10.1016/0376-7388(94)00265-Z.

GALINHA, C. F.; SANCHES, S.; CRESPO, J. G. (2018). Chapter 6 - Membrane bioreactors. Fundamental Modelling of Membrane Systems. 209–249. Elsevier. https://doi.org/10.1016/B978-0-12-813483-2.00006-X.

GUGLIELMI, G.; CHIARANI, D.; JUDD, S.; ANDREOTTOLA, G. (2007a). Flux criticality and sustainability in a hollow fiber submerged membrane bioreactor for municipal wastewater treatment. Journal of Membrane Science, 289, 241-248. https://doi.org/10.1016/j.memsci.2006.12.004.

GUGLIELMI, G.; SAROJ, D. P.; CHIARANI, D.; ANDREOTTOLA, G. (2007b) Sub-critical fouling in a membrane bioreactor for municipal wastewater treatment: experimental investigation and mathematical modelling. Water Res. 41(17): 3903-3914. https://doi.org/10.1016/j.watres.2007.05.047.

GREEN, G.; BELFORT, G. (1980). Fouling of ultrafiltration membranes: lateral migration and the particle trajectory model. Desalination 35, 129-147. https://doi.org/10.1016/S0011-9164(00)88607-5.,

HACH (2021). Oxygen Demand, Chemical-Reactor Digestion ULR Method 10211, TNTplus™ 820. Available at: https://www.hach.com/chemical-oxygen-demand-cod-tntplus-vial-test-ulr-1-60-mg-l-cod-150-tests/product-downloads?id=7640193969&callback=qs. Access on June 15, 2021.

HOWELL, J.; CHUA, H.C.; ARNOT, T. (2004). In situ manipulation of critical flux in a submerged membrane bioreactor using variable aeration rates, and effects of membrane history. Journal of Membrane Science, 242, 13-19. https://doi.org/10.1016/j.memsci.2004.05.013.

HUISMAN, I. H.; DUTRÉ, B.; PERSSON, K. M.; TRÄGÅRDH, G. (1997). Water permeability in ultrafiltration and microfiltration: Viscous and electroviscous effects. Desalination, 113(1), 95-103. https://doi.org/10.1016/S0011-9164(97)00118-5.

JOSHI, R. N.; SINGH, K.; BHATTACHARYA, A. (2011). Approaches to prepare TFC polyamide membranes by coating diamine during, and/or post formation of asymmetric membranes and their performances. Brazilian Journal of Chemical Engineering, 28(3), 457-465. https://doi.org/10.1590/S0104-66322011000300011.

JUDD, S. (2015). The status of industrial and municipal effluent treatment with membrane bioreactor technology. Chemical Engineering Journal, 305, 37-45. https://doi.org/10.1016/j.cej.2015.08.141.

JUDD, S. (2006). The MBR-Book: Principles and Applications of Membrane Bioreactors in Water and Wastewater Treatment. Elsevier Science. ISBN 1-85-617481-6.

JUDD, S.; ALVAREZ VAZQUEZ, H.; JEFERSON, B. (2006). The Impact of Intermittent Aeration on the Operation of Air-Lift Tubular Membrane Bioreactors under Sub-Critical Conditions. Separation Science and Technology, 41:7, 1293-1302. https://doi.org/10.1080/01496390600634541.

JUDD, S.; JEFFERSON, B. (2003). Membranes for Industrial Wastewater Recovery and Re-use. Elsevier Science. ISBN 1-85617-389-5.

KWON, D. Y.; VIGNESWARAN, S. (1998). Influence of particle size and surface charge on critical flux of crossflow microfiltration. Water Science and Technology, 38, 481-488. https://doi.org/10.1016/S0273-1223(98)00548-4.

LADEWIG, B.; AL-SHAELI, M. N. Z. (2016). Fundamentals of Membrane Bioreactors, Materials, Systems and Membrane Fouling. Singapore: Springer Nature, 2016. ISBN 978-981-10-2014-8.

LE-CLECH, P.; CHEN, V.; FANE, A. G. (2006). Fouling in membrane bioreactors used in wastewater treatment. Journal of Membrane Science, 284(1-2), 17–53. https://doi.org/10.1016/j.memsci.2006.08.019.

LE-CLECH, P.; JEFFERSON, B.; CHANG, I.-S.; JUDD, S. J. (2003). Critical flux determination by flux-step method in a submerged membrane bioreactor. Journal of Membrane Science, 227 (1-2), 81-93. https://doi.org/10.1016/j.memsci.2003.07.021.

LI, H.; FANE, A. G.; COSTER, H. G. L.; VIGNESWARAN, S. (1998). Direct observation of particle deposition on the membrane surface during crossflow microfiltration. Journal of Membrane Science, 149, 83-97. https://doi.org/10.1016/S0376-7388(98)00181-1.

LIN, H.; ZHANG, M.; WANG, F.; MENG, F.; LIAO, B.-Q.; HONG, H.; CHEN, J.; GAO, W. (2014). A critical review of extracellular polymeric substances (EPSs) in membrane bioreactors: Characteristics, roles in membrane fouling and control strategies. Journal of Membrane Science, 460, 110-125. https://doi.org/10.1016/j.memsci.2014.02.034.

MADAENI, S. S.; FANE, A. G.; WILEY, D. E. (1999). Factors influencing critical flux in membrane filtration of activated sludge. Journal of Chemical Technology & Biotechnology, 74, 539-543.

MELIN, T.; JEFFERSON, B.; BIXIO, D.; THOEYE, C.; DE WILDE, W.; DE KONING, J.; VAN DER GRAAF, J.; WINTGENS, T. (2006). Membrane bioreactor technology for wastewater treatment and reuse. Desalination, 187(1–3), 271-282. https://doi.org/10.1016/j.desal.2005.04.086.

MELIN, T.; RAUTENBACH, R. (2007). Membranverfahren: Grundlagen der Modul- und Anlagenauslegung. Dritte Auflage. Springer. ISBN 3-540-00071-2.

MENG, F.; CHAE, S.-R.; DREWS, A.; KRAUME, M.; SHIN, H.-S.; YANG, F. (2009). Recent advances in membrane bioreactors (MBRs): Membrane fouling and membrane material. Water Research, 43(6), 1489–1512. https://doi.org/10.1016/j.watres.2008.12.044.

MENG, F.; ZHANG, S.; OH, Y.; ZHOU, Z.; SHIN, H.-S.; CHAE, S.-R. (2017). Fouling in membrane bioreactors: An updated review. Water Research. 114, 151–180. https://doi.org/10.1016/j.watres.2017.02.006.

METCALF & EDDY, INC. (2003). Wastewater Engineering: Treatment and Reuse. 4th Edition. McGraw-Hill, New York, NY. EISBN 0071122508.

MICRODYN-NADIR. (2021a). BIO-CEL® L-2 Data Sheet. Available at: https://www.microdyn-nadir.com/bio-cel-mbr/. Access on June 7, 2021.

MICRODYN-NADIR. (2021b). NADIR® UP150 P Ultrafiltration Membrane Data Sheet. Available at: https://www.microdyn-nadir.com/flat-sheet-membrane-data-sheets/. Access on June 10, 2021.

MULDER, M. (1996). Basic Principles of Membrane Technology, 2nd Edition. Kluwer Academic Publishers B.V. ISBN 978-0-7923-4248-9.

NAESSENS, W.; MAERE, T.; NOPENS, I. (2012). Critical review of membrane bioreactor models – part 1: Biokinetic and filtration models. Bioresources Technology, 122, 95–106. https://doi.org/10.1016/j.biortech.2012.05.070.

NAVARATNA, D.; JEGATHEESAN, V. (2011). Implications of short and long term critical flux experiments for laboratory-scale MBR operations. Bioresource Technology, 102 (9), 5361-5369. https://doi.org/10.1016/j.biortech.2010.12.080.

PCI Membranes. (2021). PCI A19 Series Product Data Sheet, Product Information. Available at: https://www.pcimembranes.com/download-centre/product-information/. Access on March 23, 2021.

PINNEKAMP, J.; FRIEDRICH, H. (2006). Membrane Technology for Waste Water Treatment. FiW Verlag, Aachen. ISBN 3-939377-01-5.

ROMERO, C. A.; DAVIS, R. H. (1991). Experimental verification of the shear-induced hydrodynamic diffusion model of crossflow microfiltration. Journal of Membrane Science, 62, 249–273. https://doi.org/10.1016/0376-7388(91)80042-5.

SHIM, S.; KIM, S.-R.; JO, S.; YEON, K.-M; LEE, C.-H. (2015). Evaluation of mechanical membrane cleaning with moving beads in MBR using Box–Behnken response surface methodology. Desalination and Water Treatment. 56. 2797-2806. https://doi.org/10.1080/19443994.2014.963162.

SILVA, A. F.; ANTUNES, S.; SAUNDERS, A.; FREITAS, F.; VIEIRA, A.,; GALINHA, C. F.; NIELSEN, P. H.; CRESPO, M. T. B.; CARVALHO, G. (2016). Impact of sludge retention time on the fine composition of the microbial community and extracellular polymeric substances in a membrane bioreactor. Applied Microbiology and Biotechnology. 100(19), 8507–8521. https://doi.org/10.1007/s00253-016-7617-2.

SKOGESTAG, S. (2001). Probably the best simple PID tuning in the world. Journal of Process Control. Norwegian University of Science Technology.

SOFIA, A.; NG, W. J.; ONG, S. L. (2004). Engineering design approaches for minimum fouling in submerged MBR. Desalination, 160(1), 67-74. https://doi.org/10.1016/S0011-9164(04)90018-5.

TARDIEU, E.; GRASMICK, A.; GEAUGEY, V.; MANEM, J. (1999). Influence of hydrodynamics on fouling velocity in a recirculated MBR for wastewater treatment. Journal of Membrane Science, 156, 131-140. https://doi.org/10.1016/S0376-7388(98)00343-3.

THE MBR SITE. (2021a). LIVINGSTON, P. E. D.; PARLI, M.; SCHREIER, D.; RUTHERFORD, M. Clogging mitigation through MBR membrane module design. Available at :

https://www.thembrsite.com/features/clogging-mitigation-through-mbr-membrane-module-design/. Access on April 21, 2021.

THE MBR SITE. (2021b). What are the advantages of MBRs?. Judd & Judd Ltd. Available at: https://www.thembrsite.com/what-are-the-advantages-of-membrane-bioreactors/. Access on April 4, 2021.

TREUTEL, P. E. C. (2009). Peristaltic answer to caustic problems. World Pumps, 512, 28-31. https://doi.org/10.1016/S0262-1762(09)70183-X.

VAN DER MAREL, P.; ZWIJNENBURG, A.; KEMPERMAN, A.; WESSLING, M.; TEMMINK, H.; MEER, W. (2009). An improved flux-step method to determine the critical flux and the critical flux for irreversibility in a membrane bioreactor. Journal of Membrane Science, 332, 24-29. https://doi.org/10.1016/j.memsci.2009.01.046.

VERRECHT, B.; JAMES, C.; GERMAIN, E.; MA, W.; JUDD, S. (2001). Experimental evaluation of intermittent aeration of a hollow fiber membrane bioreactor. Water Science and Technology, 63(6), 1217–1223. https://doi.org/10.2166/wst.2011.361

VISVANATHAN, C.; BEN AIM, R. (1989). Studies on colloidal membrane fouling mechanisms in crossflow microfiltration. Journal of Membrane Science, 45, 3-15. https://doi.org/10.1016/S0376-7388(00)80841-8.

VISVANATHAN, C.; BEN AIM, R. (2000). Membrane Separation Bioreactors for Wastewater Treatment. Critical Reviews in Environmental Science and Technology, 30, 1-48. https://doi.org/10.1080/10643380091184165.

WANG, B.; ZHANG, K.; FIELD, R. W. (2018). Optimization of aeration variables in a commercial large-scale flat-sheet MBR operated with slug bubbling. Journal of Membrane Science, 567, 181–190. https://doi.org/10.1016/j.memsci.2018.09.039.

WIESE, M. (2021). Bachelors Thesis in Environmental Engineering: Planung, Bau und Betrieb eines Membranteststandes zur Bewertung von Membranen in MBR-Anwendungen. Hochschule Darmstadt, University of Applied Sciences.

WU, B.; KITADE, T.; CHONG, T. H.; LEE, J. Y.; UEMURA, T.; FANE, A. G. (2013). Flux-dependent fouling phenomena in membrane bioreactors under different food to microorganisms F/M ratio. Separation Science & Technology. 48(6), 840–848. https://doi.org/10.1080/01496395.2012.724501

WU, D.; HOWELL, J. A.; FIELD, R. W. (1999). Critical flux measurement for model colloids. Journal of Membrane Science, 125, 109-122. https://doi.org/10.1016/S0011-9164(02)00495-2.

YAMAMOTO, K.; HIASA, M.; MOHMOOD, T.; MATSUO, T. (1989). Direct solid-liquid separation using hollow fiber membrane in an activated-sludge aeration tank. Water Science Technology, 21 (4-5), 43–54. https://doi.org/10.2166/wst.1989.0209.

YOON, S.-H. (2015). Membrane Bioreactor Processes: Principles and Applications. CRC Press, Taylor & Francis Group. ISBN: 978-1-4822-5584-3.